Spatial Coordinate Systems within the Parietal Cortex

A thesis submitted for the degree of Doctor of Philosophy

by

Shaun Arthur Savio Seixas

Brain & Psychological Sciences Research Centre
Swinburne University of Technology,
Melbourne, Victoria
Australia
2014

Abstract

Spatial navigation is an important higher order cognitive function. Navigational tasks have been extensively used in neuroscience research as a tool to investigate motivational behaviour, memory and the representation of space. The role individual cortical regions play in navigation is becoming clearer through findings from functional imaging, single cell recordings in rodents and primates and clinical observations of patients. In particular, the limbic system and posterior parietal cortex have been shown to have important roles in navigation. In the case of the limbic system, there is an abundance of data from neurophysiological studies in rodents showing its role in navigation. However, in comparison, the role of the posterior parietal cortex (PPC) in spatial navigation is less established. This thesis sought to more clearly define the role of the postrerior parietal cortex in spatial navigation using functional imaging.

In the first experiment, a simple task required participants to navigate to a target position from a known starting location within a virtual 3D environment. The hypothesis was that an unexpected change in the position of the subject within the environment would require a remapping of the cognitive spatial map and that this could be detected with functional MRI. To test this, the starting location of subjects was unexpectedly shifted in a percentage of trials so that participants had to navigate from a different starting location. Two cortical regions demonstrated significant clusters of activity during the task. Initially, during the onset of the trial, the retrosplenial complex (RSC) was active, followed by a delayed activation of PFm, a

region within the PPC. RSC has been previously shown to be active during visualisation of landmarks and has demonstrated orientation selective activity, suggesting this region processes visual landmarks for navigational purposes. The subsequent activation of PPC suggests this region may be involved in remapping the spatial cognitive map and is likely to be involved in path integration. The activity in these two regions was negatively correlated during the task, implying that the navigational processes occurring in each of these regions may be mutually exclusive. Two navigational processes that are mutually exclusive are navigation by visual landmarks and navigation via internal cues when no visual landmarks are present. The latter form of navigation is often called path integration as it integrates vestibular, optic flow and efference copy signals to maintain a representation of location and orientation within the environment during navigation. Therefore it is conceivable that RSC is central to navigation processes based on visual landmarks and PFm is central to navigation by path integration, explaining the negative correlation of activity between these two regions.

To test this hypothesis, a second fMRI study was conducted that required participants to estimate their directional heading based on optic flow. This study also demonstrated activation in RSC and PFm, RSC being active during the period of time when a visual landmark was present, and PFm being active when directional information needed to be derived from optic flow information, as no landmarks were visible. The findings from this study further support the idea that RSC is involved in

processing spatial information from visual landmarks while area PFm is involved in path integration.

Acknowledgments

The completion of this doctorial thesis would not have been possible without the generous help and support of a number of people whom I wish to thank.

Before I was given the opportunity to begin this process, I had the privilege of previously working with my Principal Coordinating Supervisor Associate Professor Peter Brotchie, who gave me my first opportunity to work with functional magnetic resonance imaging. At the time, this was somewhat of a novelty, fMRI research projects were rare and expensive and most of the research coming out of my lab was focussed on EEG. It was Peter's subsequent supervision and mentorship during this period, which helped me to develop my skills as a researcher and the passion to further my academic training. I sincerely thank him for all the help, advice, opportunity and support over the last 7 years.

I also wish to thank my coordinating supervisor Dr Matt Hughes, whose assistance and knowledge was invaluable during experimental design and analysis. Matt's knowledge and enthusiasm has helped me become a better researcher and I am forever grateful. A special thanks also goes out to my other coordinating supervisor Prof David Crewther whose guidance and advice was greatly appreciated during this period of my life.

Then there are my friends and colleagues from Swinburne; Chris Anthony and Byron Silberstein, whose lunchtime philosophical discussions gave me some respite from blankly staring at a computer screen all day; Geoff Nield and Prof. Richard

Silberstein for giving me the opportunities that allowed me to see the world but more importantly giving me the time, understanding and space to finish this thesis. I also wish to thank the radiographers of Barwon Health, especially Kate Negus, for all their help and assistance with scanning.

None of this would have been possible without the help and support of my family, my parents, Phil and Mildred whose support for me during this endeavour has been unwavering. Thank you for all that you have given me: love, support, kindnesses and money, all of which has made it possible for me to complete this piece of work. I also wish to thank my sister Savannah, whom I wish the very best for.

Finally, I wish to thank Tracey Varker for all her love and support while I completed this thesis. You were there at my side while I ran this marathon, encouraging me and at times giving me a 'gentle' shove to finish. Words cannot express how grateful and lucky I am for you to have been a part of this journey with me.

Declaration

This thesis contains no material which has been accepted for the award of any other degree or diploma, expect where due reference is made in the text of the thesis. To the best of my knowledge, this thesis contains no material previously published or written by another person except where due reference is made in the text of the thesis. Disclosures are made regarding any work involving joint research or publication. All figures are original other than acknowledged adaptations.

I declare that ethical principles and procedures specified in the Swinburne University of Technology Human Research Ethics and Barwon Health Human Research Ethics document on human research and experimentation have been adhered to in the conduct and presentation of this thesis.

Shaun A. S. Seixas

Signed . . . . . .

Dated . . . . . .

“Even Noah got no salary for the first six months partly on account of the weather and partly because he was learning navigation.”

Mark Twain
in
Mark Twain in Eruption

Table of Contents

Table of Figures

Glossary of abbreviations

ACC ..... anterior cingulate cortex
AD ..... Alzheimer's disease
AIP ..... anterior intraparietal area
ATP ..... adenosine triphosphate
BA ..... Brodmann area
BOLD ..... blood oxygenation level dependent
CA1 ..... cornu ammonis area 1
CA3 ..... cornu ammonis area 2
CBF ..... cerebral blood flow
CBV ..... cerebral blood volume
CMRO2 ..... cerebral metabolic rate for oxygen
DLPFC ..... dorsolateral prefrontal cortex
EEG ..... Electroencephalogram
EPI ..... echo planar imaging
erfMRI ..... event related functional magnetic resonance imaging
ERP ..... event related potential
FEF ..... frontal eye fields
fMRI ..... functional magnetic resonance imaging
FOV ..... field of view
FWE ..... familywise error
FWHM ..... full width half maximum
GLM ..... general linear model
GRF ..... Gaussian random field
HD ..... head direction
HRF ..... hemodynamic response function
HUD ..... heads up display
IFG ..... inferior frontal gyrus
IPL ..... inferior parietal lobe
IPS ..... intraparietal sulcus
ITI ..... interstimulus interval
LIP ..... lateral intraparietal area
MCI ..... mild cognitive impairment
MEC ..... medial entorhinal cortex
MEG ..... magnetoencephalography
MIP ..... medial intraparietal area
MR ..... magnetic resonance
MRI ..... magnetic resonance imaging
MST ..... medial superior temporal area
MTL ..... medial temporal lobe

OFC ..... orbitofrontal cortex
PC ..... parietal cortex
PET ..... positron emission topography
PFC ..... prefrontal cortex
PI ..... path integration
PIP ..... posterior intraparietal area
PMC ..... primary motor cortex
PPA ..... parahippocampal place area
PPC ..... posterior parietal cortex
PRR ..... parietal reach region
PSC ..... primary somatosensory cortex
rCBF ..... regional cerebral blood flow
RF ..... receptive fields
ROI ..... region of interest
RS ..... retrosplenial cortex
RSC ..... retrosplenial complex
SFG ..... superior frontal gyrus
SMA ..... supplementary motor area
SNR ..... signal to noise ratio
SPL ..... superior parietal lobe
SPM ..... Statistical Parametric Mapping
S-R ..... stimulus-response
STP ..... superior temporal polysensory area
STS ..... superior temporal sulcus
TI ..... longitudinal relaxation
TR ..... repetition time

1 *Parietal cortex and Spatial Navigation*

1.1 **Introduction**

Spatial navigation is an important higher order cognitive function and the parietal lobe is an essential component of this process. Navigation has shared a long history in the cognitive sciences, where it was used as a tool to investigate learning and memory. This was especially evident in the early 20th century when psychologists like Edward Thorndike, Clarke Hull and Edwin Guthrie developed complex theories to explain learning behaviour, much of which was derived from animal observations. The connectionism theory (Thorndike, 1932), contiguity theory (Guthrie, 1930) and drive reduction theory (Hull, 1940) had a shared explanation of learning behaviour which was viewed as a direct result of the interaction of stimuli and the subsequent responses.

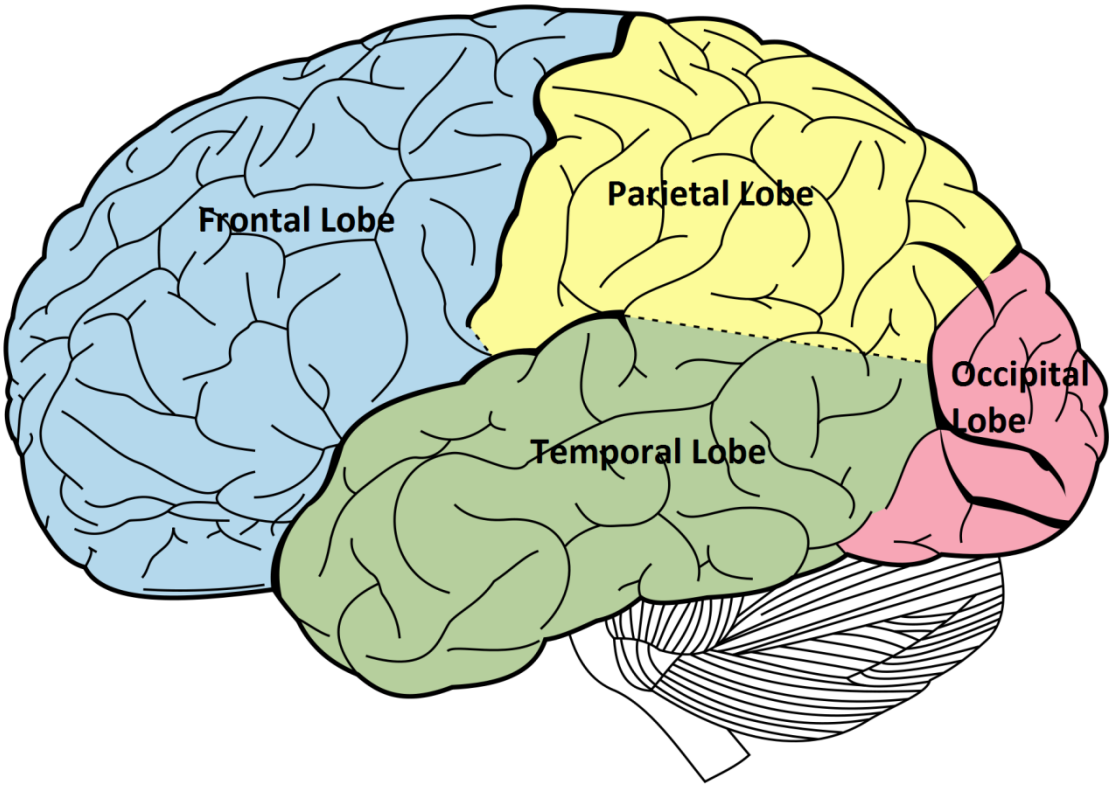

Figure 1: Lateral view of the cerebral lobes of the human brain. Adapted from Gray's Anatomy (Gray, 1918).

Navigation behaviour was often viewed in light of these theories, with much research focussing on the motivational drivers of this behaviour. A typical navigation experiment of this era involved rodents placed in a wooden constructed maze. The number of mistakes (indicated by entering dead end sections) and the time taken to reach the centre (where there was the reward of food) was then recorded. These results were often interpreted with reference to one of the stimulus-response (S-R) theories where learning was believed to be mediated by a chain of direct associations between specific stimuli and rewarded behavioural responses (Eichenbaum,

Dudchenko, Wood, Shapiro, & Tanila, 1999; Tolman, 1948). However, during some of these experiments, researchers noted that some rodents would use novel paths they had not used before. Some of these route options were considerably advantageous in terms of saving time and importantly, the S-R school of thought could not easily explain these actions.

An alternate theory was proposed by Tolman (1948) that specifically attempted to explain this aspect of rodent maze behaviour. The theory postulated the existence of a cognitive spatial map, an abstract representation of space that contained environmental information (routes, paths and environmental relationships) in which goals and self-position were represented. This was an important theory for two reasons: firstly, it marked a fundamental shift in the way navigation was viewed and secondly it was the first scientific proposal on how an abstract representation of space could be reflected in the brain.

Tolman's theory was criticised most notably by Clark Hull, because it failed to provide evidence of a cognitive or neural mechanism that could underlie a cognitive map – something akin to the physiological observations of conditioned reflexes that contributed to S-R learning (Eichenbaum, et al., 1999). It was not until further 30 years later that these neural mechanisms were discovered in the rodent hippocampus (O'Keefe & Dostrovsky, 1971), which ultimately provided the physiological evidence for Tolman's cognitive map. Single cell recording studies in rodents over the last 40 years, have revealed a number of different specialised cell types within the limbic system of

rats contributing to the representation of space, in particular, place cells in the hippocampus, grid cells in the medial entorhinal cortex (MEC) (Hafting, Fyhn, Molden, Moser, & Moser, 2005) and head direction cells in a number of cortical areas including the dorsal presubiculum, retrosplenial cortex (RS) and the lateral mammillary nuclei.

In light of these significant discoveries, spatial navigation research in humans has focused on the medial temporal lobe (MTL). Clinical observations of human patients and behavioural observations of animals with lesions to the hippocampus and neighbouring structures support a role for the region in learning and spatial memory (Corbetta, Patel, & Shulman, 2008; DiMattia & Kesner, 1988; Morris, Garrud, Rawlins, & O'Keefe, 1982). In addition, the advent of newer non-invasive functional imaging methodologies like positron emission topography (PET) and functional magnetic resonance imaging (fMRI) have helped highlight the importance of the MTL in spatial navigation (Gron, Wunderlich, Spitzer, Tomczak, & Riepe, 2000; Maguire, Frith, Burgess, Donnett, & O'Keefe, 1998)

However, the role of PPC in navigation is less well understood. Evidence concerning the importance of the PPC in spatial representations comes mainly from single cell recordings. PPC combines sensory information from different modalities, into multiple sensory-based representations of space (Andersen, 1998). The representations of space in this region are coded with respect to either the body or to the environment (Snyder, Grieve, Brotchie, & Andersen, 1998). Space coded in a body-centred reference frame would be essential for planning limb movements that need to

be made with respect to the body. In contrast, a world-centred reference frame would not be needed to plan limb movements but would be essential for navigation.

An indication of the role of PPC in spatial tasks has been determined from observations of patients with parietal lobe damage. Depending on the size and location of the damage, patients may display difficulties in performing coordinated hand and eye actions, have difficulties in representing their location in the environment or completely ignore one whole side of their body (Karnath, 1998).

Functional imaging studies investigating the role of the PPC in spatial navigation is limited. The construction of spatial navigation tasks has benefited from advances in computer processing and relatively realistic virtual environments can now be created relatively easily in order to investigate the cortical regions involved in navigation. The PC has been reported as being 'active' in many of these investigations, but teasing out the exact functional role has been somewhat problematic. This is mainly due to the measures involved, as hemodynamic time lag in fMRI & glucose metabolism in PET have temporal resolutions which are far from comparable to electrical measures of cortical activity (≈1ms). This means that observing the unique characteristics of PC neurons, such as the sustained responses during delay periods of memory tasks for example can be somewhat difficult.

In summary, two main cortical regions have been implicated as having a role in spatial navigation; the MTL and PPC. Most neuroscience research on navigation has concentrated on the MTL and in particular the hippocampus. In contrast, research into

the role of the PPC in navigation is limited. Therefore, the aim of this thesis is to investigate the role that PPC plays in navigation within the environment. It is hoped that this research will contribute to our understanding of PPC and in particular its role in spatial navigation. This has particular relevance in Alzheimer's disease (AD) where disturbances in spatial cognition and navigation can be significantly debilitating.

1.2 **Outline**

In an attempt to clarify the role of the PPC in spatial navigation, healthy human subjects were scanned using functional magnetic resonance imaging (fMRI) while they performed two separate navigation tasks. Following this introductory chapter, the cognitive processes of navigation are outlined in **Chapter 2**.

Chapter 3 describes the anatomy of PPC in both humans and non-primates, with particular focus on the intraparietal sulcus (IPS) of the PPC, a region known to be involved in spatial cognition.

The basic principles of magnetic resonance imaging are introduced in **Chapter 4** along with its application to the measuring brain activity.

Chapter 5 describes the results from one of two navigation tasks demonstrating two parietal regions that are active during different periods of the task.

Chapter 6 contains the results obtained from the second experiment that compares the brain regions that are active during two different navigation processes,

one dependent on visual landmarks and navigation without visual landmarks that uses cues such as optic flow.

In the concluding chapter, **Chapter 7,** the findings from this thesis are discussed in the context of other recent discoveries in spatial cognition to better understand the role PPC plays in the navigation process.

2 *Mechanisms of Navigation*

PPC is an integral component of spatial cognition and spatial navigation. A significant amount of our understanding of how the brain performs navigation has been derived from observing rodent maze behaviour. In the early half of last century, cognitive scientists focused on psychological drivers of navigation with much of the research being observational. Since then, single cell recordings and ablation studies have provided evidence of the underlying neurophysiological processes involved in navigation. In the 50 years since the first cognitive model of navigation was developed (Tolman, 1948), a number of other models and strategies have been proposed to explain high level navigation processes. Currently, two separate mechanisms of navigation are known to exist which both serve to determine self-location within the environment. One process relies on external cues, in particular, visual landmarks, to determine self-position. In the literature, this is sometimes referred to as allocentric or allothetic navigation although these terms are confusing and unhelpful. The second mechanism of navigation, best known as path integration, relies on an internal memory of the body's location and heading direction, updated by integrating internal signals such as vestibular, optic flow and efference copy. This has also been termed idiothetic navigation or dead reckoning. Both of these navigation strategies are required for successful navigation as visual landmarks are not always present, and both processes have been shown to occur in all animals in which navigation has been studied.

2.1 **Landmarks and Beacons**

A key component of navigation is landmarks. Landmarks provide a unique frame of reference that is required in order to identify one's location and orientation within the environment. Typically, the more unique an object is in the environment, the more likely it is to become a landmark (Stankiewicz & Kalia, 2007). For example, the tallest building in a city might become a landmark, particularly if its position amongst the other buildings offers unique positional information. Landmarks are typically fixed, but can change position in the environment (such as the Sun).

One feature of landmarks is that they persevere in their given environment, and it is this perseverance or stability which impacts on their overall salience. In both rodents and humans, landmark stability has been shown to significantly improve navigational performance (Biegler & Morris, 1993, 1996; Burgess, Spiers, & Paleologou, 2004). On a single cell level (see Section 2.6 for more detail), the presence of *distal* landmarks has been shown to be a modulating factor in the activity of hippocampal place cells (Cressant, Muller, & Poucet, 1997; Gothard, Skaggs, Moore, & McNaughton, 1996; Knierim, Kudrimoti, & McNaughton, 1995; Muller & Kubie, 1987); as well as in the activity of grid cells in the neighbouring MEC (Barry, Hayman, Burgess, & Jeffery, 2007; Hafting, et al., 2005; Moser, Kropff, & Moser, 2008). The influence of proximal landmarks on place and grid cell activity is less strong (Cressant, et al., 1997; Gothard, et al., 1996; Muller & Kubie, 1987). A classic example of landmark stability can be found in the use by various animal species of celestial bodies as navigational landmarks

such as the Sun (Baker, 1968, 1969; Santschi, 1911), Moon (Enright, 1972; Papi & Pardi, 1963) and stars (Kramer, 1951; Sauer & Sauer, 1960). Historically, human navigation (naval and land) has used celestial bodies for navigational cues.

In addition to being a unique identifier of location, landmarks can also signify the location of a target or goal, and therefore can be used as a beacon (Chan, Baumann, Bellgrove, & Mattingley, 2012). Landmarks are often classified in terms of either being proximal, distal, or beacons. While proximal landmarks and beacons share similarities, proximal landmarks serve as an associative location cue (e.g. 50 meters to the left of this landmark), whereas a beacon indicates the exact location. In rodent experiments, a beacon is likely to have been conditioned to signal the goal location. Furthermore the neural processing of beacons appears to be different to that of landmarks. For example, rodents with damage to the dorsal striatum are unable to use beacons as navigation cues (McDonald & White, 1994; Packard & McGaugh, 1992). In humans, functional evidence implicates the caudate nucleus (Miranda, Blanco, Begega, Rubio, & Arias, 2006) and striatum (Baumann & Mattingley, 2010) as regions that are active when beacons are used as navigational cues.

2.2 **Spatial Knowledge**

A key aspect of spatial navigation is the ability to understand key environmental features that may be used to identify one's position in the greater environment. McNamara et al. (2008) define this type of knowledge as object identity, where it

specifically refers to recognising entities in the environment that are important for navigation. These types of objects are known as landmarks (Siegel & White, 1975). McNamara et al. (2008) also argue that landmark knowledge is a specialised type of object knowledge.

An understanding of the shape of the environment is also required in order to successfully navigate (McNamara, et al., 2008). The behaviour of place cells (O'Keefe & Dostrovsky, 1971) and grid cells (Hafting, et al., 2005) is modulated by the shape of the environment (O'Keefe & Burgess, 1996). O'Keeffe & Burgess (1996) showed that the size and shape of place fields could be manipulated if the environment was extended out. Similarly, Rivard et al (2004) found that place fields located close to a barrier were more strongly affected when the barrier was rotated or relocated. Specifically, these place fields maintained their position relative to the barrier manipulations. Furthermore, there is strong evidence that people are sensitive to the geometry of the environment when they have to have to reorient and navigate (Hartley, Trinkler, & Burgess, 2004; Sandstrom, Kaufman, & Huettel, 1998).

2.3 **Reference Frames in Navigation**

Reference frames allow the specification of location and orientation in space (McNamara, et al., 2008). A reference frame is a set of points on an axis used to represent the location. For example, consider two individuals; one sitting in a moving convertible car, and one stationary. In this example there are two main frames of

reference, one fixed to the car and the other fixed to the earth. The person sitting in the car is moving in the earth's reference frame but stationary in the car's reference frame. If the passenger throws a ball into the air it will rise up and fall down in car's reference frame. However, to the stationary observer the ball will follow a parabolic path back down to the car. Multiple reference frames may exist in the brain, fixed to the eye (eye-centred reference frame), the head (head-centred reference frame), the body (body-centred reference frame) and the environment (world-centred reference frame). Using the example above, if a neuron encoded the location of the ball in an eye-centred coordinate reference, then the activity would remain constant as the image of the ball is stable on the retina, regardless of the eye's position in the head (Soechting & Flanders, 1992). The human memory system also uses a spatial reference system to represent the locations of remembered objects in the environment (McNamara, et al., 2008).

Reference frames can be separated in to two main spatial categories; egocentric or allocentric reference frames. Egocentric references systems represent the location of objects in space using a body-derived coordinate system consisting of eye-centred, head-centred, body-centred and limb-centred coordinate systems (Andersen, Snyder, Bradley, & Xing, 1997; Cohen & Andersen, 2002). Allocentric reference frames encode spatial relations with respect the environment (McNamara, et al., 2008).

In human navigation, allocentric reference frames are usually defined as ones' position relative to a landmark (Rodriguez, 2010). As mentioned earlier, a landmark

provides essential information to identify location and orientation within the environment. An additional subcomponent to the allocentric reference frame is the intrinsic reference frame (Marr, 1982; Rock, 1973). Landmarks consist of many different shapes and sizes and thus each comprise a unique intrinsic quality. These facets can include fronts, backs, tops or bottoms that can be used to define reference axes. Intrinsic qualities are not only limited to the individual object, but can be applied to features across a collection of objects (Mou & McNamara, 2002). A landmark with an intrinsic feature, allowing the orientation to be determined from any viewing angle, was used in the experiment described in Chapter 5.

Neurons in the PPC of primates encode targets in both egocentric (area LIP) and allocentric (area 7) reference frames (Snyder, et al., 1998), whilst neurons in the hippocampus and parahippocampus encode targets in an allocentric reference frame (Matsumura et al., 1999). Current theories of navigation maintain that successful large-scale navigation requires the use of both allocentric and egocentric coordinate systems. These representations have to be enduring, as many components of navigation are highly complex. For example, planning a route and maintaining a sense of orientation in an environment would require a stable and enduring representation of the environment in order to be completed successfully. This is because one's position within the environment constantly changes with each movement during navigation (McNamara, et al., 2008). Therefore, while allocentric and egocentric reference frames can identify one's position quite easily when stationary, a separate

method of spatial updating is required in order to maintain a stable percept of the environment. One well established process of maintaining a representation of spatial location during navigation is known as path integration, described in the next section (2.4).

2.4 **Path Integration**

Path Integration (PI), also known as dead reckoning in naval navigation, is the ability to calculate one's position based upon the speed, direction and prior position in which one was heading. It was first proposed by Charles Darwin (Darwin, 1873), and expanded by Murphy (1873) in the same year. A key feature of PI is that it allows the person or animal to return to the starting location without the use of spatial cues. However, a drawback to the use of PI, is that the process becomes unreliable after long or convoluted paths (Etienne, Maurer, & Seguinot, 1996) and is prone to accumulate drift errors (McNaughton, Chen, & Markus, 1991; Müller & Wehner, 1988).

Single cell recordings from rodents and lower order primates have identified at least three neural assemblies that are believed to contribute to PI functions. These are place cells in the hippocampus (O'Keefe & Dostrovsky, 1971); grid cells in the MEC (Hafting, et al., 2005) and head direction cells (Ranck, 1973; Taube, 1998). Place cells respond whenever the animal is in a particular region of space (O'Keefe & Burgess, 1996; O'Keefe & Dostrovsky, 1971). They are described in further detail in the next section (2.6).

Head direction cells provide the animal with an internal representation of orientation to the environment during navigation. They have been found in a number of different areas, many of which form parts of the Papez circuit; dorsal presubiculum, RS, lateral mammillary nuclei, lateral dorsal thalamus; entorhinal cortex, PPC, cingulate cortex and striatum (Ranck, 1973; Taube & Bassett, 2003; Taube, Muller, & Ranck, 1990). Unlike place cells, which show modulated activity in regards to location in space, head direction cells display orientation-specificity in regards to the position of the animal's head in the horizontal plane (Taube, et al., 1990). That is, the tuning curves of head direction cells are independent of location within the environment. When landmarks in a familiar environment are rotated, the tuning curves of head direction cells rotate with this change (Knierim, et al., 1995; Taube, et al., 1990). However, in an unfamiliar environment, head direction cells are unresponsive. Therefore, like place cells, head direction cells are modulated by visual landmarks in familiar environments (Touretzky & Redish, 1996). The firing rates of head direction and place cells display a strong coupling to each other, suggesting a unitary system of spatial orientation encoded by these two groups of cells (Knierim, et al., 1995).

When returning to a fixed base, mammals using PI to navigate will use internal cues typically derived from self-motion, such as linear and radial optic flow, vestibular signals (translational and rotational accelerations), efference copy and proprioceptive feedback from muscles and tendons (Etienne & Jeffery, 2004). These cues provide information as to speed, duration and rotation during navigation. PI is particularly

important in featureless environments, where no salient landmarks are present and can be used as the primary navigation strategy, but a limitation of this is strategy is that it accumulates errors (McNaughton, et al., 1991; Müller & Wehner, 1988).

In addition to limbic regions such as the hippocampus being directly involved in PI processes, some lesion work has also implicated the PPC. An investigation carried out by Save, Guazzelli & Pocuet (2001) found lesions to the rodent PPC resulted in more complex outward search paths when compared to hippocampal lesioned rodents. Similarly, Save, Paz-Villagran, Alexinsky, and Poucet (2005) demonstrated lesions to the rodent associative parietal cortex altered the firing of place cells, when objects from the environment were removed. In control rats, these place fields persisted, indicating these fields were anchored to olfactory and/or idiothetic cues. In associative parietal cortex lesioned rodents, these fields returned to their initial location, suggesting they relied on background cues to maintain their firing stability. The interaction of the PPC and hippocampus is likely to involve the RSC, a region that when lesioned in rodents has shown to disrupt PI (Cooper, Manka, & Mizumori, 2001). Lesions to this area in humans results in an inability to extract directional information in the presence of landmarks (Aguirre & D'Esposito, 1999).

Path integration is used to provide a stable percept of the environment when visual landmarks are absent. Although not theoretically necessary, the neural mechanism by which this occurs is the construction of a cognitive spatial map, as demonstrated by the observed activity of place cells in the hippocampus of rats

(McNaughton, et al., 1991). Presumably a cognitive spatial map is also present in other animals, including humans, yet the location of this map in humans is yet to be established.

2.5 **The Cognitive Spatial Map Theory**

The cognitive spatial map theory of navigation was first proposed by Tolman (1948), but in fact it was the German philosopher Immanuel Kant who first posed the idea that space was a fundamental organising principle of the mind (O'Keefe & Nadel, 1978). His belief was that the mind contained an a priori system that organised our sensations into a spatial framework that in turn was coupled to an absolute representation of space. The cognitive map proposed by Tolman was a representation of the environment that contained information on paths, routes and the relationships that objects in the environment have with other objects and with respect to the animal. This allowed the animal to make decisions on where to go next, and to learn the correct routes to the goal. A significant feature of this theory was the ability to take novel shortcuts between two locations. His work was primarily based on the anecdotal evidence from observations of rodent maze behaviour, which was later supported by empirical evidence from single cell recordings from the hippocampus of freely moving rodents (O'Keefe & Dostrovsky, 1971). This evidence led to the conclusion that the hippocampus was involved in the construction and maintenance of allocentric or world-centred maps of the environment (O'Keefe & Nadel, 1978).

The aspect of taking novel shortcuts when navigating was the distinguishing factor that separated Tolman's theory from the other main competing theory of his time (i.e. stimulus-response theory). This feature was later incorporated and extensively developed into the theory of O'Keefe & Nadel (1978), where the subsequent discovery and behaviour of individual hippocampal place cells formed its major foundation. According to their theory, the hippocampus contained a holistic representation of the environment including all salient environmental cues. The resulting spatial map was a 2-D abstract coordinate grid represented by a preconfigured network of intrinsic connections among hippocampal place cells (O'Keefe & Nadel, 1978).

Their theory, which was partly derived from human land navigation and from rodent hippocampal place cell behaviour, proposed an additional component to the cognitive map, which they termed a 'route'. A route, in this model was an inflexible line of movement to the goal. As landmarks are typically located at or very close to a goal, a person could navigate by simply remembering a series of landmarks (Bennett, 1996). Routes, however, contained very little environmental information, and could be easily disrupted if a landmark was removed. In contrast, the cognitive map contained a greater amount of environmental information and was highly flexible to new routes, resistant to destruction by the removal of a few landmarks and offered multiple lines of movement to the goal (Bennett, 1996). The authors argued that as the information contained in a cognitive map was greater and more detailed, travelling by this method

was far slower than using routes, as the computational requirements would be far greater (O'Keefe & Nadel, 1978). Therefore, it was deduced that animals that were able to take novel shortcuts had cognitive maps and were easily separated from those that only used a route method (O'Keefe & Nadel, 1978).

An alternate version of the cognitive map was proposed by Gallistel (1993). A major feature of this theory was that it specifically dealt with how representations of space were organised in the brain, something that was not discussed by O'Keefe & Nadel (1978). Gallistel defined a cognitive map as "a record in the central nervous system of macroscopic geometric relations among surfaces in the environment used to plan movements through the environment". According to his definition, any representation of space, including routes proposed by O'Keefe & Nadel (1978), were akin to having a cognitive map. This meant that Gallistel considered that all animals had cognitive maps, as their brains contained at least one representation of space. Gallistel (1993) proposed four versions of cognitive maps that could be used by the brain: Euclidean, affine, topological and projective. The generation of these maps came from the combining of two sources of positional information. The first of these was egocentric vectors, which would specify the locations of landmarks in a body-centred coordinate system and secondly, geocentric vectors which specify the position of the animal in an earth-centred coordinate system (see Figure 2).

Figure 2: Schematic View of the Egocentric Vector system.

The animal's geocentric position vector is computed by the dead-reckoning (PI) mechanism. The egocentric position vector for the landmark – its direction (or bearing, b) and distance from the animal is computed by the animal's perceptual system. Rotating the egocentric vector by the animal's geocentric orientation (its heading, h) gives a vector of the same length with orientation h+b (heading+bearing). Adding that vector to the animal's geocentric position vector a_g gives the landmark's position in the geocentric coordinate framework established by dead reckoning. Algebraically, $l_g=R(h)l_e+a_g$, where l_g is the landmark's geocentric position vector, le is its egocentric position vector, ag is the dead reckoning vector and R(h) is the rotation matrix. Adapted from Gallistel & Cramer, (1996).

2.6 **Neuronal Representations of Space**

A primary component of O'Keefe & Nadal's (1978) cognitive map theory was the single cell behaviour of hippocampal place cells. Typically observed by recording extracellular activity from the CA1 and CA3 regions of the freely moving rodents, hippocampal place cells show location-specific activity (Fox & Ranck Jr, 1975; O'Keefe & Dostrovsky, 1971). As the rodent engaged with the environment, performing stereotypical behaviours such as foraging and preening, place cell activity increased in preference to a particular location within the environment regardless of the behaviour (Markus et al., 1995). The behaviour of a small population of place cells was sufficient

to calculate an animal's trajectory in the environment without any prior information (Zhang, Ginzburg, McNaughton, & Sejnowski, 1998). In a preferred position known as a 'place field', the firing rates of place cells were quite dramatic and can exceeded 100Hz from a relatively calm baseline rate of $\leq$1Hz (Eichenbaum, et al., 1999).

Place fields are not continuous, but typically cover the entire available region with a significant overlap between fields. This clustering of activity implies that some environmental features are overrepresented at the expense of others (Eichenbaum, et al., 1999; O'Keefe & Nadel, 1978). To investigate this behaviour further, O'Keefe & Conway (1978), removed some of the cues in an environment and found that place cell activity persisted in those locations. This implies that any subset of cues sufficient to define the global configuration could support the location-specific activity of the place cell system (Eichenbaum, et al., 1999). Place fields also appeared to change when the environment changed. Muller & Kubie (1987) reported a scaling up in the overall size and shape of the place field when their circular environment was expanded outwards. Similarly, O'Keefe & Burges (1996) found that the size, shape and location of place fields were determined by the spatial relations of walls within the environment.

Evidence supporting the existence of place cells has been reported in non-human primates (Matsumura, et al., 1999), as well as in the human hippocampus (Ekstrom et al., 2003). Complementary spatial information in an orientation-specific format has also been found within the population coding of head direction cells, which are large contributors to PI (Taube, et al., 1990). A similar representational system has also been

found in the hippocampal and parahippocampal regions of humans (Ekstrom, et al., 2003) and non-human primates (Rolls & O'Mara, 1995; Rolls, Robertson, & Georges-Francois, 1997). Spatial view cells show modulated activity in response to the direction in which the animal is facing. Spatial view cells differ from place cells as they do not localise in space and they differ from head direction (HD) cells as they do not represent orientation, but only represent a direction *to* a specific object within the environment (Rolls & O'Mara, 1995; Rolls, et al., 1997).

More recently another spatial representational system has been discovered in the rodent MEC. These class of neurons termed grid cells, fire when the animal's position matches the vertices of a periodic tessellating triangular field that encompasses the entire available environment (Franzius, Vollgraf, & Wiskott, 2007; Hafting, et al., 2005; Sargolini et al., 2006, see Figure 3). This 2-dimensional representation of the environment is represented equally amongst grid cells where different grid cells fire at different locations in the environment (Sargolini, et al., 2006). Unlike place cells in the neighbouring hippocampus, grid cell activity is not modulated by salient environmental features such as landmarks (Moser, et al., 2008; Moser & Moser, 2008). Grid cell activity incorporates speed, direction and prior position of the animal through PI processes. The exact mechanism in which this occurs however, is not yet fully understood (Moser & Moser, 2008).

As mentioned above, a key difference between place cells and grid cells is the locus of activity. Individual place cells typically only fire in one location in the

environment, whereas individual grid cells fire in multiple locations (see Figure 3). Grid cells also begin to fire immediately in a new environment (Hafting, et al., 2005; Moser, et al., 2008), unlike place cells which can take a few minutes before stable place fields are established (Guzowski, Knierim, & Moser, 2004; M. Wilson & McNaughton, 1993). However, the most significant difference between regions is the representation created by grid cells which is created completely within the nervous system and is not mediated by external factors (Moser & Moser, 2008). Such a feature allows for the broad investigation of neuronal interactions of pattern formation in the brain (Moser & Moser, 2008). The abundance of electrophysiological evidence concerning the behaviour of MTL place and grid cells indicates the representation of space constructed by these neurons is allocentric in nature, that is, with respect to the environment.

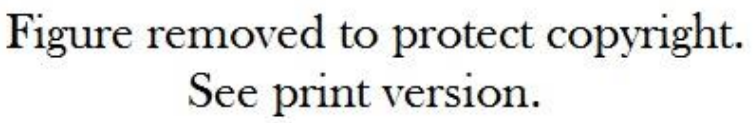

Figure 3: Place cell activity vs Grid cell activity.

Place cell in the hippocampus (a) and grid cell in the MEC (b). Spike locations (red) are superimposed on the animal's trajectory in the recording enclosure (black). Whereas most place cells have a single firing location, the firing fields of a grid cell form a periodic triangular matrix tiling the entire environment available to the animal. Adapted from Moser, Kropff and Moser (2008).

Egocentric representations of space, which are most commonly found in the parietal and frontal lobes, are also involved in spatial cognition, including navigation. Egocentric representations are often thought to be a short-term representation, as changes in body position are much more dynamic than the relative stability of fixed environmental landmarks. As mentioned in Section 2.3 (Reference Frames) egocentric representations represent the location of objects in space using a body-derived coordinate system consisting of an eye-centred, head-centred, body-centred or limb-centred coordinate system (Andersen, et al., 1997; Cohen & Andersen, 2002). At the most basic level these interactions typically reflect the reference frame of the receptor

involved (for example a retinotopic coordinate system by visually responsive neuron), that is then transformed into the appropriate coordinate system for action. There is evidence for these coordinate transformations within neurons of PPC (Andersen, 1998).

A number of regions within the PPC show egocentrically tuned responses that are modulated by the body's position and orientation in space. In particular, area 7a, the lateral intraparietal area (LIP) of the IPS and the parietal reach region (PRR) display gain modulated responses, where the overall gain of the signal is modulated by body signals (eye plus head) and world signals (trunk signals relative to the external environment; Cohen & Andersen, 2002; Snyder, et al., 1998). This type of coding allows for the coordinate transformation of locations between difference reference frames (Andersen & Zipser, 1988) and may subserve object tracking and self-movement (Bremmer, Klam, Duhamel, Ben Hamed, & Graf, 2002; Bremmer, Schlack, Duhamel, Graf, & Fink, 2001).

In addition, PPC neurons often show sustained responses during the delay period of delayed-response tasks (Chafee & Goldman-Rakic, 1998; Gnadt & Andersen, 1988). The true nature of this sustained response is still debated with evidence either supporting a role in motor intention (Andersen & Buneo, 2002; Andersen, et al., 1997; Snyder, Batista, & Andersen, 1997, 2000) or a role in visuo-spatial attention (Bisley & Goldberg, 2003; Colby & Goldberg, 1999). Further evidence obtained from single cell recordings from posterior parietal and dorsolateral frontal regions also suggests the

representations created by these areas during spatial working memory tasks is egocentric in nature (Compte, Brunel, Goldman-Rakic, & Wang, 2000).

In summary, electrophysiological evidence suggests a parallel yet, functional dichotomy between the parietal cortices and MTL areas regarding the representation of space. Namely, the MTL regions, the hippocampus and MEC, contain specialised neurons that show place or location-modulated activity. The close association of MTL areas in long term memory processes support the belief that this type of allocentric representation is best utilised by long-term, large-scale tasks such as navigation (Byrne, Becker, & Burgess, 2007). In contrast, the neural dynamics of parietal neurons are closely coupled with body position and are key contributors to egocentric representations. Current evidence suggests that egocentric representations are best served by small-scale, short-term tasks. The anatomy and function of the parietal cortex is described in detail in the next chapter (3).

2.7 **Summary**

The mechanisms reviewed in this chapter represent over 65 years of research and theory regarding an aspect of cognition that is extremely important for nearly all animals. Our knowledge of the neural mechanisms of spatial navigation, spatial cognition and spatial memory has increased enormously since Tolman (1948) first proposed the cognitive spatial map.

3 *The Neuroanatomy of the Parietal Cortex*

3.1 **Introduction**

Traditionally seen as a classical sensory association area, the parietal lobe is also implicated in spatial ability and motor planning (Snyder, et al., 2000). A prominent example of this occurs in visual sciences where the parietal lobe is referred to as the dorsal stream or "where" and "how" pathways (Goodale & Milner, 1992; Ungerleider & Mishkin, 1982). This stream accounts for the location and any subsequent motor actions towards objects in space and forms an important part of not only our perception, but also of our spatial awareness. The discovery of the multimodal nature of parietal neurons has changed the way we think of spatial representations in the brain. While the traditional view has been that of a single representation of space in the brain, single cell recording studies of primate parietal neurons have shown single brain regions can encode space in multiple frames of reference. Many parietal neurons are multimodal in nature, responding to visual, somatosensory and auditory cues (Andersen, 1989; Colby, Duhamel, & Goldberg, 1993, 1996; Heiser & Colby, 2006), with attention modulating these responses (Andersen & Buneo, 2002; Colby, et al., 1996). These findings have changed the way we view the role of the parietal lobe from merely being a sensory association area to a region that is involved in higher order spatial processing.

Architectonic studies of Brodmann (1909; see figure 4), Vogt & Vogt (1919), von Economo (1929) and later from von Bonin and Bailey (1947) and Pandaya and Seltzer

(1982) showed that the parietal lobes are made of many regions of different architectonic types that project to different areas within the cortex. Single cell recordings of primates in the 70s and 80s helped to distinguish these different regions functionally and provided insight into the functional specificity of a number of parietal areas.

A significant amount of our understanding concerning the human parietal lobe has come primarily from studying the brain after an injury. More recent advances in structural and functional imaging have contributed to this body of knowledge, with new human parietal regions being classified using functional methods.

So while the discovery and the subsequent separation into functionally distinct areas in the primate parietal lobe offers some insight into the possible functional organisation of the human parietal lobe, a comparative anatomical framework across the two species currently remains unclear. The following sections of this chapter describe the anatomy and function of the parietal lobe both in humans and non-human primates and will focus on the connectivity of parietal regions to other cortical areas.

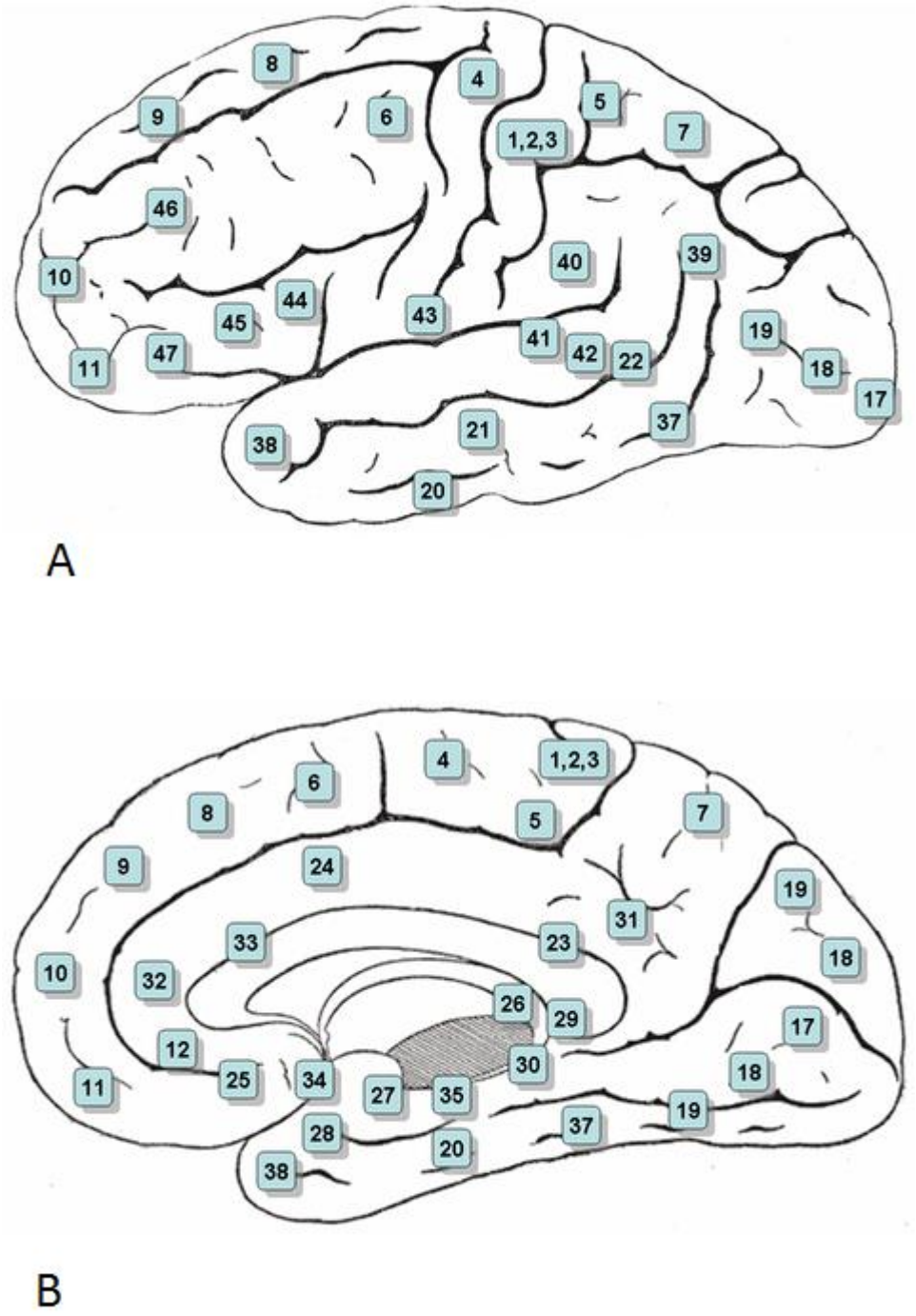

Figure 4: Lateral (A) and medial (B) view of the human cortex with Brodmann architectonic subdivisions.

3.2 **Anterior Section of the Parietal Cortex**

At present, there are a number of naming conventions that define the various cytoarchitectonically regions in the brain. Of these, the most popular and widely used convention is that of Brodmann (1909). Subsequent investigations, (see Vogt & Vogt, 1919; von Economo, 1929; von Bonin and Bailey, 1947 and Pandaya & Seltzer, 1982) were further able to divide regions of primate parietal cortex into smaller functional parts, resulting in a combination of naming conventions being commonly used (see Figure 4). Relative homogeny exists in the anterior parietal lobe between non-human primates and humans, where primary somatosensory cortex (Brodmann areas 3,1, 2) is located caudally to the central sulcus on the postcentral gyrus and is responsible for the conscious perception of touch, vibration, temperature, pressure, pain and taste via relay from the thalamus. The cortex at this site is organised into somatotopic columns that reflect the degree of nerve innervation. This differs between anatomical areas, with some areas such as the lips and fingertips receiving a greater cortical representation compared to areas such as the trunk and legs. Each somatotopic column receives inputs from thalamic, commissural and association fibres that terminate at cellular levels IV, III and II. Resulting output signals originate from layers V and VI (Waxman, 2003).

The surface of the body is represented on the surface of the somatosensory cortex in a map-like function and is usually described as a sensory homunculus. This representation shows the location and amount of cortical area dedicated to a

particular function (Amaral, 2000; Penfield & Rasmussen, 1950) and similarly has also been demonstrated in non-human primates, where at least four separate body representations have been found (Kaas, Nelson, Sur, Lin, & Merzenich, 1979; Paul, Merzenich, & Goodman, 1972; Powell & Mountcastle, 1959). In humans the main systems that relay sensory information to the cerebral cortex are the dorsal column (lemniscal system) and the ventrolateral system. The former carries touch, joint sensation, two-point discrimination and vibratory sense while the latter is responsible for nociceptive and temperature related changes (Waxman, 2003).

Figure 5: The different architectonic subdivisions of the posterior parietal cortex in Cercopithecus & Macca Mulatta.

Adapted from Cavada & Goldman-Rakic (1989a). Original work of Brodmann (1909) & Vogt and Vogt (1919, Cercopithecus); Von Bonin and Bailey (1947) & Pandya and Seltzer (1982a, Macaca Mulatta).

3.3 **The Posterior Parietal Cortex**

The posterior parietal cortex (PPC) sits immediately behind the postcentral gyrus and is divided into superior and inferior sections by the intraparietal sulcus (IPS). It comprises of Brodmann areas 5,7,39 and 40 and receives inputs and projects to both sensory and motor areas (Averbeck, Battaglia-Mayer, Guglielmo, & Caminiti, 2009; Cavada & Goldman-Rakic, 1989a, 1989b; Pandya & Seltzer, 1982). Traditionally it is viewed as a higher cortical sensory integration area, but in recent years single cell recordings from this area indicate that this region plays a role in spatial coordinate transformations. PPC neurons are typically bimodal in nature, responding to two different types of sensory stimulation and have been found to encode locations of objects in space and encode intention to perform an appropriate motor action (Andersen & Buneo, 2002; Burgess, Jeffery, & O'Keefe, 1999; Colby & Goldberg, 1999). Furthermore, some PPC cells have also demonstrated retinal receptive fields, modulated by gaze, thus appearing to hold information pertaining to the retinal position, eye position and head position , contributing to a body centred representations of space (Andersen, Brotchie, & Mazzoni, 1992; Brotchie, Andersen, Snyder, & Goodman, 1995; Snyder, et al., 1998).

The PPC has also been implicated in other cognitive functions, including attention (Corbetta, et al., 2008; Corbetta & Shulman, 2002). This is not surprising given the development of attentional neglect in patients with parietal lobe lesions (see section 3.8). Furthermore, the region is also implicated in memory retrieval (Rugg, Fletcher,

Frith, Frackowiak, & Dolan, 1997) and the guidance and planning of movement (Snyder, et al., 1997).

3.4 **Neuroanatomy of the Superior Parietal Lobule**

The anterior section of the superior parietal lobe (SPL) is confined anatomically by the upper section of the post central sulcus, whilst being bound caudally by the lateral section of the parietooccipital fissure. It is separated from the inferior parietal lobe by the intraparietal sulcus that passes through the base of the SPL. Architectonically, it is subdivided into areas PE and its regional variant PEc which is located caudally at the apex of the lobe. The medial intraparietal area (MIP) and area PEa which are located in the medial and dorsal banks of the IPS also comprise the SPL. Areas PE and PEc extend onto the medial wall of the hemisphere where PEci is situated on the caudal tip of the cingulate sulcus and area PGm (Caminiti et al., 2010; Pandya & Seltzer, 1982). The SPL forms one half of what is commonly described as the posterior parietal cortex (PPC).

3.5 **Neuroanatomy of the Inferior Parietal Lobule**

The inferior parietal lobe (IPL) sits below the IPS and is bound by both the post central gyrus and transverse occipital sulcus. Like the SPL, it also is subdivided into architectonic sections based upon cytological appearance. PF, PFG and PG occupy the main area on the gyral surface, whilst caudally sitting adjacent to SPL area PEc is the fourth area, OPT. SPL areas PF, PFG and PG also show a trend to having better laminar

definition rostrally to caudally (Pandya & Seltzer, 1982). The IPL also extends onto the anterior intraparietal and lateral intraparietal areas of the IPS. The IPL forms the seconds half of the PPC.

3.6 **The Intraparietal Sulcus**

The intraparietal sulcus of primates has received a great deal of interest mainly due to its proximal, yet architectonically and functionally different areas that are encompassed within its borders. These regions have been shown to integrate information derived from multiple senses, with each afferent being attached to a different (motor) action or region of space (Andersen & Buneo, 2002; Brotchie, et al., 1995; Colby & Duhamel, 1991; Snyder, et al., 1998). The true nature of this integration in terms of whether it is used for planning actions (Snyder, et al., 1998) or sensory integration (Goodale & Milner, 1992; Ungerleider & Mishkin, 1982) however, is currently unknown. The IPS is segmented into lateral, ventral, anterior and medial intraparietal areas (lateral intraparietal area, LIP; ventral intraparietal area, VIP; anterior intraparietal area, AIP; medial intraparietal area; MIP).

3.6.1 The Lateral Intraparietal area

The LIP is located on the lateral bank of the IPS, posterior to MIP and lateral to the VIP, and contributes to the representation of space that is covered by the eyes (Andersen, 1989; Andersen, et al., 1992; Colby, et al., 1996; Mountcastle, Lynch,

Georgopoulos, Sakata, & Acuna, 1975). In most cases the region is often treated as a whole, but can be separated further into two distinct areas; LIPd and LIPv based on differing patterns on myelination, connectivity and immunohistochemistry (Lewis & Van Essen, 2000a, 2000b; Medalla & Barbas, 2006). LIPd is located deep within the lateral bank of the IPS and is far more densely myelinated than LIPv (Lewis & Van Essen, 2000b; Medalla & Barbas, 2006). The LIP is heavily connected with frontal and peristriate visual areas, and in particular with visual areas V4, V3, V3a, V2, V6A, the frontal eye fields (FEF) and dorsolateral prefrontal cortex (DLPFC, Averbeck, et al., 2009; Lewis & Van Essen, 2000a; Medalla & Barbas, 2006; Neal, Pearson, & Powell, 1990). With respect to the two distinct LIP regions, LIPv is more strongly connected to V3, the posterior intraparietal area (PIP), parietal-occipital area (PO), whilst LIPd is more strongly connected with V4, V4 transitional area (V4t), area TEa plus TEm (TEa/m), temporal parietal occipital area (TPOr) (Lewis & Van Essen, 2000b; Medalla & Barbas, 2006).

The visual receptive fields of LIP neurons are stored in retinal coordinates, with position of the eye modulating the gain of the signal (Andersen, Essick, & Siegel, 1985). Commonly, LIP neurons are active when light is presented in the visual field and the monkey is required to look at it, but they can also remain active before or after this event (Colby, et al., 1996). Similarly, stimulation of this areas results in the generation of spontaneous saccadic eye movements (Andersen, Essick, & Siegel, 1987). The behavioural characteristics of this response can therefore represent a visual signal, a

motor signal, an attention signal or an intentional signal (Colby & Goldberg, 1999). Originally, LIP responses were originally thought to reflect motor planning (Gnadt & Andersen, 1988), however they are now believed to reflect either visual attention (Bisley & Goldberg, 2003, 2010; Colby & Goldberg, 1999) or motor intention (Andersen & Buneo, 2002; Cohen & Andersen, 2002; Snyder, et al., 1997).

3.6.1.1 Visual Attention Responses of the LIP

The activity of LIP neurons is behaviourally modulated with approximately two-thirds displaying higher firing rates when a monkey is going to make a motor movement to a behaviourally important stimulus (Goldberg, Colby, & Duhamel, 1990). Importantly this activity is independent of intended actions even when the stimulus becomes unimportant (Colby, et al., 1996) and does not predict any upcoming behaviour (Bisley & Goldberg, 2003). A number of investigations have looked at the attentional enhancement of LIP responses (see Colby & Goldberg, 1999 for review) with a more recent investigation that included components designed to measure both temporal and spatial aspects of visual attention (Bisley & Goldberg, 2003). The authors used a contrast sensitivity method to measure the animal's attention, which meant the locus of attention was also within the visual receptive field and a two-stage behavioural response phase. The first phase included planning a saccade to a remembered location and the second phase was deciding whether to make an additional movement on the basis of GO/NO GO signal (1/3 of GO signals were not placed in the RF). For half of the trials, a distracter visual stimulus was also flashed on

the screen. Importantly their results showed that there was an attentional advantage for both upcoming saccades and for distracters events with the perceptual advantage at the attended location being the equal. Furthermore, it was impossible to identify the locus of attention from a single LIP neuron, but rather from an LIP population, that provides attentional priority for visual targets within the subtended visual field.

3.6.1.2 Intention Responses of the LIP

An alternate view on the activity of LIP neurons is that the activity in part represents *intention* or the plan to make a movement. Intention is a cognitive representation that specifies both the goal and movement, but does not include the necessary proprioceptive information needed to complete the task itself (Andersen & Buneo, 2002). Since initial sensory information is encoded in eye-centred coordinates, the sustained responses of LIP neurons may be responsible for the coordinate transformations from sensory to motor coordinates. This evidence is supported by patients with PPC lesions who don't have specific sensory or motor but display difficulties when performing motor tasks to sensory stimuli. The exact nature of PPC lesions and the effect it has on cognitive functioning will be detailed further on in this chapter.

One common method, of distinguishing sensory from motor components is the memory task first described by Hikosaka & Wurtz (1983). In this task, the animal is required to make a movement to a cued location only when given a go signal. While PPC responses reflect sensory and motor behaviour they also show persistent activity

during the memory period of this task (Gnadt & Andersen, 1988; Snyder, et al., 1997). Therefore, in order to separate out sensory and motor signals from PPC neurons, an additional target stimulus is added and the subsequent motor response is also cued. This means the animal now has to memorise two target stimuli and make movements to both locations. For eye and arm movements, the activity in the delay period is only present for the next planned movement, even though the animal is required to memorise the two cued locations (Batista & Andersen, 2001). This implies that sensory memory of the target location is either stored in a small portion of PPC neurons or stored elsewhere in the brain (Andersen & Buneo, 2002; Tian, Schlag, & Schlag-Rey, 2000).

3.6.2 The Medial Intraparietal area

Located on the medial wall of the intraparietal sulcus, the medial intraparietal area (MIP) forms part of the parietal reach region (PRR) and is specialised for reaching movements. It is also traditionally considered to be part of Brodmann's Area 5 (BA 5) and therefore is part of the SPL. MIP neurons mainly project to the frontal cluster PM-D (see Figure 1-2), which consists of the premotor and primary motor cortices (Averbeck, et al., 2009; Caminiti, et al., 2010). Importantly, MIP neurons display unique firing characteristics with neurons displaying purely visual behaviour, purely somatosensory behaviour or both (Colby & Duhamel, 1991). Visual and auditory targets are stored in eye-centred reference frames by MIP neurons (Brotchie, et al., 1995; Cohen & Andersen, 2000; Snyder, et al., 1998), with this activity being

modulated in part auditory signals, eye position, visual signals, head position, limb position and efferent copies of motor commands (Cohen & Andersen, 2002). Visually active cells also increase activity based on the proximity of the stimulus, suggesting preparatory behaviour for reaching movements. These receptive fields are also dynamic, allowing for the expansion of reach related space. This behaviour suggests the temporary incorporation of the grasped object into the brain's representation of the body (Colby & Goldberg, 1999). The MIP area is considered along with V6a & area 5 to form the PRR (parietal reach region). This network receives inputs from several extrastriate visual and somatosensory areas and projects to the dorsal premotor cortex (Snyder, et al., 2000). Similarly, activity within the LIP which is greatest when planning saccades, while activity within the PRR is greatest when planning reaching movements and is believed to reflect motor intention (Andersen, et al., 1997; Snyder, et al., 1997, 2000)

Figure 6: Distribution of neural response properties in the IPS.

The anterior part of the sulcus is shown at the top of the figure. The posterior part of the sulcus is shown at the bottom, where the banks of the sulcus have been separated. Each column depicts responses recorded along a single 10 mm penetration through the

lateral or medial bank. Penetrations are spaced 1 mm apart. Adapted from Colby & Duhamel (1991).

3.6.3 The Anterior Intraparietal Area

Area AIP is located at the lateral most anterior bank of the IPS and includes the fundus and is involved in the processing of visually guided hand and grasp movements (Colby & Goldberg, 1999; Frey, Vinton, Norlund, & Grafton, 2005; Sakata, Taira, Kusunoki, Murata, & Tanaka, 1997; Taira, Mine, Georgopoulos, Murata, & Sakata, 1990). This region has strong connections to parietal areas PG, PF & PFG (both are derived from 7b), the lateral subdivision of the LIP and SII; frontal areas F5, premotor area 46 & 12 and inferotemporal areas TEO, TEpd, TEm and TEa (Borra et al., 2008). Neurons in AIP display preferences towards the size and shape of the objects within reach and broadly classified into three major classes; motor dominant, which are active when grasping in light and dark conditions; visual and motor, discharging fervently when only grasping in light conditions and visually dominant which are only active in light conditions (Sakata, Taira, Murata, & Mine, 1995; Taira, et al., 1990). Furthermore, the visually responsive neurons are further classed into two categories: Object-type and non-object type. Object-type neurons fire during object fixation, which imply these neurons are coding of the object's intrinsic 3-D properties. Non-object type neurons are not active during object fixation periods but display selective visual activity during grasping, which implies the coding of hand shape or hand-object interactions (Borra, et al., 2008). The connections that emanate and depart from AIP, along with

single cell recording from non-human primates indicate that this region of cortex has a very specific role that is dedicated to visual arm guidance and grasping.

While connections to frontal areas are required to control and execute arm movements, and connections to parietal areas would be responsible for integrating eye position, connections to inferotemporal areas offer a new possibility in terms of functional significance. Firstly, these temporal regions form part of the ventral stream relating to object identification, which is more colloquially referred to as the 'what' pathway (Ungerleider & Mishkin, 1982). This pathway was originally believed to be separate from the dorsal or 'where' pathway and connections from AIP to ventral areas challenge the dichotomy that is purported to exist between the two regions. Specifically it has been hypothesised that primate IPL convexity is part of a separate pathway that incorporates visual information from the dorsal stream with multisensory information from the superior temporal sulcus (STS) to create and control perceptually based motor commands (Rizzolatti & Matelli, 2003; Rozzi et al., 2006). Using this model, grasping actions would not only require information pertaining to 'how' an object is made but also to 'what' the is object is (Borra, et al., 2008). Importantly there is functional evidence of an equivalent region in humans which is active during grasping and reaching actions (Binkofski et al., 1999).

3.6.4 The Ventral Intraparietal Area

The ventral intraparietal area (VIP) is located deep within the IPS and adjacent to LIP and MIP within the fundus of the IPS. Historically, it was first classified as a

projection zone of MT within the IPS (Maunsell & van Essen, 1983; Ungerleider & Desimone, 1986), but was given a new name once it was discovered one of its functions involved the processing of direction and speed of moving visual stimuli (Colby, et al., 1993; Maunsell & van Essen, 1983). VIP has reciprocal connections with V1 and V2, but also projects to area 7a, F4 of the motor cortex and the frontal eye fields (FEF, Maunsell & van Essen, 1983). In addition, the VIP is connected to several subcortical regions; the basal ganglia, thalamus, mesencephalon, and pons (Maunsell & van Essen, 1983). Neurons within the VIP are multimodal in nature, responding to visual, tactile, vestibular and auditory stimuli (see Figure 6, Colby & Goldberg, 1999). Visual information is stored with reference to head, so when eye position changes the receptive fields of VIP neurons also change to maintain the representation of spatial location (Colby, et al., 1993). Interestingly, tactile receptive fields are also restricted to the face and head and therefore also provide a head-centred representation of space. Importantly, they also share the same size and shape of visual receptive fields, which are referenced to the eyes, head or lie in an intermediate frame (Duhamel, Bremmer, BenHamed, & Graf, 1997). Thus, a neuron that responds to visual stimulus presented in the upper left quadrant will also respond to a tactile stimulus presented to upper portion of the face (Colby & Goldberg, 1999). In addition, visual and tactile receptive fields also match each other with respect to direction preference. That is, the neurons are preferentially responsive to visual motion and head rotation in the same direction

(Bremmer, et al., 2002). Additionally, VIP neurons have also been shown to code for head velocity, acceleration and position (Klam & Graf, 2003).

One suggested function of VIP posits its role might involve facilitating planning actions that involve the mouth area (Colby & Goldberg, 1999) or near extrapersonal space (Bremmer, et al., 2002). For example, if a monkey were to move in a forest to search for food, it would involve visual (approaching branches), tactile (touching the branches) and vestibular information (perception of head movement) (Grefkes & Fink, 2005). Interestingly, when the region is electrically stimulated the animal displays avoidance behaviour, such as eye closure, contraction of facial muscles, shoulder shrugs and arm movements which do not occur when the cortex surrounding VIP is stimulated (Cooke, Taylor, Moore, & Graziano, 2003). Thus, VIP may also be involved in defensive behaviours when a stimulus is close or near the head (Cooke, et al., 2003). Alternatively, another possible function of VIP could be contributing head-related signals to the other parietal and frontal areas for generation of a head-centred reference frame for motor intention.

3.6.5 Brodmann's Area 7

Brodmann's area 7 forms part of the IPL and is usually further subdivided into functional areas 7a (also referred to as PG by Pandya & Seltzer, 1982) and 7b (also referred to as PF, Neal, Pearson, & Powell, 1987) as described first by Vogt & Vogt (1919) and then by Von Bonin & Bailey (1947) . Area 7a has widespread connections to other cortical areas, particularly visual areas V2, V3 and V4; PO; both anterior and

posterior cingulate; superior temporal sulcus (Neal, Pearson, & Powell, 1988; Neal, et al., 1990). Area 7b is reciprocally connected to somatosensory area SI & SII, area 5, posterior cingulate and the STS (Neal, et al., 1987). In addition, there are also connections to frontal motor areas; PMv, area 6 (supplementary motor area, SMA and premotor cortex), area 45 and pontine nuclei (Andersen, Asanuma, Essick, & Siegel, 1990; Averbeck, et al., 2009; May & Andersen, 1986).

The stimulation of 7a typically evokes non-saccadic eye movements (Sakata, Takaoka, Kawarasaki, & Shibutani, 1973), whereas the stimulation of LIP typically evokes saccadic eye movements (Shibutani, Sakata, & Hyvarinen, 1984). This is not unexpected as both regions are adjacent to each other and both project to visual areas. Areas 7a also displays saccade related activity like LIP neurons, but many of the responses in this region are postsaccadic, whereas LIP responses are presaccadic (Andersen, Bracewell, Barash, Gnadt, & Fogassi, 1990; Andersen, et al., 1987). Furthermore the visual receptive fields in 7a are larger and bilateral (Motter & Mountcastle, 1981) when compared to the receptive fields in LIP which are smaller and contralateral. In addition, 7a neurons also display gain field modulation, where the amplitude of the visual response is modulated by the position of the eye (Andersen & Mountcastle, 1983). This allows for the coding of external targets in difference reference frames and provides a mechanism for coordinate transformations (Cohen & Andersen, 2002). The gain field mechanism is described in detail further in this chapter.

Another unique feature of area 7a neurons is the coding of locations using a world-centred coordinate frame. Area 7a neurons have vestibular gain fields and respond when the head is positioned with respect to the external world (Snyder, et al., 1998). It is important to note that while body-centred representations, like the ones created by LIP neurons would be required when planning and executing body movements (like gaze control and limb reaching) which would need to made with respect to the body, a world –centred representation of space would only be useful if it were used for navigation or tasks that required an absolute reference frame (Snyder, et al., 1998). Area 7a projects heavily to the parahippcampal gyrus and the presubiculum, two regions that have been heavily implicated in topographical memory and allocentric navigation in primates and rodents (Aguirre, Detre, Alsop, & D'Esposito, 1996; Epstein & Kanwisher, 1998; McNaughton, Barnes, & O'Keefe, 1983). The world-referenced gain fields of 7a neurons could support the activity seen within these two areas by providing information on gaze direction in a compatible allocentric format.

Area 7b (also referred to as PG by Pandya & Seltzer, 1982) lies rostral to 7a and in contrast to 7a, area 7b is primarily concerned with somatosensory processing. This is reflected in the greater number of connections with somatosensory areas, although this region also projects to PO (most commonly known as V6), MST (medial superior temporal area), STP (superior temporal polysensory) and TE (inferotemporal cortical visual association area) all of which form part of the visual extrastriate network (Andersen, Asanuma, et al., 1990). In addition, 7b is the source of the only connections

between the SPL and IPL though is direct connection with area 5, a known somatosensory association area. In addition, lesions to this area result in hemineglect in the contralateral peripersonal space. This is evidenced by a transient deficit in mouth grasping movements towards contralaterally presented stimuli and finally postural abnormalities and a reluctance to use the contralateral hand. This has led some researchers to believe that 7b's function lies in the perception of peripersonal space and in the organisation of movements of towards stimuli that is presented in that space (Matelli, Gallese, & Rizzolatti, 1984).

3.6.6 Brodmann's Area 5

Brodmann's area 5 forms part of the SPL and is located posterior to the primary somatosensory cortex (Sakata, et al., 1973; Taira, et al., 1990) and thus encompasses MIP. In non-human primates, area 5 has dense cortico-cortical connections to all subdivisions of SI and even receives interhemispheric connections from contralateral area 5 and SI (Pandya & Kuypers, 1969). Furthermore area 5 is also connected to the primary motor cortex via area 6 (Jones, Coulter, & Hendry, 1978) Neurons in area 5 are mainly concerned with processing somesthetic stimuli from the truck and limbs. These inputs include passive movements of the joints, light palpation over muscle bellies, palpation of deep tissues and muscle stretch. These proprioceptive responses demonstrate that at some level sensory processing also occurs in area 5. However the most significant finding in the last 20 years has been its involvement in the planning of reaching and guiding arm movements. Neurons in area 5 display directional firing

patterns for arm movements in a preferred direction with concurrent similar activity in the primary motor cortex (Kalaska, Caminiti, & Georgopoulos, 1983). In this regard, area 5 is sometimes considered to be part of PRR, a region in the reach networks that provides a gateway between sensory and motor areas (Caminiti, Ferraina, & Johnson, 1996).

3.7 **The Human Parietal Cortex**

Brodmann's parcellation of the human brain is currently the most accepted cytoarchitectural organisation of the human cortex. With regards to the parietal lobe, it shares a similar, albeit less defined organisation, with the non-human primate parietal lobe. This is particularly evident in the PPC, where there are considerably more areas identified in primates compared to humans (Averbeck, et al., 2009; Pandya & Kuypers, 1969; Pandya & Seltzer, 1982; Seltzer & Pandya, 1980; Von Bonin & Bailey, 1947). The anterior section of the human parietal lobule contains the somatosensory cortex and is described in the aforementioned paragraphs. This section will focus primarily on the IPS by comparing and contrasting the differences between humans and non-primates. The human IPS is considerably larger and more expanded than the monkey IPS, consisting of a complex folding and branching pattern (Grefkes & Fink, 2005). This feature can make it difficult to localise the human IPS, especially when the sulcus is split into several anatomical segments (Grefkes, Geyer, Schormann, Roland, & Zilles, 2001). Unlike the primate brain, very little is known about cortical connections

in the human brain. Connectivity so far has been assumed to resemble that of the primate brain and initial evidence from non-invasive imaging is complementary (Rushworth, Behrens, & Johansen-Berg, 2006).

3.7.1 Human Ventral Intraparietal area

A main feature of the macaque VIP is the polymodal processing of motion in primarily a head centred reference frame. Bremmer & colleagues (2001) attempted to identify a putative human equivalent using a polymodal protocol and fMRI. In their study, participants experienced either a visual (moving starfield pattern), tactile (airflow across the forehead) or auditory (binaural beats) motion stimulus or stationary controls. The authors reported a bilateral intraparietal activation when testing for common activations in all conditions that conveyed motion information, relative to the perception of a stationary modality matched stimulus. Furthermore, single subject data confirmed the location of activation to be indeed within the fundus of the IPS. As this is the only area within the macaque IPS that responds to multimodal motion stimulation (Bremmer, Schlack, Duhamel, et al., 2001; Bremmer, Schlack, Shah, et al., 2001; Colby, et al., 1993; Colby & Goldberg, 1999), the authors concluded that the human VIP is in a similar topographical location as the macaque VIP (Bremmer, Schlack, Shah, et al., 2001).

3.7.2 Human Anterior Intraparietal Area

As mentioned in Section 3.6.3, the AIP in non-human primates is involved in visually guided hand and grasp movements. In humans, damage to the anterior region of the IPS results in disturbances in visually guided hand actions (see section 3.8). Furthermore functional research in healthy human participants has demonstrated an area within the anterior IPS that is involved in tactile shape processing (Bodegard, Geyer, Grefkes, Zilles, & Roland, 2001; Grefkes, Weiss, Zilles, & Fink, 2002), grasp planning (Jacobs, Danielmeier, & Frey, 2010), cross modal information transfer (Grefkes, et al., 2002) and error detection when executing visually guided reaching (Tunik, Frey, & Grafton, 2005). Based on this evidence, it would appear that the human AIP performs in a role that is equivalent to the macaque AIP.

3.7.3 Human Medial Intraparietal Area

The macaque MIP has been implicated in reaching actions, and as such forms part of the parietal reach region, which also included areas V6a and intraparietal area PE. In humans, only a few investigations have specifically investigated the cortical regions that are involved in the reaching and visuospatial motor transformation, but nonetheless these investigations have demonstrated the crucial role the human IPS plays in these abilities (Chaminade & Decety, 2002; Grefkes, Ritzl, Zilles, & Fink, 2004; Simon, Mangin, Cohen, Le Bihan, & Dehaene, 2002).

3.7.4 Human Lateral Intraparietal Area

As discussed in section 3.6.1, the macaque LIP is located within the lateral wall of the IPS and is involved in the processing of saccadic eye movement, as well as demonstrating attention and intention related activity. In humans, a number of functional investigations have previously demonstrated the role of the IPS in attention and in the control of eye movements (Berman et al., 1999; Corbetta & Shulman, 2002; Petit & Haxby, 1999; Pierrot-Deseilligny, Milea, & Muri, 2004), but importantly the majority of these activations occur within the medial wall of the IPS (Shulman et al., 2003). Likewise, studies employing variations of the double-step saccade task have reported activations largely in the superior parietal cortex and medial sections of the IPS, with activity also extending into the adjacent inferior parietal cortex (Heide et al., 2001). More recently, an fMRI investigation compared the activations of humans and monkey performing the identical saccade task (Koyama et al., 2004). In this task, both sets of subjects were required to make saccades either to the left or to the right, while maintaining a fixed head position. In the monkey group, the dorsal area of the LIP was most strongly activated, whereas the corresponding activations in humans were located within the posterior section of the MIP. Taking this finding in light with the previous research into this area, it can be concluded that the putative human equivalent of the LIP is located within the medial wall of the IPS.

3.7.5 Connectivity of the Parietal Lobule

The parietal lobe is heavily interconnected, with many of these connections being reciprocal (Jones, et al., 1978; Pandya & Seltzer, 1982). In the somatosensory cortex, there are differences in the connectivity between regions 3, 1 and 2 respectively. Projections that emanate from area 3 primarily project to area 1 with smaller projections to areas 2, 3a and somatosensory area II (S II) (Jones, et al., 1978). Area 1 primarily projects to areas 2, S II, 4 and the supplementary motor cortex (M II) and to a lesser extent areas 3, 3a and 5. Area 2 projects to areas 1, 3a, S II, M II, 4, 6, 7 and extensively to area 5. This pattern of connectivity reveals a sequential outflow of sensory information originating in somatosensory area 3 to the sensory association areas in the parietal lobule (Jones, et al., 1978). Afferent and efferent connections of the PPC are primarily comprised of reciprocal connections to primary and premotor cortices, temporal and occipital visual areas and the cingulate and prefrontal cortex (Averbeck, et al., 2009; Caminiti, et al., 2010). Parietal connections to the hippocampus and amygdala are few and thus there are no inputs from these areas (Caminiti, et al., 2010).

3.7.5.1 Fronto-parietal connections

Parietal connections to frontal areas are reciprocal in nature and are distributed topographically, in a dorsal to ventral fashion. The majority of these connections originate from the subdivisions within area 7, with each specific subdivision connecting to a different area within the frontal lobe (Cavada & Goldman-Rakic, 1989b). Area 7m

is connected with the dorsal premotor cortex (PM-D) whilst 7b is connected with the ventral premotor cortex. Both 7b and 7m are interconnected with the supplementary motor area (SMA). However, the posterior region of the SMA is only connected to 7m. Area 7a, 7m and 7ip are reciprocally connected with the rostral frontal eye fields (FEF) and area 7ip is also reciprocally connected with the caudal FEF. Averbeck and colleagues (2009) proposed a connectivity map of parietal connections based on statistical analysis that clusters architectonically defined areas based on their inputs. They identified four spatially adjacent parietal clusters that form bifurcations in a hierarchical tree (Figure 2.1). From their analysis we can see these clusters project to separate sections of the frontal lobes with very little overlap.

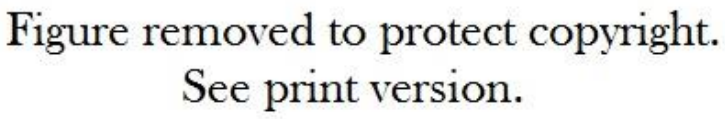

Figure 7: Hierarchical statistical analysis of the parietofrontal system

Each colour represents the dominant connections between parietal to frontal areas and vice versa. Clusters of the frontal areas: Red (dorsal premotor area (PM-D); Blue (M1); orange (ventral premotor cluster (PM-V); Green (cingulate cluster (CING); Yellow (prefrontal cluster (PFC). Clusters of parietal areas: Red (PAR-D); Blue (SS); Orange

(PAR-V); Yellow (PAR-ML). Numbers represent percentage of total input to each area that corresponds with each input while arrows represent connectivity. Image from *Caminiti et al, 2010.*

3.7.5.2 Parieto-occipital connections

Parietal connections to occipital visual cortex are reciprocal in nature and originate from area 7a and PG and terminate at the prestriate cortex (Neal, et al., 1990). Connections that originate from the posterior wall of the IPS[1], near area PG, appear to terminate at visual area V4 on the prelunate gyrus (Neal, et al., 1988). This region has also been shown to connect to other areas in the visual system: V2, V3v, V3d and V3A (Cavada & Goldman-Rakic, 1989a). These regions are topographically organised with peripheral lower field representation in V2 being connected mainly with 7m and 7a; visual peripheral representation in PO is connected with parietal areas 7m, 7a and 7ip; upper visual field representation in the anterior section of PO is connected to parietal area 7m and 7a; lower visual representation in the posterior section of PO is reciprocally connected with 7ip(Cavada & Goldman-Rakic, 1989a). These connections are structured and support the general consensus of visual representations being processed in and around the proximal region of area 7a or PG, which have well-

[1] This region has also been labelled as area PO (Seltzer & Pandya, 1980) and 7IP (Cavada & Goldman-Rakic, 1989).

established roles in the processing of saccadic eye movements in non-human primates (Andersen, Bracewell, et al., 1990; Snyder, et al., 1998).

3.7.5.3 Parieto-temporal connections

Connections between parietal and temporal lobes originate from three separate regions on the IPL and terminate on various regions in the temporal lobe. The majority of these connections arise from the caudal third of the lower bank of the IPL (primate cortex area 7) and terminate in three different regions on the ventral temporal lobe; the parahippocampal place area, angular retrosplenial cortex, presubiculum and the perirhinal cortex (Cavada & Goldman-Rakic, 1989a; Seltzer & Pandya, 1984; Seltzer & Van Hoesen, 1979). The mid-inferior and medial surface project reciprocally to the caudal bank of the superior temporal sulcus (STS) (Cavada & Goldman-Rakic, 1989a). The remaining sections of the parietal lobe, including the SPL do not project to temporal lobe. There are no direct connections with the parietal lobe and the hippocampus.

3.8 **The Neuropsychology of Parietal Cortex Lesions**

A great deal of our understanding on the role the PC plays in spatial cognition has come from clinical examination of patents who have suffered lesions to the area. These findings are also supplemented by selective ablation of the equivalent parietal structures in rodents (DiMattia & Kesner, 1988; Rogers & Kesner, 2006) and in lower

order primates (Rushworth, Nixon, & Passingham, 1997a, 1997b). Typically when the PC is damaged, disruptions to spatial perception, spatial cognition and motor behaviour in space become apparent, and the type of deficit and its magnitude are dependent on the relative size and location of the lesion. Visual processing in parietal cortex is often characterised in terms of the dorsal or "where" processing stream (Ungerleider & Mishkin, 1982). This processing stream is not only responsible for representing the locations of objects or stimuli, but is also thought to perform coordinate transformation that allows for accurate motor actions.

Evidence obtained from lesion studies in rodents has suggested a funtional dissociation between parietal and hippocampal areas regarding spatial processing. Lesions to the hippocampus impair the body's allocentric reference system of space, while PPC lesions impact the egocentric reference system. Rodents with hippocampal lesions display marked disruptions in spatial navigation, difficulties in spatial learning (acquisition) during maze navigation (Faraji, Lehmann, Metz, & Sutherland, 2008; Rogers & Kesner, 2006; Etienne Save & Poucet, 2000) and deficits in retention of previously learned mazes (DiMattia & Kesner, 1988; Faraji, et al., 2008; Rogers & Kesner, 2006).

Clinical observations of patients with damage isolated to the posterior section of the right parietal lobe has found that these patients fail to respond to contralateral space with either limb or eye movements, a disorder termed unilateral spatial neglect or hemineglect (Karnath, 1998). A striking example of this is failure to represent the

contralesional side of space when drawing and can be as extreme as failing to address the contralesional side of the body when shaving or dressing (personal neglect). Neglect can affect contralesional space within reaching distance or space beyond reaching distance (Buxbaum et al., 2004).

A common symptom often reported by neglect patients is a lack of awareness of the disorder itself, a condition which itself is termed anosognosia. In their famous experiment, Bisiach & Luzzatti (1978), asked patients with left-side neglect to imagine viewing the Piazza del Duomo (Cathedral Centre; a well-known landmark in Milan, Italy) from the cathedral which was in the centre of the square. Patients failed to report buildings or roads to the left of this viewpoint, but when their imagined viewpoint was shifted by 180 degrees, they then failed to report roads and landmarks which they had previously reported prior to the imagined rotation.

Bilateral damage to the IPL results in the impaired planning and execution of arm movements toward the contralesional egocentric space; a condition which is known as directional hypokinesia (Caminiti, et al., 2010). Patients with this disorder make slower limb movements, have longer reaction times and display reduced accuracy in reaching tasks regardless of the limb used. This disorder shares many similarities with optic ataxia but a key difference is the presence of perceptual aspects of hemineglect.

In contrast to IPL lesions, SPL lesions generally produce optic ataxia, which manifests itself as impaired arm reaching to a visual target often with incorrect hand orientation and grip prehension (Balint, 1909; Battaglia-Mayer & Caminiti, 2002;

Holmes, 1918). Optic ataxia is usually comprised of three main features. The first of these is a defect in the directional control of hand movement, affecting the perception of the direction of the movement (Critchley, 1953). Secondly, the real time control of hand movements is affected. The third factor is that it occurs only when visual control of the movement is required. Patients with optic ataxia do not have any other motor deficits, can execute movement correctly under prioprioceptive control do not display hemineglect (Battaglia-Mayer & Caminiti, 2002).

In their report of 10 pure optic ataxia unilateral patients, Perenin & Vighetto (1988) found that when lesions were located in the right SPL reaching was affected only in the contralesional space, while for left-sided lesions, patients experienced difficulties when reaching in both contra- and ipsi-lesional space.,

Numerous cases of optic ataxia have been reported with the literature (Ando & Moritake, 1990; Auerbach & Alexander, 1981; Balint, 1909; Battaglia-Mayer & Caminiti, 2002; Perenin & Vighetto, 1988) with the symtoms best represented by case 2 of Holmes (1918):

> The most striking symptom in this case... the patient's inability to localize correctly in space objects which he could see and recognize perfectly well. When, for instance he was asked to touch a piece of paper attached to the end of the metal rod, he rarely reached it directly, but brought his hand to one or other side of it, or above or below it, and continued to grope until his hand came into contact with it.

Perhaps the most compelling evidence supporting the PPC role in spatial navigation comes from spatial disturbances seen in egocentric disorientation.

Although the condition is quite rare, it is believed to emanate from bilateral or right unilateral lesions to the PPC, including the SPL (Aguirre & D'Esposito, 1999). While patients with this disorder show intact visuospatial attention and memory for people and objects, they have difficulty in reaching for identified objects or describing the relationships between two objects in their environment., These patients also show deficits in a wide range of visuo-spatial tasks including mental rotation and spatial span tests (Aguirre & D'Esposito, 1999). One of the earliest cases of egocentric disorientation was described by Holmes and Horrax (1919);

> If spoken to suddenly he first stared in a wrong direction and then moved his eyes about until they fell, as if by chance, on the observer's face; he was extremely slow and inaccurate in his attempts to fix or bring into central vision any object when its image fell in the periphery of his retinae, especially if it were small. When, however, requested to look at his own finger or to any point of his body which was touched he did so promptly and accurately, moving as a rule both his head and eyes in the normal manner.
>
> On one occasion he explained, "Your hand seemed to come nearer to me, but I had no idea how near it came, I thought it was plenty far off." But on another day he said, "I did not see that it was coming toward my face." If, however, his own hand was suddenly jerked by the observer toward his eyes he always reacted normally to the threat.
>
> His visual memory, for both form and colour, of impressions obtained in earlier years was apparently intact; he was evidently a strong visualist and described as a visualist does his house, his family, a hospital ward in which he had previously been, etc. But, on the other hand, he had complete loss of memory of topography; he was totally unable

> to describe the route between the house in a provincial town in which he had lived all his life and the railway station a short distance away, explaining "I used to be able to see the way but I can't see it now." …The most prominent symptom, however, from the time he came under our observation till he left the hospital three months later, was his inability to orientate and localize correctly in space objects which he saw. When within the first few weeks he was asked to take hold of or point to, any object, he projected his hand out vaguely, generally in a wrong direction, and had obviously no accurate idea of its distance from him.

Kase et. al. (1977) described the behavioural symptoms of patient MVV, who had bilateral parietal lobe damage and exhibited the symptoms of egocentric disorientation. In MVV's case, she was not unable to localise objects by vision, nor could she properly localise sound. In addition, she could not navigate around the hospital where she stayed nor she could not find her bed in a six-bedroom ward and found it very difficult to find the correct position to lie down in it. She consistently got lost in the street and often bumped into objects she could see and recognise (Kase, et al., 1977; B. A. Wilson et al., 2005). A case of pure egocentric disorientation was patient GW, who developed the condition from a neurodegenerative disorder of unknown aetiology (M. Stark, 1996). She exhibited no visual field disturbances and her reaching was relatively normal, unlike like some of Holmes & Horax's patients. GW's symptoms manifested in navigational difficulties in familiar surroundings, like her town and in her house. She found it difficult to sit down in chairs or even to position herself in her bed, and described her left arm 'wandering' off. GW could not localise the origin of sounds and often turned in the wrong direction when someone greeted her.

In their seminal review of the literature concerning topographic disorientation, Aguirre & D'Esposito (1999) reclassified patients exhibiting the above symptoms into a new group of topographically disorientated patients, which they termed egocentric disorientation. They defined egocentric disorientation as having difficulties in the ability to represent the location of objects with regards to oneself, or describe any relationships the object might have with others in the local environment (Aguirre & D'Esposito, 1999). The findings from these patients are consistent with the evidence from single cell recording studies of primates that suggest PPC neurons represent spatial location of objects information in an egocentric coordinate frame (M. Stark, 1996).

3.8.1 Lesions to the Rodent Parietal Lobe

In rodents, the bilateral lesions of the hippocampus resulted in deficits in the acquisition of new information (DiMattia & Kesner, 1988; Kesner, Farnsworth, & Kametani, 1991; Rogers & Kesner, 2006), known as anterograde amnesia (Eichenbaum, 1997; Penfield, 1968; Scoville, 1954; Scoville & Milner, 1957; Squire, 1987). When the PPC was lesioned in rodents the effects were similar (DiMattia & Kesner, 1988; Kesner, et al., 1991; Rogers & Kesner, 2006), however DiMattia & Kesner (1988) reported PPC lesioned rodents were more severely affected in the acquisition and retention of spatial knowledge in the Morris water maze task. This deficit was seen as an increase in the distance travelled to find the target location and the effect was replicated in later investigations (Kesner, Farnsworth, & DiMattia, 1989; Kesner, et al., 1991; Rogers

& Kesner, 2006). Another deficit present in PPC lesioned rodents was an impaired ability to recognise the changes in spatial distributions in objects (Goodrich-Hunsaker, Hunsaker, & Kesner, 2005; E. Save, Poucet, Foreman, & Buhot, 1992). Those rodents took more time to habituate to a previously familiar environment when objects in that environment were topologically rearranged. Hippocampal lesioned rodents, however, only displayed deficits when the distance between those objects changed (Goodrich-Hunsaker, et al., 2005). This led some researchers to suggest the separation in function between the PPC and hippocampus lies in the processing of metric and topographic space respectively. However, as rodent maze tasks such as the Morris water maze, are allocentric in nature, this evidence implies the rodent PPC also processes allocentric information. Evidence concerning the rodent PC's involvement in egocentric processing comes from the work of Save, Guazzelli & Poucet (Etienne Save, et al., 2001), who demonstrated lesions to PPC resulted in deficits in PI. Specifically, these rodents took more complex outward paths, which were also related to a greater amount of errors made. In contrast, hippocampal lesions resulted in a general learning deficit that affected subsequent behaviours in the task (such as PI).

Current lesion evidence from rodents highlights the role of the PPC in both allocentric and egocentric processing in the rodent brain. Similarly, the single cell recordings from primates have also demonstrated allocentric and egocentric processing (Snyder, et al., 1998).

3.9 **Retrosplenial Cortex**

There has been some ambiguity in the labelling of the retrosplenial cortex (RS) and the retrosplenial *complex* (RSC) and the two labels are sometimes used interchangeably. However Epstein (2008) defines the RSC as the functionally defined scene-response region (which will be discussed in detailed further on in this chapter) which is not identical to the anatomically defined RS. The RSC is located in the retrosplenial cortex-posterior cingulate medial parietal region near the region where the calcarine sulcus joins the parietal-occipital sulcus (Epstein, 2008). This next section will detail the anatomical connections and function of the RS and RSC.

In primates, the RSC is located caudally to the bulbous portion of the corpus callosum, the splenium, and is comprised of Brodmann's areas 29 and 30. It forms part of the cingulate cortex and is separated from the precuneus by BA 23. The RSC is often implicated in memory function and this is reflected in the strong connections the region has with well-established memory centres in the MTL including the hippocampal formation and the parahippocampal region. The connections to the hippocampus are densest from BA 29 and BA 31 (Kobayashi & Amaral, 2003), suggesting that region of the RSC is likely to contribute to hippocampal functions (Vann, Aggleton, & Maguire, 2009). Other reciprocal connections include projections to prefrontal areas BA 46 (dorsolateral prefrontal cortex, DLPFC), BA 9, BA 10 and BA 11 (Rugg, et al., 1997).

The rodent posterior cingulate region differs considerably from the primate region and does not have areas analogous to the primate BA 23 and BA 31, so the

entire region is often classed as the retrosplenial cortex (Vann, et al., 2009). Like the primate, this region is also separated into granular (BA 29) and dysgranular (BA 30) regions with granular regions further subdivided into granular a (Rga) and granular b (Rgb). These granular regions are reciprocally connected to the anterior and laterodorsal thalamic nuclei, which contain HD cells (Corbetta & Shulman, 2002). In contrast, the dysgranular region is reciprocally connected to the visual areas BA 18b and 17 (Fox & Ranck Jr, 1975). As in the primate cortex, the region is reciprocally connected to the hippocampal formation and the anterior cingulate (M. Wilson & McNaughton, 1993).

3.9.1 Lesions to the Retrosplenial Cortex

The majority of lesion studies on RS are in rodents as the area is reasonably accessible, occupying most of the dorsal midline cortex to the body of the fornix (Aggleton, 2010). Further information as to RS function has been derived from clinical observations of patients who have suffered stroke to this area. However, there have been only a handful of reported case studies (Aguirre & D'Esposito, 1999; Greene, Donders, & Thoits, 2006; Ino et al., 2007; Katayama, Takahashi, Ogawara, & Hattori, 1999). Navigation difficulties are commonly reported by patients with lesions to the RS and the neighbouring posterior cingulate cortex (Aguirre & D'Esposito, 1999; Ino, et al., 2007; Katayama, et al., 1999; Takahashi, Kawamura, Shiota, Kasahata, & Hirayama, 1997). Patients have reported getting lost in familiar environments without being able to use landmark information to provide directional heading cues (Ino, et al., 2007;

Takahashi, et al., 1997). For example, one patient was unable to recall the direction of travel from one location to another (allocentric heading) and appeared to have lost his ability to use landmarks to locate his position (Ino, et al., 2007). Another patient who suffered a stroke within RS while walking home was able to recognise the building in front of him, but was unable to determine the direction to his house. The same patient attempted to go to the hospital but was unable to determine the direction to take and consequently got lost several times on the way (Takahashi, et al., 1997). This aspect of topographic disorientation is not limited to familiar environments and also occurs in novel ones (Greene, et al., 2006). These symptoms have been reported for both left and right-sided lesions. Interestingly the symptoms diminish with time, presumably as the undamaged hemisphere takes on extra processing to compensate for the loss of function (Ino, et al., 2007; Takahashi, et al., 1997). However, when damage occurs bilaterally, there is no recovery of lost function (Greene, et al., 2006). While some patients were able to describe what they could see from a particular viewpoint (Katayama, et al., 1999), they were unable to determine the spatial relationship between two landmarks, if one landmark was not visible from the other (Takahashi, et al., 1997). In their review, Aguirre & D'Esposito (1999) described the deficits arising from RS lesions as “heading disorientation”, which was classified as an inability “to represent direction of orientation with respect to the external environment”.

The RS has been reported to be hypoactive in patients diagnosed with mild cognitive impairment (MCI), often the prodromal phase of Alzheimer’s disease (AD).

There is evidence to suggest that hypoactivity of the retrosplenial cortex during this early stage is consistent with the memory complaints and topographic disorientation patients with early AD often report (deIpolyi, Rankin, Mucke, Miller, & Gorno-Tempini, 2007; Desgranges et al., 2002; Grossi, Fasanaro, Cecere, Salzano, & Trojano, 2007).

In rodents, approximately 10% of cells in the RSC are head direction cells. Head directions cells are an orientation-specific class of neuron, that discharge in relation to the animal's head position in the horizontal plane (Taube, et al., 1990). The firing rates of HD cells are strongly coupled to the firing rates of place cells in the hippocampus suggesting a unitary system of spatial orientation between these two regions (Knierim, et al., 1995). HD cells, place cells and grid cells in the medial entorhinal cortex form part of the rodent's triumvirate of spatial navigation ability (Vann, et al., 2009).

Studies of rodents with lesions of the retrosplenial cortex have demonstrated impairment in spatial memory (Aggleton & Vann, 2004; Harker & Whishaw, 2004b; Vann, et al., 2009), impaired performance when completing the Morris water maze, a test of dynamic learning (Harker & Whishaw, 2004a; Vann & Aggleton, 2004; Vann, Kristina Wilton, Muir, & Aggleton, 2003) and reduced performance in working memory mazes such as the radial arm and T- maze (Pothuizen, Davies, Aggleton, & Vann, 2010; Vann & Aggleton, 2004). However, the magnitude of spatial deficits in rodents with RS lesions is much smaller than those seen in rodents with lesions of either the hippocampus or the anterior thalamus Vann et al. (2009), suggesting that the role

played by the RS in spatial learning is secondary to the functions provided by the hippocampal formation and the anterior thalamus.

Further deficits from RS lesions became apparent when the animals were required to shift between modes of spatial learning (Pothuizen, Aggleton, & Vann, 2008), for example, when they had to switch from local to distant cues (Pothuizen, et al., 2008; Vann & Aggleton, 2004). These lesions also impacted performance on idiothetic tasks involving path integration (Whishaw, Maaswinkel, Gonzalez, & Kolb, 2001). This has led some researchers to conclude that the role of RS is in performing transformations between allocentric (world-centred) and egocentric (body-centred) reference frames (Byrne, et al., 2007; Epstein, 2008; Vann, et al., 2009).

3.10 **Multimodal Integration of Spatial Information and Coordinate Transformations**

A likely role of PPC is to translate sensory coordinates into motor coordinates. PPC neurons, particularly those that reside within the IPS, often display bimodal responses to visual and somatosensory stimuli (Colby & Duhamel, 1991), and also may respond to auditory stimuli (Cohen & Andersen, 2000). Importantly, the responses to these stimuli are often modulated by the position of the eyes and head (Andersen, Snyder, Li, & Stricanne, 1993; Cohen & Andersen, 2002; Snyder, et al., 1998).

3.10.1 Eye and Head Coordinate Space and Gain Fields

Parietal neurons in area 7 and LIP encode the locations of visual targets in retinal coordinates with head and eye position signals modulating this activity (Andersen, et al., 1993; Brotchie, et al., 1995; Brotchie et al., 2003; Snyder, et al., 1998). LIP, sometimes referred to as the parietal eye fields, is heavily connected with visual areas and is specialised for planning saccadic eye movements. LIP neurons have retinotopic receptive fields and therefore encode visual targets in eye centred coordinates. However, this activity is modulated by the position of the eyes in the head, thereby also providing a representation of visual targets in a head-centred coordinate frame (Andersen, et al., 1992; Andersen, et al., 1993; Brotchie, et al., 1995; Snyder, et al., 1998). This modulation of activity by eye position is known as a gain field. Gain field modulation of LIP neuronal activity has also been observed with head position (Andersen, 1998). Individual LIP neuronal activity does not encode specific locations. However, stimulus location is encoded in head-centred and body-centred space across populations of LIP neurons (Andersen, 1998). Approximately half of the neurons in LIP that had eye position gain fields also had gain fields to head position (Brotchie, et al., 1995)

Similarly, neurons within area 7a also encode visual targets in retinal coordinates and have activity modulated with respect to eye position (Brotchie, et al., 1995). However, the activity of neurons within this area is also modulated by the position of the body in the environment thereby providing a world-centred representation of

space (Snyder, et al., 1998). In one aspect of this experiment, Snyder and colleagues rotated the monkey's body under the head, which was fixed relative to the external world. Vestibular cues were absent, as the head was stationary with respect to the environment, so only neck proprioceptive cues indicated body orientation. Neurons within LIP displayed neck proprioceptive gain fields, indicating the orientation of the head relative to the body and thus allowing encoding of locations in a body-centred coordinate frame (Andersen, 1998; Snyder, et al., 1998) whereas neurons in area 7a displayed vestibular gain fields identifying the position of the head in space and therefore allowing an encoding of locations in world-centred coordinates (Andersen, 1998; Snyder, et al., 1998).

The PPC was initially found to be a visually responsive area, but more recently it has been discovered that neurons in this region also process the spatial locations of auditory stimuli. Visual information is processed in terms of an eye-centred coordinate frame, whereas auditory information must be processed from intra-aural time, intra-aural intensity and spectral cues arriving at the two ears. This type of processing would provide a head-centred coordinate frame (Andersen, et al., 1997). Neurons in LIP have demonstrated processing related to the sensory integration of these two reference frames allowing for the perception of visual and auditory cues originating from the same location to be perceived as spatially coincident (Andersen, et al., 1997). A study conducted by Mazzoni et al. (1996) found LIP neurons not only displayed sustained activity during the delay period of a delayed response task, they also displayed activity

during the presentation of the auditory stimulus. In this particular experiment, the monkey was required to memorise the location of an auditory target in the dark, and make a saccade to it after a delay. Effects of eye and head position were not assessed by this study. However, Stricanne et al. (1996), found forty-four percent of auditory responding neurons in LIP encoded the auditory location in eye-centred coordinates, thirty-three percent in head-centred coordinates and 23 precent in an intermediate manner between eye and head-centred frames. The behaviour of LIP neurons indicates the region is concerned with the spatial location of visual and auditory stimuli (Stricanne, et al., 1996).

3.11 **Functional Imaging of Navigation**

Functional imaging has allowed us to noninvasively investigate what roles the human PPC and the RSC play in navigation as they are commonly reported in studies of spatial navigation (Epstein, 2008; Spiers & Maguire, 2007a). Some observations imply the PPC is involved in the processing of heading direction (Spiers & Maguire, 2007a). London taxi drivers were required to navigate to destinations in a highly detailed representation of London. During this journey the end goal was sometime changed, which required the driver to recalculate a new route to the new goal. Of interest in this study was the bilateral activity of the parietal lobe, which was positively correlated with egocentric direction to the goal. Egocentric direction was determined by subtracting heading direction from the heading direction pointing to the goal.

Similarly, Rodriguez (2010) also investigated navigation in human participants, but chose to use a visually austere environment and two elements that are common to more complex forms of navigation. The first of these involved navigating to a location that is relative to a landmark (akin to allocentric navigation), while the second involved picking the correct cue directly from a landmark (egocentric navigation). The PPC was bilaterally active in calculating the heading vectors to goal locations, similar to the actoivations reported by Spiers & Maguire (2007a). Furthermore, patients with parietal lobe lesions showed impaired performance when navigating in a virtual maze with no landmarks, but normal performance when landmarks were present, suggesting that idiothetic strategies may reside in the parietal lobe (Weniger, Ruhleder, Wolf, Lange, & Irle, 2009) (Aguirre & D'Esposito, 1999; Snyder, et al., 1998; Spiers & Maguire, 2007a).

The retrosplenial cortex, like the PPC, is highly activated during spatial tasks including passive viewing of navigation footage, mental navigation, familiar scenery and navigation with 3-D virtual reality environments. In addition, the RS is also active during the retrieval of long-term spatial knowledge especially if used in making judgements (Epstein, Parker, & Feiler, 2007). The area appears to be active during all aspects of spatial navigation, that is, the learning of a new environment, navigating in a recently learned environment and navigating in a familiar environment (Vann, et al., 2009). In a recent investigation, Spiers & Maguire (2006) imaged participants while they navigated through a highly detailed representation of London. Activity within the

RSC increased specifically when topological representations had to be updated for route planning or when new topological information was acquired, supporting the idea that RS is a short-term store for translating between reference frames (Byrne, et al., 2007; Vann, et al., 2009). Additionally, these findings also highlight the area's importance in the processing of directional heading.

A functionally defined subsection of the RS termed the retrosplenial complex (RSC) displays scene responsive activation, similar to that of the parahippocampal place area (PPA, Bar, 2004; Epstein, 2008; Epstein, Higgins, Jablonski, & Feiler, 2007; Epstein, Parker, et al., 2007). The RSC is active during the viewing of scene imagery (O'Craven & Kanwisher, 2000) and navigation through virtual environments (Baumann & Mattingley, 2010; Rauchs et al., 2008). However, unlike PPA, the familiarity of the scene modulates the strength of RSC activation (Epstein, Parker, et al., 2007). Bar (2004) and Epstein (2008) advocate that the RSC's role lies in the processing of scene-relevant relationships rather than supporting spatial navigation and orientation. In the study conducted by Epstein (Epstein, Parker, et al., 2007) the RSC was active in conditions in which there was some familiarity of the local scene. The familiarity was based in part on the 'background' environmental information which allowed the participant to place the location of the scene. Some retrieval of information would be required in order to identify the background cues in order to place the scene in the greater context of the environment and secondly some translation of the scene would need to occur as the original information would have been encoded into memory from

a different viewpoint or angle. Similarly, Wolbers & Buchel (2005) also reported RSC activation which the authors believed to reflect the integration of egocentric information into allocentric processing.

A recent study by Baumann and Mattingley (2010) suggests that the RSC also encodes perceived heading direction when navigating. The authors used a simple task that represented simulated heading. The task consisted of two phases, a learning phase and a test phase. The learning phase included free roaming and also allowed participants to become familiar with the landmarks situated around the periphery of the maze. In the test phase, the participants were shown two images separated by a delay that represented travelling in one direction/ heading (e.g. north) or travelling in a novel heading (e.g. north-west). The RSC was active during both same and different heading trials but this activity was greater in trials that had a different heading (e.g. north-west). The reduction in blood oxygenation level dependent (BOLD) signal for same heading trials can be explained by neural adaption. The findings from this study support previous observations of RSC activity during the presentation of scene viewing, scene imagery and scene memory (Epstein & Kanwisher, 1998; Epstein, Parker, et al., 2007), but also add the interesting finding of sensitivity to heading direction in RSC.

Figure 8: Schematics of the virtual environment and spatial judgment task used to examine the representation of allocentric heading.
A, Aerial perspective of the virtual maze (never seen by participants) used in the learning phase. The red dots indicate the locations of the 20 symbols that acted as landmarks; the single blue spot represents the center of the virtual maze. The arrows represent the 16 different vantage points from which participants viewed the landmarks during the test phase. *b*, Example of a single image viewed by participants during the test phase. *c*, Sequence of events in a typical experimental trial, consisting of a pair of images depicting landmarks representing the same heading direction (repeated trials) or different heading directions (novel trials). Note that participants never viewed the same landmark symbol twice within a trial pair. Adapted from Baumann & Mattingley (2010)

In contrast to the view proposed by Bar (2004) and Epstein (2008), an alternate theory on RS function is that it processes the stability of environmental landmarks, a process which could be considered a critical component of navigation (Auger, Mullally, & Maguire, 2012). Auger and colleagues used fMRI to measure changes in BOLD activation when participants viewed images of common everyday outdoor items. A major factor of the landmarks was the perception of permanence, with some

landmarks such as buses, having low permanence (or high non-permanence), while other landmarks such as light poles have high permanence (or low non- permanence). Both the parahippocampus and RS were significantly active. The parahippocampus was equally active during the viewing of landmarks in both low and high permanence categories, while RS was most strongly engaged by landmarks in the high permanence category. In addition, when the sample was subdivided into good and poor navigators, individuals in the latter group had significantly reduced responses in the RS. Based on these findings, the authors have suggested one possible function of the RS is to identify stable landmarks in the environment, a task which would undoubtedly aide in navigation. This type of processing may lead to the overall salience that landmarks have amongst other objects present in the environment. Given the strength of connections to the hippocampus (Kobayashi & Amaral, 2003), and the fact that landmark stability has been shown to influence place fields (Cressant, et al., 1997; Gothard, et al., 1996; Knierim, et al., 1995; Muller & Kubie, 1987), it is possible that processing conducted by the RS is shared with temporal lobe regions. This type of processing is consistent with the observation that temporary inactivation of the rodent RS transiently alters the spatial tuning of place cells (Cooper & Mizumori, 2001). It should be noted that the RS activations reported in this investigation fall within the boundary of BA 29/30 and do not correspond to the RSC of Epstein (2008).

In summary, both the RS and PPC are activated by a wide variety of spatial and memory tasks. The functional evidence concerning the PPC largely appears to support

the region's involvement in egocentric processing. In particular, one current theory supports the notion of the RS being involved in scene translation between allocentric and egocentric reference frames (Bar, 2004; Byrne, et al., 2007; Epstein, 2008; Vann, et al., 2009). An alternate theory of RS function states the region's involvement lies in the processing of landmark stability, a notion which is largely supported from single cell investigations conducted in rodents (Cooper & Mizumori, 2001; Cressant, et al., 1997; Gothard, et al., 1996; Knierim, et al., 1995; Muller & Kubie, 1987), and from human functional research (Auger, et al., 2012).

4 *Functional Magnetic Resonance Imaging of Neural Activity*

4.1 **Introduction**

Magnetic Resonance Imaging (MRI) is an imaging technique that is used to view internal body structures, primarily used in clinical diagnosis. Specialised imaging sequences can indirectly measure neural activity via changes in the ratio of oxyhaemoglobin/deoxyhaemoglobin in cerebral brain tissue. FMRI has superior spatial resolution (as fine as $1mm^3$ voxel size) when compared against electric (electroencephalogram; EEG) and positron emission topography (PET). Unfortunately, due to the nature of BOLD signals, the temporal resolution (12-16 seconds) is far inferior to electrical measures of brain activity (1ms). Functional magnetic resonance imaging using the BOLD contrast is a sensitive measure of changes in blood oxygen, and can be used to make inferences about regionally specific activations in the brain (Frackowiak, Friston, & Frith, 2003), interpreted as static representations of averaged dynamic brain activity (Nair, 2005). In the studies presented in this thesis, whole brain-fMRI was acquired to investigate brain activity in healthy volunteers who performed navigation tasks in a virtual 3D environment.

4.2 **The Biophysics of functional Magnetic Resonance Imaging**

When a charged body such as the Earth spins on its axis, a magnetic moment is produced, resulting in a magnetic field. This process also occurs in protons whose

rotational movement causes tiny magnetic moments to occur. In a normal environment, the spins of protons are random and overall their net magnetic charge is zero. But when a strong magnetic field is applied, the spins of protons align with the direction of the magnetic field (B0). The spins however, are not stable and precess or 'wobble'. The rate of precession is determined by the strength of the external magnetic field and is described as the Larmor frequency:

$$\omega = \gamma \mathcal{B}_0$$

Where;

ω = Frequency of precession

γ = gyromagnetic ratio

$\mathcal{B}_0$ = Strength of external magnetic field

When a radio frequency (RF) pulse is at the Larmor frequency, the protons absorb the energy and move into a higher energy state. The degree to which they are flipped into the higher energy state is determined by α, a function of the magnetic field strength and RF duration. The protons precess in the XY plane until the RF pulse is switched off. Then their spins in the XY plane decay and to alignment with B0. When this happens, electromagnetic energy is released in the form of a photon, which is detected and used to construct an image, whilst the remaining energy is transferred to surrounding tissue as heat. Three types of MR signal can be detected when during this process: T1, T2 and T2*. T1 is categorised by longitudinal relaxation along the Z-axis, and the constant for different tissues is defined when 63.2% of magnetisation has

recovered alignment with B0. T2 is categorised by exponential signal loss in the XY plane as a result from interactions between neighbouring protons (known as a spin-spin interactions) and is defined when signal amplitude has been reduced to 36.8% of its original value. In real world situations, the decay of MR signals occurs at a faster rate and than predicted by T2. The assumption behind T2 is that the external magnetic field is homogeneous, and that the resulting signal loss occurs completely from spin-spin interactions. This however is not the case, as there are inherent inhomogeneities present within the magnetic field emanating from the magnet itself or from the patient. Therefore T2* is a combination of fixed (spin-spin interactions) and random (magnetic field inhomogeneity) effects. As hydrogen is the most ubiquitous element in the human body with roughly two-thirds of the body weight in the form of water, it is the main element being imaged in MRI (Martini, 2001).

4.3 **The BOLD Response**

The blood oxygenation level dependent signal is the specific magnetic resonance (MR) contrast that is used to detect the macroscopic changes that occur as result of neuronal activity. The source of neuronal energy is adenosine triphosphate (ATP) which is synthesised through oxidative glucose metabolism. As neurons do not have their own internal stores for glucose and oxygen, they are transported to the neurons via capillary networks. When there is an increase in neural activity, increased glucose and oxygen (as oxyhaemoglobin) is transported to the active brain regions via

increased regional blood flow. The changes in BOLD signal arise from the fundamental differences in magnetic susceptibilities between oxyhaemoglobin and deoxyhaemoglobin. Oxyhaemoglobin is diamagnetic and has no influence on the external magnetic field. When the oxygen molecules are lost to the local neurons, oxyhaemoglobin becomes deoxyhaemoglobin, which in contrast is paramagnetic. This results in increases in the local magnetic field, whilst creating differences in the susceptibility between venous vasculature, surrounding tissue, and blood stream. An increased presence of oxyhaemoglobin will produce less inhomogeneity in the magnetic field, result in a slower T2* decay and produce a stronger BOLD signal. The converse is true of deoxyhaemoglobin, which produces a greater inhomogeneity in the magnetic field, results in a quicker T2* decay and produces a weaker BOLD signal. Therefore, BOLD signal is dependent on a complex relationship between the cerebral metabolic rate of oxygen consumption (CMRO2), cerebral blood flow (CBF) and cerebral blood volume (CBV). The change in oxygen saturation however is somewhat predictable and can modelled by modelling the dynamic changes in CBF (See Figure 2.1)(Buxton). These models are time-locked with stimulus presentation and are known as the hemodynamic response function (HRF; see Figure 9).

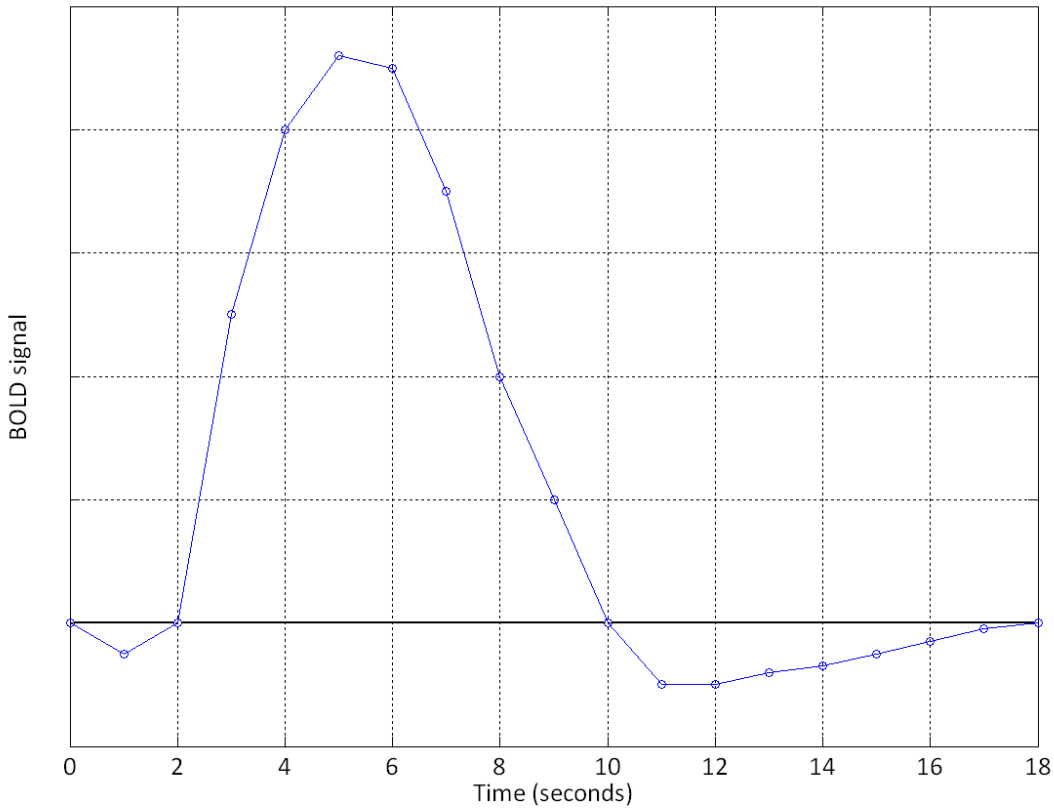

Figure 9: A typical HRF response to a single stimulus.

Maximal signal occurs 4-6 seconds post stimulus and returns to baseline 8-12 seconds post stimulus, followed by an undershoot. At high magnetic fields (> 3T), an initial undershoot can also be observed. Haemodynamic responses are known to differ between individuals (Aguirre, Zarahn, & D'Esposito, 1998).

As seen in Figure 9, the initial dip in BOLD signal is a result of a transient increase of deoxyhaemoglobin within the local cortical area that is under cognitive load. This effect is regarded as potential means to increase the spatial selectivity of the BOLD effect even though this particular response is rarely seen at magnetic field strengths of less than 3T (Aguirre, et al., 1998; Hu & Yacoub; Yacoub et al., 2001). It is generally

accepted that the initial dip predominately reflects changes in the microvascular circulation with this specific BOLD contrast expected to scale quadratically with the magnetic field (Hu & Yacoub). Following this, there is an increase in BOLD signal due to the change in the ratio of oxy/deoxyhaemoglobin. When the consumption of oxygen increases, the regional increase in cerebral blood flow to the area causes an increased BOLD signal, believed to reflect the underlying neural processes underpinning the cognitive task, occurring approximately 4-6 seconds after stimulus presentation (Aguirre, Zarahn, & D'Esposito, 1997). After the stimulus ends, the BOLD signal returns back to baseline approximately 4-6 seconds after reaching its maxima and then undershoots it. This undershoot effect is not fully understood and could potentially be explained as a metabolic effect where there is a slow recovery of CMRO2 or a hemodynamic effect where blood capacity causes cerebral blood volume to normalise at slower rates than changes in cerebral blood flow (Buxton). See Figure 10 for a visual representation of a typical BOLD response with respect to time.

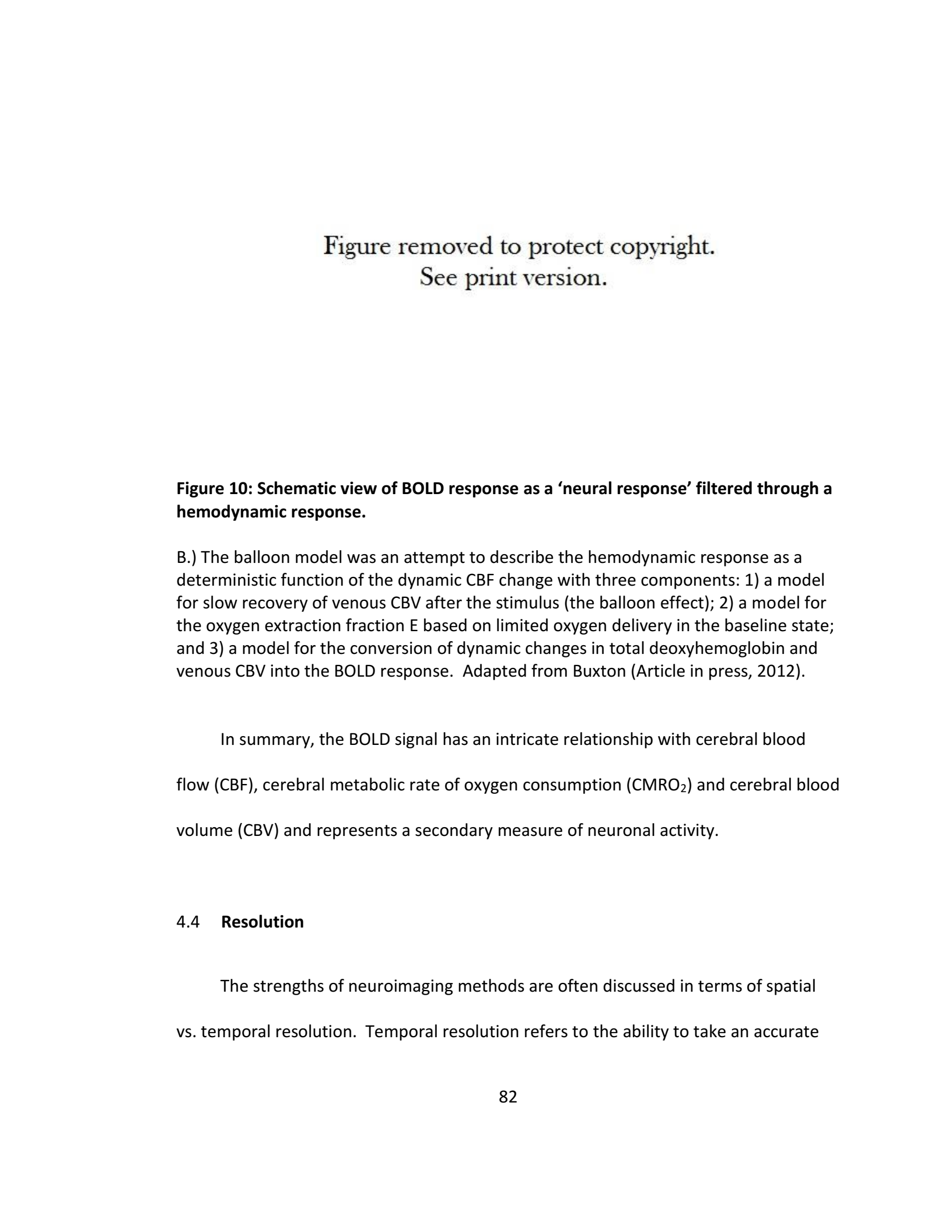

Figure 10: Schematic view of BOLD response as a 'neural response' filtered through a hemodynamic response.

B.) The balloon model was an attempt to describe the hemodynamic response as a deterministic function of the dynamic CBF change with three components: 1) a model for slow recovery of venous CBV after the stimulus (the balloon effect); 2) a model for the oxygen extraction fraction E based on limited oxygen delivery in the baseline state; and 3) a model for the conversion of dynamic changes in total deoxyhemoglobin and venous CBV into the BOLD response. Adapted from Buxton (Article in press, 2012).

In summary, the BOLD signal has an intricate relationship with cerebral blood flow (CBF), cerebral metabolic rate of oxygen consumption ($CMRO_2$) and cerebral blood volume (CBV) and represents a secondary measure of neuronal activity.

4.4 **Resolution**

The strengths of neuroimaging methods are often discussed in terms of spatial vs. temporal resolution. Temporal resolution refers to the ability to take an accurate

measurement with respect to time. In contrast, spatial resolution refers to the spatial detail of an image acquired by an imaging device such as a MRI or EEG. While it is possible to take several fMRI images every second (every 40ms in new scanner using an EPI scanning sequence), the temporal smoothing of the BOLD response effectively limits the overall temporal resolution. The BOLD response behaves like a low pass filter, so high frequency activity is underestimated (Nunez & Silberstein, 2000). In contrast, electrical measures of neural activity such as EEG and MEG (magnetoencephalography) have far superior temporal resolutions in the order of milliseconds.

With respect to other imaging modalities (EEG, MEG & PET), one of the biggest strengths of fMRI is the exceptional spatial resolution it offers, which can be as high as $1mm^3$. This is dependent on the TR or repetition time – the time it takes for the scanner to complete the imaging of one brain volume. The shorter the TR, the less spatial resolution or brain coverage is available.

An important caveat regarding spatial resolution of fMRI images is that the overall resolution for these images is likely to be less than the recorded voxel. Pre-processing involves spatial smoothing which removes a considerable amount of spatial specificity. Variations in anatomy may also reduce the overall spatial resolution when images are combined for group analyses. Also, it is still difficult to identify the exact source of neural activity due to the BOLD mechanism. Nonetheless, the spatial

resolution of fMRI is still considerably superior to other metabolic and electric measurements of neural activity.

4.5 **Study Design**

FMRI investigations are designed to measure the cognitive impact of a single task or paradigm on the modulation of the BOLD response. Unlike EEG, which has a far superior temporal resolution, fMRI designs have to incorporate stimulus timing within the timing constraints of the BOLD response. In this regard, stimuli can be presented as either blocked or event related designs. This next section will detail some basic principles of these two designs.

4.5.1 Block designs

Block designs string together multiple conditions from an experiment into condition blocks that alternates with rest condition blocks (Amaro & Barker, 2006, see Figure 11). Hemodynamic responses to repetitive stimuli are additive. By introducing a rest condition, this allows the response to return to a baseline level, thus providing maximum variability within the signal. This allows block designs to have greater signal to noise ratios than event related designs (Friston, Zarahn, Josephs, Henson, & Dale, 1999). However, this method is subject to several shortcomings. Firstly, as randomisation within a condition block is impossible, expectation and habituation effects are common within block designs. Secondly, block designs are very sensitive to

signal drift from head motion. Thirdly, there is strong evidence that the brain is not idle during rest conditions, hence elevated brain activity during this period would make it difficult to draw significant conclusions (C. E. L. Stark & Squire, 2001).

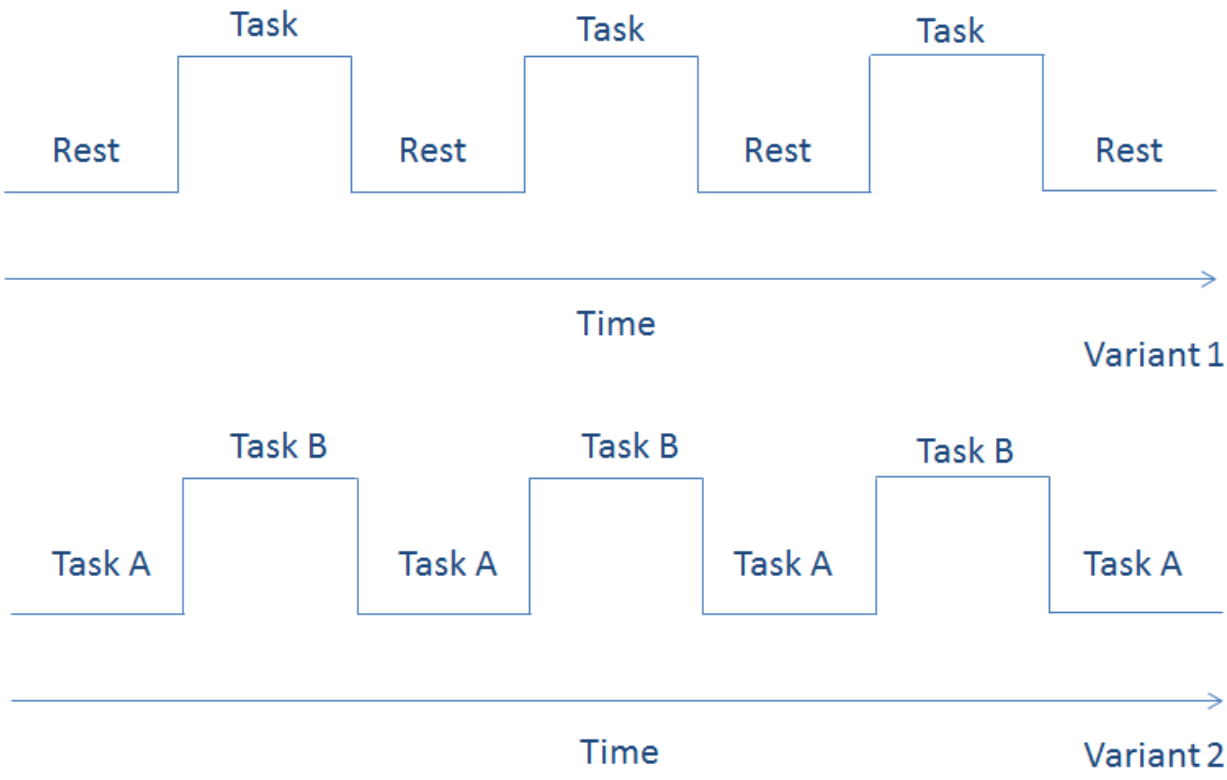

Figure 11: Schematic representation of block design paradigms.

Variant 1 involves having a rest condition following an experimental condition, whilst variant 2 has two different experimental conditions alternating between each other.

4.5.2 Event-related designs

Event related fMRI (erfMRI) designs measure transient variations in BOLD responses to repetitive stimuli and allow for the temporal characterisation of BOLD signal changes (see Amaro & Barker, 2006). This is based on the observation that

changes in hemodynamic response are rapid and typically occur after the stimulus presentation (Buckner, 1998). Thus, event related designs differ from blocked designs, which test a particular stimulus response across a long period of time, by presenting stimuli from different conditions in a randomised order during the image acquisition. Importantly, event related designs provide the means to investigate the neural correlates of behavioural responses, as the neural response to each trial is analysed. This is particularly useful in measuring effects that are not stable, but are rather dynamic, such as novelty effects. Event-related designs are generally less susceptible to habituation and expectation effects (if they are multiple conditions) at a cost of being more complex in terms of design and analysis.

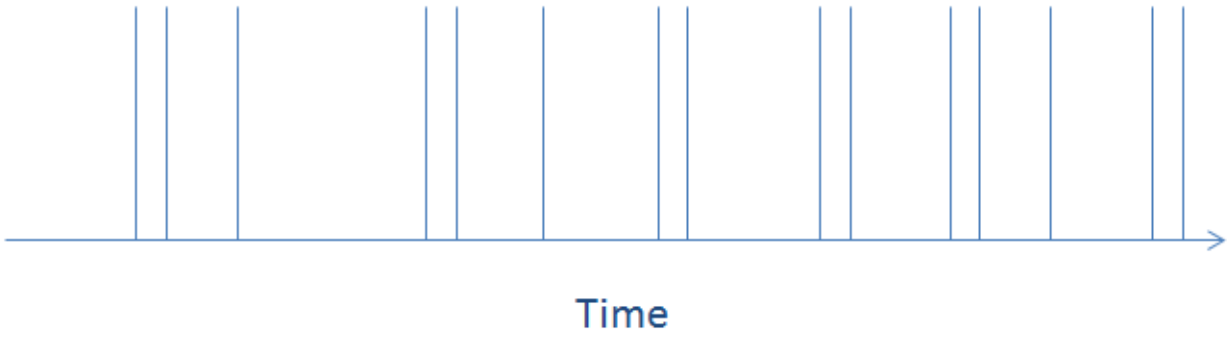

Figure 12: Schematic representation of Event-related design.
The horizontal lines represent the brief stimuli which presented over a period of time.

4.5.3 Mixed Designs

Mixed designs are the combination of event related and blocked design and thus offer the ability to potentially measure the impact of sustained (block) versus transient

(event) neural activity. This allows for the subsequent investigation of brain regions that display item-related (transient) or task-related (sustained) patterns of activation and the ability to draw conclusions that are broadly based on the functional role of the region and not just specifically its anatomical location (Amaro & Barker, 2006; Donaldson, 2004).

4.6 **Statistical modelling**

The analysis of functional images allows identification of brain regions that are active during the task. A number of freely available programs are available for the statistical analysis of functional images. The work presented in this thesis will use the statistical parametric mapping (SPM) approach first defined by Friston, Jezzard & Turner (1994) and later implemented in the SPM analysis package (Wellcome Department of Neurology, UCL, London).

4.6.1 Spatial Image Pre-processing

Standard SPM analysis denotes a pipeline of image transformations that are designed to reduce the amount of unwanted variance that is typically introduced by motion artefacts. The premise is that data from a particular image voxel is derived from a particular location in the brain (Friston, 2003). Motion artefacts essentially change the 3-D position of the voxel in space and have the propensity to show functionally inactive areas as active. This makes isolating a particular region of activity to a

particular region in the brain difficult. Therefore the first step in pre-processing is usually realignment. Realignment in SPM involves the estimation of an 'affine' rigid body transformation that minimises the sum of squared differences between each successive scan and a reference scan. This transformation is applied by re-sampling the data using either a sinc, tri-linear or spline interpolation (Friston, 2003). Additionally the motion parameters can be included as multiple regressors in the design matrix to remove or model out nonlinear effects. These nonlinear effects include movement between slice acquisition, interpolation effects (Grootoonk et al., 2000), nonlinear distortion due to inhomogeneities within the magnetic field (Andersson, Hutton, Ashburner, Turner, & Friston, 2001) and spin-excitation history effects (Friston, Williams, Howard, Frackowiak, & Turner, 1996).

As each individual brain is anatomically different, it would be impossible to compare or combine results between subjects unless they were represented in a standard anatomical space. The normalisation procedure in SPM accomplishes this using a voxel intensity based method which mathematically minimises the sum of squared differences between the original image and a template. Typically the final step in pre-processing is spatial smoothing, which aids in eliminating noise effects due to differences in anatomy by 'blurring' activations with a Gaussian kernel. As noise is a random occurrence, smoothing the data distributes the errors in a normal probability distribution with a cluster around the value of zero. This is also a reasonable representation of an underlying Gaussian field which SPM uses to make inferences

about regional effects. Overall, smoothing improves the overall signal-to-noise (SNR) at the cost of image resolution. An example of a SPM analysis pipeline can be seen in Figure 13.

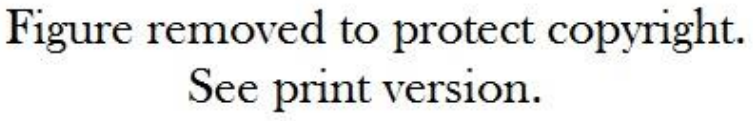

Figure 13: Schematic representation of image transformations that start with an imaging data sequence and end with a SPM.

Note slice timing correction would typically occur before motion correction in event related designs. Voxel-based analyses require the data to be in the same anatomical space: This is effected by realigning the data (and removing movement-related signal components that persist after realignment). After realignment the images are subject to nonlinear warping so that they match a template that already conforms to a standard anatomical space. After smoothing, the general linear model is employed to (i) estimate the parameters of the model and (ii) derive the appropriate univariate test statistic at every voxel (see Figure 4). The test statistics that ensue (usually T or F statistics) constitute the SPM. The final stage is to make statistical inferences on the basis of the SPM and Random Field theory and characterize the responses observed using the fitted responses or parameter estimates. Adapted from Friston el al (2007).

4.6.2 Statistical Analysis and model specification

Statistical parametric mapping uses both the general linear model (GLM) and Gaussian random field (GRF) theory to analyse and make inferences about spatially extended processes through statistical parametric maps (SPMs). Standard GLM design involves modelling data according to this mathematical notion:

$$Y_i = \beta_0 + \beta_1 X_{i1} + \beta_2 X_{i2} + \ldots\ldots + \beta_p X_{ip} + \varepsilon_i$$

Where *p* represents the number of predictors and $\beta_1 \ldots\ldots \beta_p$ represent the independent contributions of *i*th observation of Y, the dependent variable. B_0 represents the set of intercepts, while the error term ε is assumed to be identically and normally distributed. Within SPM, this regression model is calculated within a design matrix where for *i* observations of Y, the above formula can now be expressed in matrix formulation:

$Y = X\beta + \varepsilon$

where Y is the column vector of observed responses, β is the column vector of regression coefficients, including intercepts and the column vector ε which is an unexplained error term. The term X refers to a design matrix that contains all the explanatory variables and corresponds to some effect that has been built into the experiment or that may confound results (like motion parameters, Friston, 2003). Typical GLM analyses rely on the assumption of normality of residuals and errors, but not in the case of timeseries data. FMRI scans are considered to be functions of time, as BOLD signal will correlate with successive scans. As a result they can no longer be

treated as independent samples (Henson, 2003). In order to correct these autocorrelations, the GLM implementation in SPM applies a temporal smoothing function to the timeseries and adjusts the degrees of freedom accordingly (Henson, 2003).

Condition-specific regressors specify the onset of each experimental condition. A boxcar or delta function is convolved to the onset of these trials depending on whether the experimental design is event related or block design. These functions are then convolved with the canonical HRF to account for the temporal characteristics of the BOLD response. Additional user-specified regressors can be added to the design matrix to house conditions that do not need to be convolved with a HRF. These regressors may introduce unwanted effects into the experiment and should be controlled. A common example of this is motion related artefact. Motion regressors were generated during the realignment process of our data and were added to the matrices of Study One and Study Two (Chapters 5 and 6) to covary out any movement related effects.

Inferences on parameter estimates are made using their estimated variance, using either F or T-statistics. F-statistics are used to test whether the null hypothesis is true for all estimates, whilst the T-statistic is used to test whether a particular linear combination of estimates is true for the null hypothesis. Due to the nature of SPM, which essentially conducts a univariate test (also referred to as mass univariate testing) on each individual voxel, this ultimately results in the increase of a type-I error, where a true null hypothesis is accepted as true (i.e. there is no effect in a specified region of

the brain, but it is accepted as if true). For example, if we consider that in a given SPM analysis that roughly 100,000 voxels are subject to mass univariate testing, an alpha level of 5 percent will produce 10,000 voxels that will show up as active even though there is no true effect in the data. Typically, in general statistics, pairwise comparisons would be controlled using a Bonferroni correction, which adjusts the p-value by taking into account the number of comparisons that have been made. In most cases this type of correction is too conservative and also increases the possibility of producing false negatives or type-II errors. This would mean that voxels that should show an effect are below the corrected threshold and do *not* appear as active. SPM uses GRF theory as an alternative to Bonferroni correction by adjusting p-values on the notion that neighbouring voxels are not independent by virtue of continuity in the original data (Friston, 2003). Essentially, while a Bonferroni correction would be expected to control for the number of false positive voxels, a GRF correction would control for the expected false positive regions. As such, a GRF correction is a much more sensitive method than a Bonferroni correction. A GRF correction is dependent on two assumptions,

(i) on the smoothness of the data which is assumed to be a lattice approximation to an underlying random field with a multivariate Gaussian distribution and

(ii) that these fields are continuous, with a differentiable and invertible autocorrelation function (Friston, 2003).

In summary SPMs are image processes with voxel values that under the null hypothesis are distributed according to a probability density function of either the Student's T or F distributions, with each individual voxel being subject to a univariate test (Friston, 2003). SPMs are interpreted as spatially extended statistical processes that fall under the probabilistic behaviour of Gaussian fields. Gaussian random fields model both the univariate probabilistic characteristics of a SPM and any non-stationary spatial covariance structure (Friston, 2003).

4.6.3 Mixed Effects Group Analysis

Standard general linear model assumes one source of independent and identically distributed variation, when in fact there are at least two sources, within subject variance (fixed) & between subject (random) variance. A mixed model accounts for both these sources of variation by modelling fixed and random sources of variation. In a fixed effects model, the assumption is the specific effect of each individual is correlated to the independent variable and thus only accounts for within-subject variability. This means that the only source of variation is measurement error and therefore the magnitude of the overall response is fixed. Results from fixed effects models are difficult to generalise given that a significant effect can be driven by a small proportion of participants. In contrast, random effects analyses assume subject specific effects are 'random' and are not correlated to the independent variable. The two sources of variation are measurement errors and response magnitude is random over subjects. In other words, we are estimating whether the effect size in each

subject is relative to variance between subjects. If this is true, and is usually dependent on sample size, then we can assume a similar effect exists in the greater population. In the case of fMRI, a suitable sample size of ≥ 12 is common for mixed models.

In SPM a mixed model is executed in two levels, a first level or within-subjects level and a 2nd level or between-subject level. Firstly parameter estimates are calculated for each subject at the first level before being entered into a 2nd level analysis. A common 2nd level analysis is a one sample t-test where the estimated effect size or contrast is greater than zero across all subjects.

4.7 **Repetition-Suppression**

Study one (Chapter 5) in this thesis used an fMRI adaption paradigm to investigate BOLD signal changes to repeated and novel conditions. This method results in very specific changes in BOLD responses, namely a reduction in repeated trials. When stimuli are repeated in perceptual or conceptual tasks, a typical response is the increase in performance (e.g. reaction time) when that particular stimulus is encountered again. This phenomenon is referred to as the repetition priming effect. In the brain, this increase in performance is often mirrored by a reduction in neural activity. This reduction in neural activity is referred to as the repetition-suppression effect and has been reported at different spatial scales of brain activity, from the single cell level (Lueschow, Miller, & Desimone, 1994), to the summed macroscopic level of extracranial recordings (EEG, Busch, Groh-Bordin, Zimmer, & Herrmann, 2008) and to

the hemodynamic level (Baumann & Mattingley, 2010; Epstein, Parker, & Feiler, 2008; Grill-Spector, Henson, & Martin, 2006). In the specific case of fMRI, this phenomenon is usually referred to as fMRI-adaptation. BOLD responses to repeated stimuli follow a monotonic decrease in signal strength and typically reach a plateau after 6-8 repetitions (Grill-Spector, et al., 2006). The use of this approach in fMRI has a significant advantage in that it allows for the investigation of sub regions within fMRI voxels (Grill-Spector, et al., 2006). FRMI-adaptation has been demonstrated in multiple brain regions, medial temporal cortex (Stern et al., 1996), frontal cortex (van Turennout, Bielamowicz, & Martin, 2003), visual cortex (Fang, Murray, Kersten, & He, 2005) and PPC (Baumann & Mattingley, 2010). It has been demonstrated in both block (Grill-Spector et al., 1999) and event related paradigms (Baumann & Mattingley, 2010).

4.7.1 Mechanisms underpinning Repetition-Suppression

Four mechanisms are believed to play a role in repetition-suppression effects, firing-rate adaptation, synaptic depression, long-term depression and long-term potentiation (Grill-Spector, et al., 2006). Firing-rate adaptation refers to the reduced excitability of the neuron as a result of an increase in the number of potassium ions which hyperpolarize the membrane potential thereby increasing its conductance. Synaptic depression is believed to occur as a result of a reduction in the presynaptic neurotransmitter release. This has the net effect of reducing the overall efficacy in the neuron's synaptic transmission (Markram & Tsodyks, 1996). Long term depression is a long lasting reduction in synaptic efficacy that reflects plasticity within an area (Ito,

1989). Long-term potentiation is an increase in synaptic efficacy through Hebbian processes. These mechanisms form the basis for three models that have been developed to explain the origin of repetition-suppression effects. These are the fatigue model, the sharpening model and the facilitation model.

The fatigue model states that all neurons that respond to a stimulus show a proportionally equivalent decrease in response to repeated presentations of the same stimulus. Therefore, although the mean neuron population firing rate decreases, there are no changes in the relative pattern of responses from neurons (Grill-Spector, et al., 2006).

The sharpening model differs from the fatigue model in a number of ways (Desimone, 1996). Firstly, in this model not all neurons respond to a stimulus but those that do show repetition-suppression effects. Secondly, these neurons that show repetition-suppression effects code irrelevant information for stimulus identification (Grill-Spector, et al., 2006). Therefore the responses are sharpened resulting in a sparser distributed representation with only a few responsive neurons.

The facilitation model is arguably the simplest of all these models and states repetition-suppression effects occurs as a result of the faster processing of stimuli (Grill-Spector, et al., 2006). One potential explanation of this effect is that repeated information is accrued faster following stimulus presentation (James & Gauthier, 2006). Therefore, neurons that first respond to a stimulus would display reductions in firing latencies for repeated stimuli. This model has some implications for fMRI

investigations as presented stimuli are summed over a few seconds as a result of BOLD lag. Therefore decreases in neural activity would be reflected as decreases in BOLD signal amplitude.

4.8 **Summary**

In summary, fMRI is a useful and non-invasive tool for investigating functional brain activity in humans. The superior spatial resolution offered by this methodology, when used in conjunction with an appropriate study design, makes it a powerful tool for investigating the neural networks that underpin spatial navigation.

5 *Study One: Orientation Specific Activity in Opposing Regions of Retrosplenial and Posterior Parietal Cortex during Navigation: Part A*

5.1 **Abstract**

Functional imaging and clinical evidence suggests the posterior parietal cortex (PPC) and the retrosplenial complex (RSC) are both involved in navigation. In this study we used functional magnetic resonance imaging (fMRI) during the performance of a simple navigation task. Participants were required to navigate to a single target location from a *known* starting orientation. One group of participants (Group A) always had a different starting orientation for every trial whilst the other group (Group B) had three quarters of trials starting from the same *known* orientation. The starting orientation of the remaining quarter of the trials was randomly and unexpectedly *shifted*. We found that brain activations during this task initially occurred within the RSC (Brodmann area 31) with a persistent delayed response within PFm of the PPC. Interestingly, the magnitude of activations was greater for the shifted trials than the control trials of Group B participants, consistent with suppression of activity occurring during trials with repeated starting orientation, suggesting that the activity in both RSC and PPC was specific for orientation within the 3D environment.

5.2 **Introduction**

In primates, navigation is a complex task that requires high level visual processing of landmarks within the environment in order to orient oneself relative to those landmarks. This level of complexity is also reflected in the number of regions that have been implicated in this process, with much of our understanding derived from clinical observations of patients with lesions to specific cortical areas. In particular, an impaired ability to navigate, termed topographical disorientation, arises from damage to any of three main cortical regions that can produce different forms of this disorder (Aguirre & D'Esposito, 1999). These regions are the parahippocampal cortex, the retrosplenial cortex and the posterior parietal cortex (PPC). Patients with damage to the parahippocampal cortex display an impaired ability to represent environmental stimuli such as visual landmarks and consequently have difficulty perceiving and identifying previously familiar buildings or landscapes (Aguirre & D'Esposito, 1999; Barrash, 1998; Barrash, Damasio, Adolphs, & Tranel, 2000; Takahashi & Kawamura, 2002). Those with damage to the retrosplenial cortex display selective deficits in the ability to orientate themselves within the environment and are unable to use landmark information to provide directional cues (Aguirre & D'Esposito, 1999; Ino, et al., 2007; Takahashi, et al., 1997). Damage to the third area, the PPC results in egocentric disorientation, or an inability to represent the location of objects with respect to oneself (Aguirre & D'Esposito, 1999; Barrash, 1998).

The functions of the PPC and RSC have been well-studied using fMRI. An area of the parahippocampal cortex, near the border of the angular lingual gyrus, referred to as the parahippocampal place area (PPA) displays preferential activation during the viewing of visual imagery and is believed to be involved in the perception or encoding of the local scene (Epstein, 2008; Epstein & Kanwisher, 1998). The PPA responds strongly to visual scenes such as landscapes, weakly to non-scene objects like appliances or vehicles and scrambled images. The region does not show any preference for faces like the adjacent fusiform face area within the fusiform gyrus (Downing, Chan, Peelen, Dodds, & Kanwisher, 2006). While the PPA shows preferential activation for the viewing of buildings, the response is smaller than the response to the viewing of landscapes or scenes and therefore the region is commonly known as the scene area (Epstein & Kanwisher, 1998).

Similarly, a region within the retrosplenial cortex, known as the retrosplenial complex (RSC) is also activated on viewing scenes, but the pattern of activation in this area differs from the activity seen in the PPA in that if there is familiarity with the scene, the activation is stronger than if the scene is unfamiliar (Epstein, Higgins, et al., 2007; Sugiura, Shah, Zilles, & Fink, 2005). Additionally, the region is also encodes heading direction (Baumann & Mattingley, 2010).

Much of the electrophysiological data on the PPC concerns eye movements and indicates that the spatial information of visual stimuli is represented within the neuronal activity of many parietal neurons (Andersen, 1989; Andersen, et al., 1992;

Colby, et al., 1996; Duhamel, Colby, & Goldberg, 1998; Heiser & Colby, 2006). This information is task dependent and reflects the upcoming saccade.

PPC neurons display both presaccadic and postsaccadic responses to visual stimuli (Andersen, Bracewell, et al., 1990; Andersen, et al., 1987; Colby, et al., 1996) and current debate is whether this activity is providing spatial information necessary for the generation of the upcoming saccade or reflecting a remapping of the visual environment for the upcoming saccade. Many of the investigations of the PPC neurons have focused on the lateral intraparietal region (LIP) of the intraparietal sulcus (IPS) and area 7a where visually responsive neurons have been shown to reside (Andersen, et al., 1997). These are typically based on a memory saccade paradigm which separates the occurrence of the visual stimulus and the saccade in time. In this task, a monkey is required to memorise the position of a visual stimulus and subsequently reach or look to the location after an intervening delay. The delay period between the visual stimulus and saccade onset is associated with sustained discharge in a significant number of LIP neurons (Andersen, et al., 1992; Colby & Goldberg, 1999; Snyder, et al., 1997; Snyder, et al., 1998). This persistent discharge occurs throughout the delay period and has been postulated to reflect either visuospatial attention (Bisley & Goldberg, 2010; Colby, et al., 1996) or motor planning activity (Andersen & Buneo, 2002; Andersen, et al., 1997).

Area LIP has monosynaptic connections to superior colliculus and the frontal eye fields and appears to be predominantly concerned with saccadic eye movements.

These presaccadic responses are modulated in a monotonic fashion by eye and head position to transform spatial coordinates from the visually acquired retinal coordinates into a body-centred coordinate system (Brotchie, et al., 1995; Snyder, et al., 1998). A neighbouring region, area 7a, also has visually responsive neurons whose activity is modulated by head and eye position (Snyder, et al., 1998). Electrical stimulation of this region also produces spontaneous eye movements in a similar vein to LIP stimulation (Sakata, et al., 1973), but visual responses are postsaccadic in nature and do not appear to play a direct role in saccades (Barash, Bracewell, Fogassi, Gnadt, & Andersen, 1991). Furthermore, the visual receptive fields of 7a neurons are large and bilateral (Motter & Mountcastle, 1981) when compared to the receptive fields in LIP which are smaller and contralateral (Blatt, Andersen, & Stoner, 1990).

Recent experiments have shown that nearly half of 7a neuron activity is modulated by the orientation of the body within the environment, thus providing a world-centred coordinate system of the visual stimuli (Snyder, et al., 1998). While reference frames in body-derived coordinates would be needed to make limb movements which would have to be made with reference to the body, a reference frame in world centred space would be required to maintain a stable percept of the environment during navigation and may also be used to plan limb actions with reference to the external world. This suggests that perceptions of space are derived from a combination of world-centred (allocentric) and body-centred (egocentric) representations.

An area analogous to the primate LIP has been found in humans and is commonly referred to as the parietal eye fields (Brotchie, et al., 2003). This area is located bilaterally in the posterior parietal cortex and displays increased BOLD signal during saccades and is modulated by the position of the head relative to the body. This suggests that the human and non-human primate brains both use a body-centred reference frame for planning saccades. An area that processes the environment in world-centred coordinates has not been found in the human cortex to date.

Recent technological advances in functional magnetic resonance imaging (fMRI) and computer-generated graphics have given researchers the opportunity to study real world navigation in healthy human participants. Most functional imaging investigations of spatial navigation have focussed on identifying the regions involved in navigation rather than the underlying mechanisms. These investigations have used large and sometimes very realistic representations of real world environments (Gron, et al., 2000; Rauchs, et al., 2008; Spiers & Maguire, 2007a). Not surprisingly, a number of cortical areas were active during these tasks including the PPC, hippocampus, RSC, which makes identifying the function of these areas somewhat problematic.

To specifically investigate cortical regions specific to orientation within a virtual environment, we developed a navigation task with repetition suppression of orientation.

5.3 **Methods**

5.3.1 Participants

Thirty-one healthy adults (sixteen males and fifteen females), with no significant history of illness, gave voluntary consent and participated in the study. MRI has no harmful effects on healthy people but in some instances it poses a risk to individuals with certain medical conditions. Exclusion criteria included the presence of implanted metal objects such as cardiac pacemakers, aneurismal clips, inner ear implants, shrapnel, intrauterine devices, ocular prostheses, artificial heart valve, embolisation coils or were pregnant during testing. In addition to this, participants were also screened and excluded if they had a history of movement disorders, neurosurgery, cardiac surgery, currently pregnant and were currently using illicit substances. Written informed voluntary consent was obtained from all participants, and they were advised that they were free to withdraw from the study at any stage. This research was approved by the Human Research Ethics committees of Swinburne University of Technology and St Vincent's Hospital. Participant ages ranged from 18-25 years (M = 21.5 years) and were all right handed. Participants were assigned to either Group A (12 participants) or Group B (19) participants. Group A participants also completed the task in Study Two during their data acquision. The order in which these particpants completed both tasks was fully counterbalanced in order to eliminate any order effects.

5.3.2 Paradigm

The paradigm was designed to perturb a subject's location within a virtual environment while controlling for visual stimulation and motor responses. Prior to functional scanning, participants were made familiar with the sparse virtual 3D virtual environment, presented on an LCD monitor. The environment consisted of a single room with 4 walls in which was positioned a single visual landmark, always situated in the centre of the visual field. The landmark was shaped as a rectangle with only 3 sides so that one's orientation within the room could always be determined by viewing the landmark from any angle. The task consisted of a number of trials in which the subject would move from a starting location to a known destination by pressing either the left or right mouse button (see Figure 14). Pressing the mouse buttons caused the subject to shift sideways to the left or right while always facing the landmark. The destination point was the location at which the landmark was seen face on (see Figure 14). During training, the initial location and orientation of the subject within the environment was always the same, with the subject viewing the landmark from the side. During data acquisition, most trials also commenced from this location so that the subjects remained expectant of this starting location. However, a quarter of the subject's starting locations were slightly rotated within the virtual environment so that they were facing the landmark from a slightly different position. This rotation in position was always less than 45 degrees from the expected starting orientation to allow easy identification of the new location.

Group A participants had different starting orientations for each trial in order to eliminate repetition suppression effects. In 1/3 of these trials the starting orientation was the same as the target orientation so no button press was required. In the remaining trials the starting orientation was randomly selected and different from the target location, requiring a button press to complete the task (Move Condition). In the Move Condition, the starting orientation was either rotated leftward (Left Move Condition) or rightward (Right Move Condition) from the target orientation (30 degrees).

Group B participants had three quarters of the trials start from the exact same orientation so that suppression effects would be maximized (Control Condition). In one quarter of the trials, the starting orientation was randomly shifted (Shifted Condition). The trials with a shifted orientation were never repeated so that neuronal suppression would only exist in the non-shifted trials. These trials had a variation of 15 degrees to 25 degrees from the control condition. In half of these shifted trials, the starting orientation was the same as the target orientation so no button press was required (No Move Condition). The delay period between the onset of the trial and the "GO" signal was randomized between 2 and 6 seconds (M = 4). The "GO" signal was indicated by changing a round visual stimulus from red to green. In order to ensure the effects of orientation on baseline activity were unconfounded or orthogonal as possible, we included a long interstimulus interval (ISI) of 12 seconds. These were included to

ensure we were able to disambiguate orientation effects on transient haemodynamic responses.

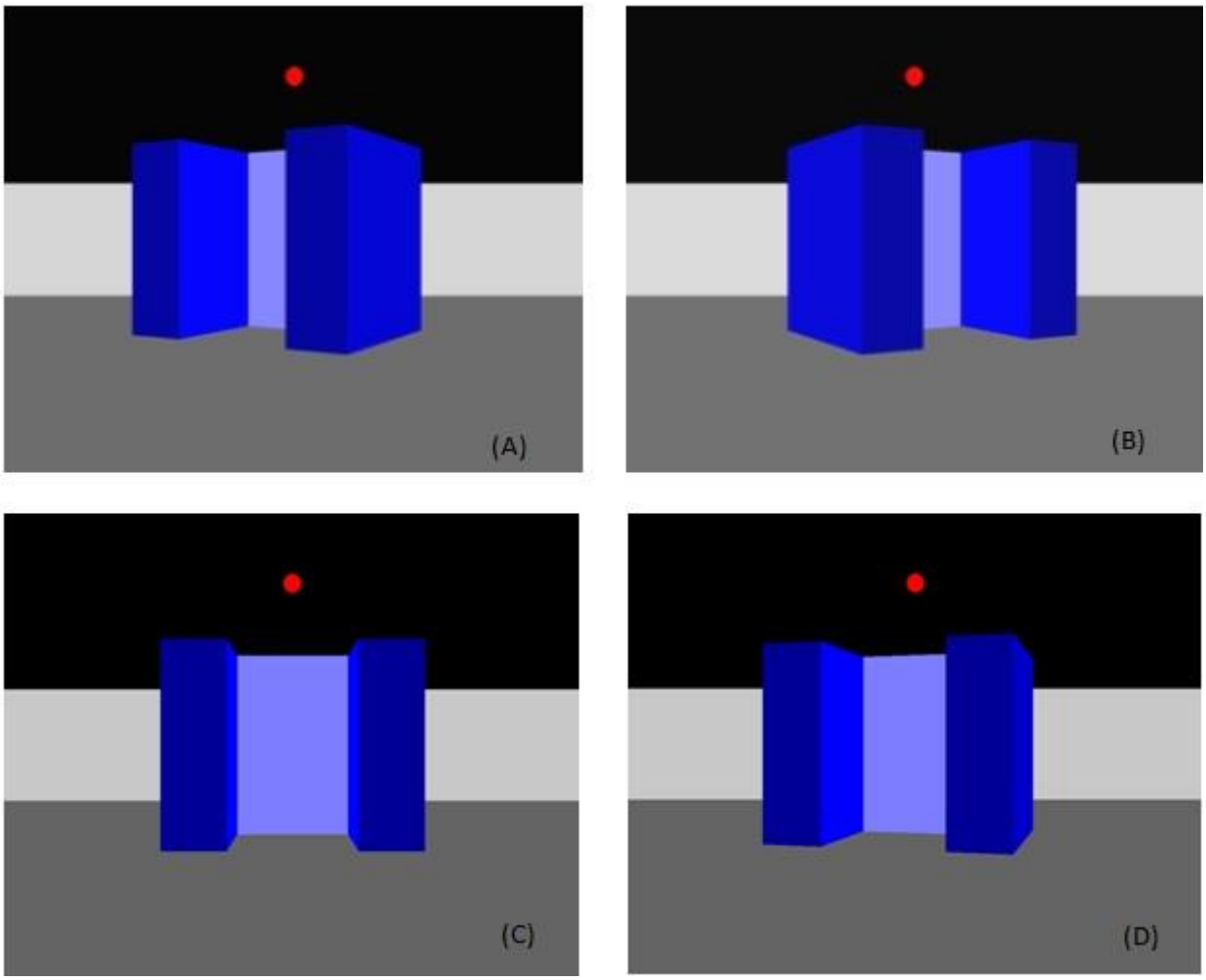

Figure 14: Different event conditions of the simple navigation task.

Starting position for Group A participants was either (A), (B) or (C) with (C) being the final target location. The probability of starting a trial in one of these three conditions was 1/3. Group B participants had ¾ of trials start from (A) and ¼ of trials start from (D). The position of (D) varied from 5 to 25 degrees from (A).

5.3.3 Imaging

Group A: Blood oxygenation level dependent (BOLD) imaging was performed on a 3 Tesla Siemens TIM Trio scanner with a 32-channel head coil (Siemens, Munich, Bavaria, Germany). Thirty-Two BOLD sensitive T2* echoplanar images were obtained in the axial plane with a repetition time of 2.5 seconds (Flip angle = 90°, TE = 30ms, 64 x 64 matrix, 192 x 192 FOV, voxel size = 3x3x3) at 3mm thickness for full brain coverage. In addition a 3-D T1 weighted image (208 images; TR = 1900ms; E = 2.25ms; TI = 900ms; flip angle 9°; 23cm FOV; 232x256 matrix) was also acquired.

Group B: BOLD imaging was performed on a 3 Tesla GE Signa LX scanner with a 32 Channel birdcage quadrature coil (General Electric, Milwaukee, WI, USA). Twenty-one BOLD sensitive T2* echoplanar images were obtained in the sagittal plane with a repetition time of 2.5 seconds (Flip angle = 90°, TE = 40ms, 128 by 128 matrix, 24cm FOV, voxel size = 2x2x2) at 5mm thickness for full brain coverage. In addition, a 3-D T1 weighted image using a fast spoiled gradient recovery sequence (TR = 13.8ms; TE = 2.7; TI = 500ms; flip angle = 20°;25cm FOV; 512 by 512 matrix) was also acquired for each subject.

5.3.4 Data analysis

Subject data was individually screened for outliers, and corrected using algorithms within the ArtRepair toolbox (Centre for Interdisciplinary Brain Sciences Research, Stanford University). Firstly, signal spikes and slow variations were removed using a 17-point moving point average of the data. Signal change greater that 4% of

mean signal was clipped to this value. Secondly, subject (movement) and scanner induced artefacts were screened and corrected using an interpolation function. Subsequent pre-processing and statistical analyses were performed using SPM8 (Wellcome Department of Neurology, UCL, London). Differences in slice acquisition were corrected using the central slice as a reference. All images were aligned to the first image acquired in the time series and a mean image produced. This mean image was warped to a standard EPI template in SPM8 with the parameters from this transformation subsequently applied to all EPI images. Normalised EPI images were smoothed with an 8mm FWHM Gaussian kernel. A high-pass filter with a cut-off of 128s was applied to each participant's data to remove baseline signal drift. Please refer to Appendices (Section 9.1) for the MATLAB script used to perform SPM8 individual participant pre-processing.

5.3.5 First Level Modelling

FMRI time series were modelled as an event related paradigm and analysed by fitting two convolved canonical HRFs and its temporal derivatives to the onset of each trial. The second HRF was specified as an epoch, with corresponding duration being aligned with the pseudorandom delay present at the beginning of each trial. For each participant statistical parametric maps of the t-statistic were generated from the linear contrast of Shifted Onset>Control Onset, Control Onset<Shifted Onset, Shifted Delay>Control Delay and Control Delay>Shifted Delay. The contrast images from this analysis were subsequently included in a second level analysis using the single sample

t-test statistic (please refer to Appendices section 9.2 for the MATLAB script used to create this model). Using standard GLM notation the formula used in this model was expressed as;

$Y = \beta_0 + \beta_1 * X_1 + \beta_2 * X_2 + \beta_3 * X_3 + \beta_4 * X_4 + \xi$

Where;

β_0 = Parameter estimate for implicit baseline

β_1 = Parameter estimate shifted onset

β_2 = Parameter estimate for shifted delay

β_3 = Parameter estimate for control onset

β_4 = Parameter estimate for control delay

ξ = Error Term

5.3.6 Second Level Modelling

Several random effects models were calculated to investigate the effects of orientation change on cortical areas. This was first accomplished by computing the model on each individual's data, followed by running one sample t-tests on the aforementioned contrasts.

5.3.7 Determining functional neuroanatomy

SPMs were overlayed with probabilistic cytoarchitectonic maps using the SPM Anatomy tool box in standard Montreal Neurological Institute space (MNI, Eickhoff et al., 2005)

5.3.8 Region of interest (ROI) analyses

Functional ROIs were defined from the subsequent SPMs and the time course of the average blood oxygenation level-dependent (BOLD) signal change were extracted using MarsBar (http://marsbar.sourceforge.net, Brett, Anton, Valabregue, & Poline, 2002).

5.4 **Results**

5.4.1 Functional brain activation

5.4.1.1 Group A participants

No statistically significant activity was detected between the Left Move contrast>Right Move contrast and Right Move contrast> Left Move contrast for both onset and delay time periods. The combined effects of the movement contrasts were subsequently added to a single contrast (Move condition) and compared to conditions where no button press was required (No Move condition). No statistically significant activity was detected during the onset period for the contrast of Move Condition>No

Move Condition. For the delay period of this contrast, a second level whole brain analysis revealed a number of significantly activated clusters which are displayed below in Table 1: Group activation for Move Condition > No Move Condition.

Table 1: Group activation for Move Condition > No Move Condition contrast

Anatomical regions, Brodmann's Areas (BA) & stereotactic coordinates of the voxels of peak activation for the contrast of Move Condition>No Move Condition delay period.

Anatomical Region	BA	x	y	z	t-value	Cluster Size
SMA	6	-6	-2	54	14.42	3540
V4	18	-32	-82	-4	11.79	1411
hIP2	7c approx.	42	-38	44	9.63	79
Cerebellum Vermis	NA	4	-66	-34	9.58	2174
Precuneus	7a	26	-58	54	8.72	117

Note: FWE corrected, $p<0.05$

As seen above in Table 1, a number of cortical areas were strongly and significantly activated during the delay period of this contrast. Not surprisingly, as this condition required a planned button press, the majority of these activations occur

within regions that have well established motor related and visual responses. This network included HIP2, SMA, 7a, V4 and Cerebellar Vermis.

In contrast, no significant activity was seen in onset period of the No Move Condition>Move. However, during the delay period of this contrast, a small network of very focal activation in the right lateralised cortical regions was found (Table 2). These areas include the primary motor and somatosensory cortices, hIP1 and superior frontal gyrus (SFG).

Table 2: Group activation for No Move Condition > Move Condition contrast

Anatomical regions, Brodmann's Areas (BA) & stereotactic coordinates of the voxels of peak activation for the contrast of No Move Condition> Move Condition delay period.

Anatomical Region	BA	x	y	z	t-value	Cluster Size
PMC & PSC	3&4	34	-30	60	10.77	315
hIP1	7c approx.	40	-60	46	10.06	161
Cuneus	18	-6	-72	18	7.48	425
SFG	NA	30	20	50	5.91	65
SFG	6	-4	24	56	5.14	75

Note: FWE corrected, $p<0.05$

SFG = superior frontal gyrus

PMC = primary motor cortex

PSC = primary somatosensory cortex

5.4.1.2 Group B participants

Second-level whole brain analysis was performed comparing the Shifted and Control Conditions during the trial onset and delay periods of the task, resulting in four comparisons.

1. For the contrast of Shifted > Control during the delay period, one significantly activated cluster was observed ($T(18) = 9.11$, $p<0.05$, FWE), located in the left posterior parietal cortex, (Figure 15, MNI coordinates of peak voxel = -58 -42 38, area PFm, see Eickhoff, et al., 2005).

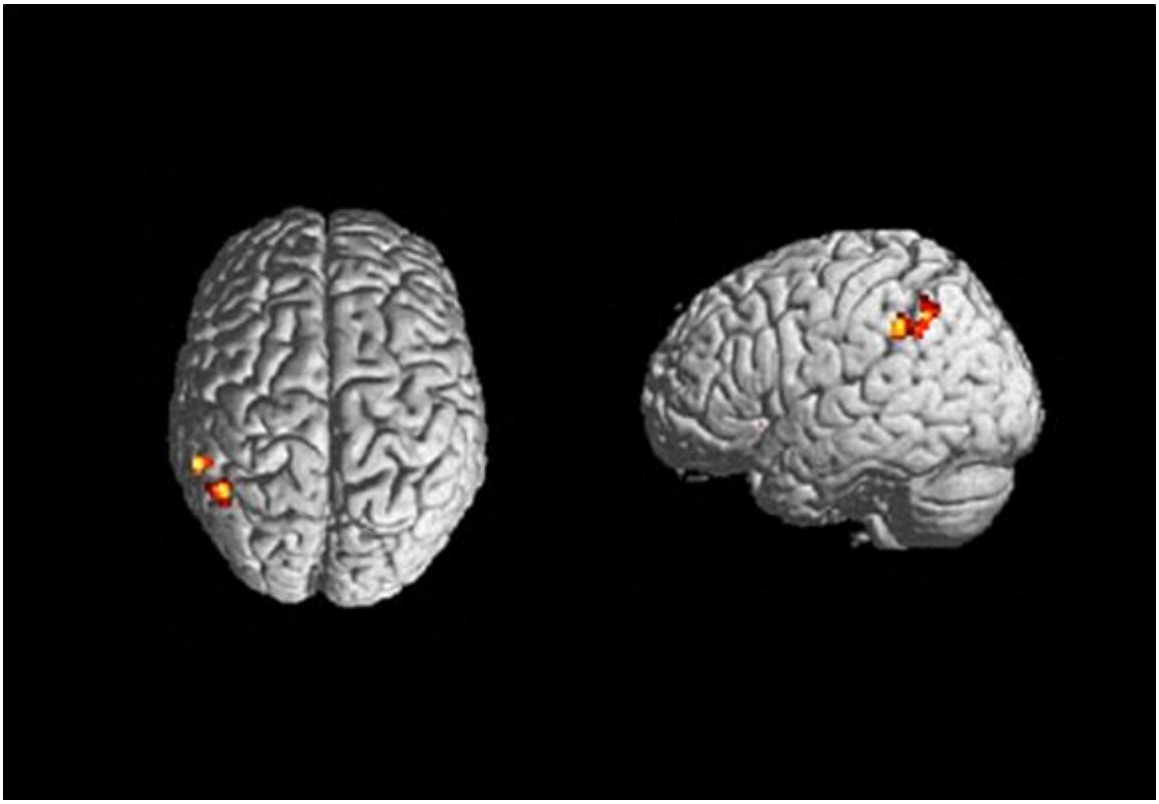

Figure 15: Delayed activity of PFm.

Statistically significant cluster of activity in PFm for Group B participants during the delay period comparing of the Shifted Condition minus the Control Condition (P<0.05, FWE). Image is in neurological coordinates.

2. For the contrast of Shifted > Control during the onset period, one significantly large cluster was activated in the left retrosplenial area (T (18) = 5.34, p<0.05, FWE, MNI coordinates of peak voxel -10 -60 6), corresponding to the location of the left retrosplenial complex (see Figure 16).

3. For the contrast of Control > Shifted during the delay period, significant activation was again seen in the left retrosplenial complex.

4. For the contrast of Control > Shifted during the onset period, significant activation was observed in PFm of left PPC.

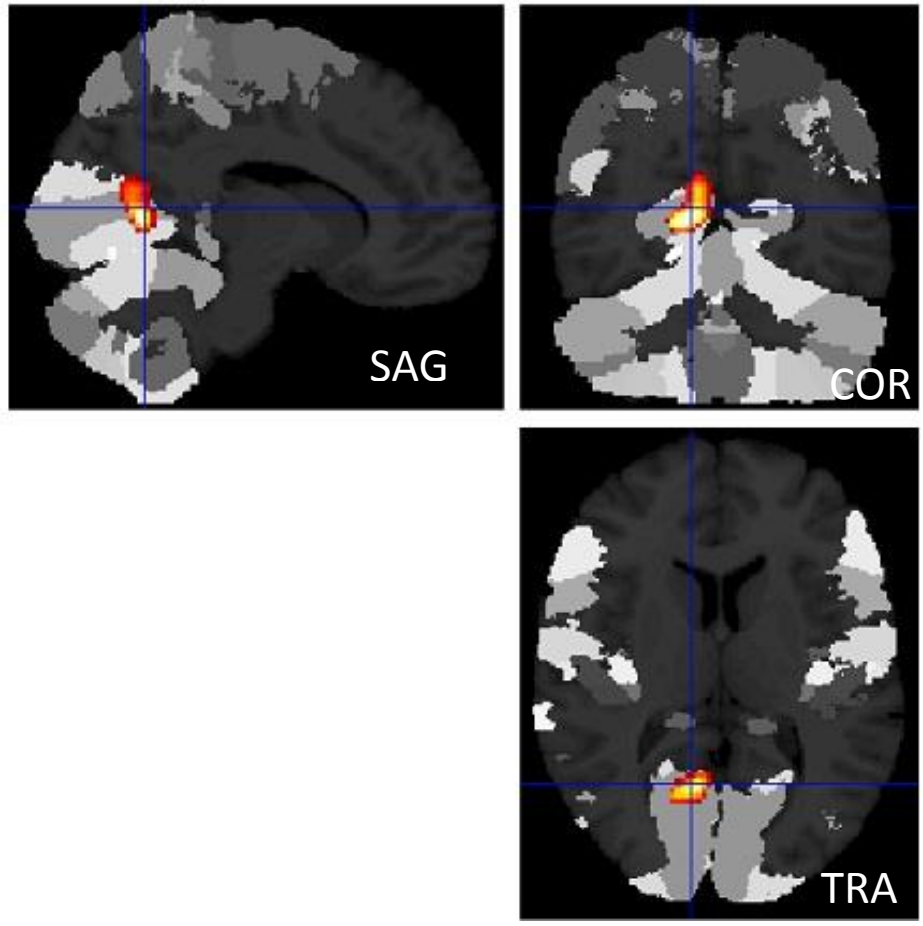

Figure 16: Early response of RSC

Statistically significant cluster of activity (P<0.05,FWE) in RSC of the left posterior parietal cortex in Group B participants during the onset period comparing the Shifted Condition minus the Control Condition. This image was generated using the cytoarchitectonic maps of the SPM Anatomy toolbox (Eickhoff, et al., 2005). Image is in neurological coordinates.

So for each of the four contrasts, either the retrosplenial complex or area PFm of the left PPC was significantly activated, but never in the same contrast. For the contrasts that subtracted the Control from the Shifted Conditions, RSC was activated during the onset period and PFm was activated during the delay period. For the opposite contrasts, PFm was activated during the onset period and RSC was activated in the delay period. To better understand these findings, it is necessary to examine the time-course of the signal within these two regions during the trials. Furthermore, it should be noted that the activation of PFm appears to be bilateral, but due to FWE set-level thresholding this activation is predominately left lateralised.

5.4.2 Region of interest (ROI) analyses

Cytoarchitectonic probability maps were used to identify the regions of activation from the above SPMs using the Anatomy toolbox for SPM (Eickhoff, et al., 2005). Marsbar toolbox for SPM was used to construct a 5mm sphere that was centred on the peak voxel and also used to extract the mean timecourses (percent change of fMRI signal) from these two regions (Figure 17).

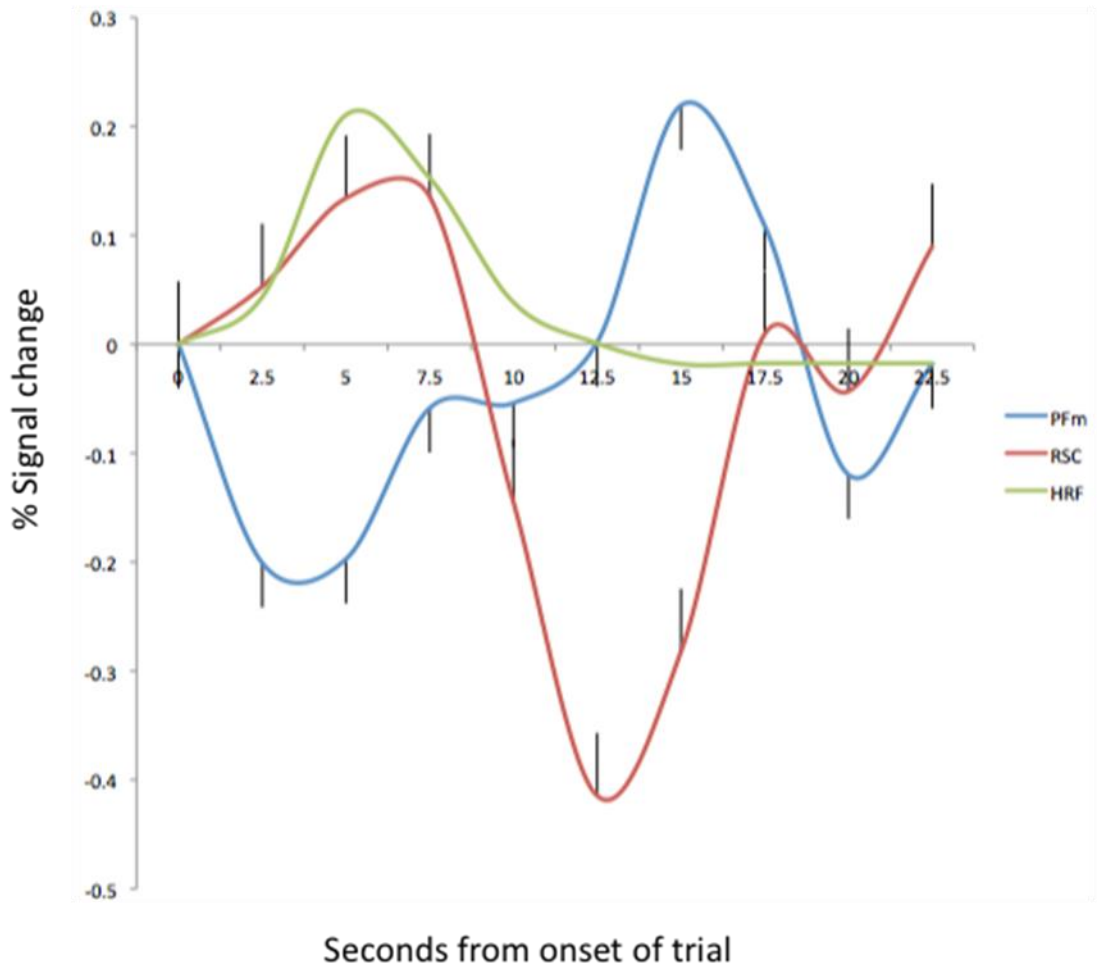

Figure 17: Extracted timecourse from RSC & PFm

Timecourse of signal within the RSC (red) and PFm (blue) of the left PPC of Group B subjects for all trials. Activity in RSC increases at the start of the trial with a similar timecourse to the simulated HRF from SPM8 (grey), then decreases during the delay period. PFm displays a timecourse that is negatively correlated to that of RSC (Pearson's r coefficient $r(18)=-.52, p<0.05$).

Figure 17 shows the time-course for the signal change within the regions of PFm and RSC of the left PPC for all trials for the Group B subjects. A negative correlation for the time-courses between the 2 regions is observed ($p<0.05$). For each region there is a period of increased signal and a period of decreased signal, corresponding to the

onset period and delay period of the task. The signal in RSC increases at the commencement of the trial when the presentation of the visual landmark occurs, whereas the activity decreases in PFm during this period. Later during the delay period, the activity increased in PFm and decreased in RSC. When taking the timecourse into account, it is clear that the activity we observed in each of the four contrasts is due to the inter-trial suppression of the signal in the Control trials for both time periods in both RSC and PFm. Figure 18 shows the timecourses in RSC for the Control and Shifted trials, demonstrating the reduced activity during the Control trials due to inter-trial suppression.

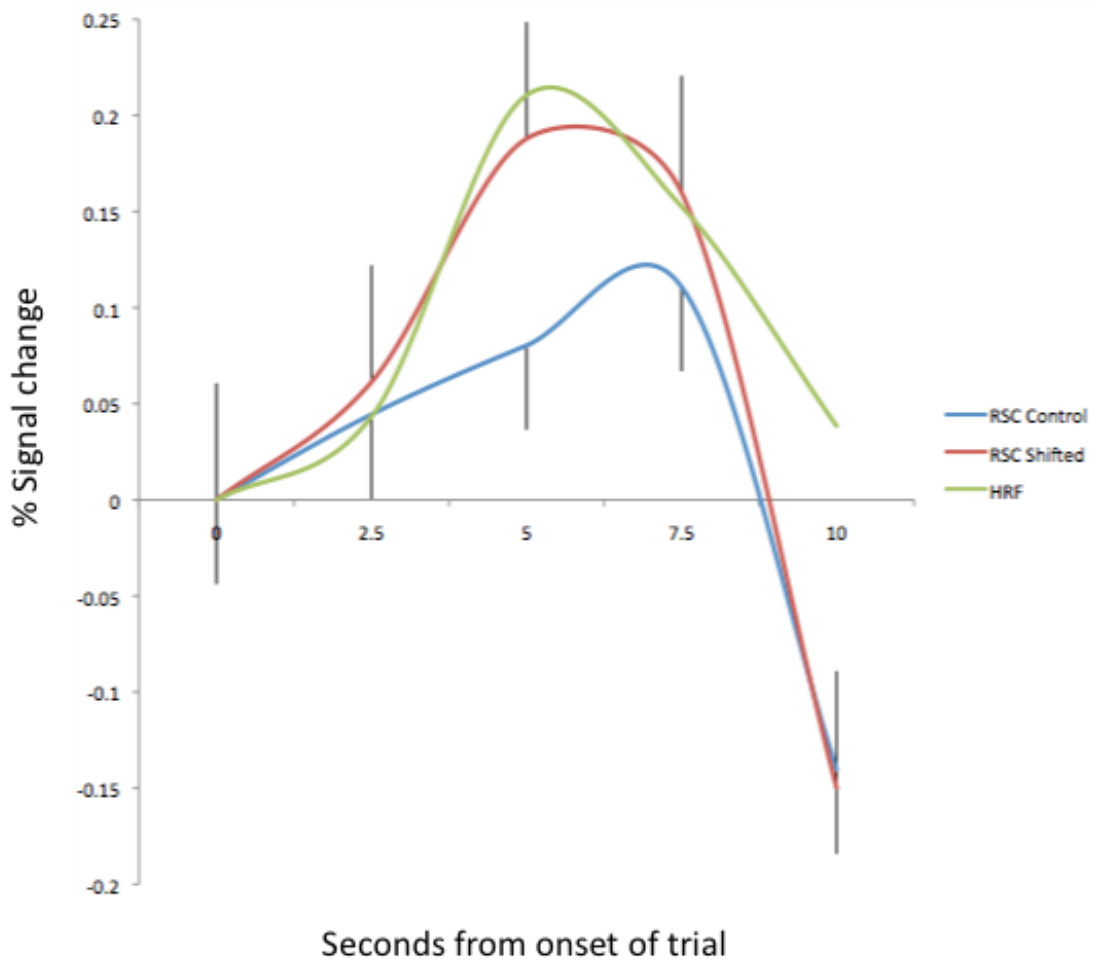

Figure 18: Percent signal change vs. Time

Timecourses in RSC for the Control and Shifted trials, demonstrating the reduced activity during the Control trials due to inter-trial suppression.

5.5 **Discussion**

The goal of the present study was to investigate the functional role of human PPC during navigation. Using a repetition suppression method during fMRI BOLD acquisition, sensitivity of brain activations to orientation within a virtual environment was assessed.

Two time periods in the first task were assessed, the onset period, when the participant first saw the landmark and the delay period, during which the participant planned the appropriate button press. Two cortical regions demonstrated activity specific for the subject's orientation within the environment, RSC and area PFm of the left posterior parietal lobe. RSC was activated in the onset period and PFm was activated during the delay period.

5.5.1 Group A Participants

For Group A participants, the starting position was either shifted 30 degrees to the left, 30 degrees to the right or at the target location in which case no button press was required. There was no significance difference in activity for both onset and delay time periods in trials where participants had to move either left or right to face the target location. The combination of both left and right movement trials (Move) vs. the no movement trials (No Move; participant was already at the target location and did not need to make a button press), saw no significant differences in functional activation during the onset period. However, during the delay period a network of areas was significantly activated. This included the SMA (BA6), hIP2, V4, 7a and the cerebellar vermis. This network of activations can be categorised into either motor or visual areas. When Left and Right movement trials were compared, no significant difference was seen. This suggests that the topography of cortical regions that are sensitive to orientation is of a higher resolution than can be detected by fMRI. The use of fMRI-adaptation techniques on Group B participants highlights the importance of

the technique in investigating these orientation-specific regions, as it allows for the investigation of sub regions within fMRI voxels (Grill-Spector, et al., 2006).

5.5.1.1 Motor-related processing

The SMA and cerebellar vermis were active in the comparison of movement minus no movement trials (bilateral activation in the case of the SMA). In previous research, the SMA has been observed to be active in the delay period of motor tasks most likely reflecting the preparation or planning of a movement (Hanakawa, Dimyan, & Hallett, 2008; Picard & Strick, 2003). Similarly, the role of the cerebellum in executing coordinated motor commands is well established (Waxman, 2003). A significant cluster of activity was also found within hIP2, a region that is located within the IPS. HIP2 is a newly defined human parietal region that is believed to be analogous to AIP of the macaque IPS (Choi et al., 2006). Patients with lesions to this area demonstrate impaired fine motor control (Abela et al., 2012) and difficulties in 3-D object recognition (Hömke et al., 2009). In primates, AIP is responsible for processing visually guided hand and grasp movements (Colby & Goldberg, 1999; Frey, et al., 2005; Sakata, et al., 1997; Taira, et al., 1990). When this area is inactivated by muscimol, the monkey's ability to appropriately shape its hand to grasp an object is comprised, but not its ability to reach for that object. The significant activity seen in hIP2, during Move> No move contrast may be indicative of the processing required to correctly hold the mouse whilst lying in the MRI scanner.

5.5.1.2 Visual processing

Activations occurred in V4 during the first task. Single cell recordings from V4 in primates respond to luminance, colour and the features of objects in the environment (McAdams & Maunsell, 2000; Moran & Desimone, 1985; Motter, 1994). A major aspect of this activity is feature-selective responses, which suggests that V4 may highlight objects in the visual scene at the expense of the background (Motter, 1994). The landmark used in this experiment was clearly distinct from the surrounding background, and the functional activation of V4 during this particular time period suggests that activity is likely to reflect the visual processing of the landmark.

Hippocampus and parahippocampus did not show activation in our data analysis. This is most likely due to the fact that we were comparing conditions that both had landmarks visible. Therefore, even though these regions were most likely active during the task, they were active to similar degrees in the 2 conditions and therefore the activity was subtracted out.

5.5.2 Group B participants

The study of Group B participant used a repetition suppression method to investigate fMRI adaptation for the contrasts of shifted>control & control>shifted in both onset and delay time periods. FMRI responses to repetitive stimuli display a monotonic decrease for subsequent trials that are the same and often reach a plateau typically after 6-8 repetitions (Sayres & Grill-Spector, 2006). This method allowed us to specifically investigate the functional properties of subpopulations of neurons within a

voxel (Krekelberg, Boynton, & van Wezel, 2006). In the onset period of this task, we observed increased BOLD signal within the left RSC. This increase occurred upon initial viewing of the visual landmark and is consistent with previous reports suggesting that viewing visual landmarks specifically activates this region (Epstein, 2008; Epstein, Higgins, et al., 2007). We also observed greater signal change in the region during the Shifted Condition (see Figure 17), indicating specificity of the activity for the orientation of the subject within the environment. This finding is in agreement with recent studies suggesting that this region encodes heading direction or at least detects heading direction after viewing known visual landmarks (Baumann & Mattingley, 2010; Epstein, 2008).

In the delay period, increased activity was seen in area PFm of the left PPC and was greater for the Shifted Condition (See Figure 17), indicating that the activity was specific for the orientation of the subject within the environment.

A number of possibilities exist for what this activity in PFm represents. Since the activity follows that of RSC and retains orientation selectivity, PFm may be taking the spatial information from RSC for the purpose of:

1. Retaining it in short term memory,
2. Transforming the spatial information to generate a motor plan,
3. Transforming the information from allocentric to egocentric coordinates,
4. Creating a cognitive map of space,

5. Combining it with internal cues using path integration to maintain a percept of location and orientation in space.

None of these possibilities are mutually exclusive and the region may be performing any or all of them. It is unlikely that the persistent activity observed in area PFm is related to motor preparation for the button press, as activity related to the preparation for the button press was observed in the supplementary motor area but did not show inter-trial suppression for orientation like the activity in area PFm.

The magnitude of BOLD signal change in area PFm and RSC was greater for the Shifted condition in both time periods due to inter-trial suppression of the Control condition, indicating specificity of their activity for orientation. These two areas were the only cortical regions in the brain exhibiting such behaviour during our navigation task and highlight their importance in navigation. Interestingly, a significant negative correlation of activity was observed between these two regions during the performance of the task. This relationship implies they are inhibitory towards each other.

Two separate mechanisms of navigation are known to exist that both serve to determine self-location within the environment. One process is navigation based on landmarks and relies on external cues, usually visual, to determine self-position. The second mechanism, called path integration relies on an internal memory of the body's location and heading direction in space, and is updated by internal cues such as optic flow and vestibular signals. It is logical that, to some extent, these two mechanisms

would be inhibitory towards each other as they could otherwise output different and incompatible trajectories. Since the activity in RSC is closely related to viewing visual landmarks, it is likely that this region is central to the landmark-based process of navigation. The inhibitory relationship that area PFm and RSC appear to have suggests that PFm may be central to the competing process of path integration. This would fit with the current theories of PPC function, which is known to integrate sensory information from multiple sources such as optic flow and vestibular signals.

6 *Study Two: Orientation Specific Activity in Opposing Regions of Retrosplenial and Posterior Parietal Cortex during Navigation: Part B*

6.1 **Précis**

The results from Study One suggested that RSC is central to landmark-based navigation and PFm is central to path integration. To further examine this hypothesis, a second experiment was developed to compare navigation using a visual landmark to determine orientation versus navigation relying on optic flow to determine orientation.

6.2 **Introduction**

Functional imaging has helped to highlight the distributed network of cortical areas active during navigation (Maguire et al., 1998; Maguire, Frackowiak, & Frith, 1997; Spiers & Maguire, 2007a, 2007b). This network often comprises the hippocampus, RSC, anterior & posterior parietal cortex, and the motor and memory regions of the frontal cortex.

The results obtained from Study One are in line with the findings from previous literature regarding RSC function and provide evidence implicating the PPC in orientation selective processing. The navigation task in Study One required participants to reorient themselves within a virtual environment with a prominently featured landmark from a known starting location, to a known target location. Using an fMRI adaptation technique, we unexpectedly shifted the starting position in some

trials, while the majority of trials began from the known starting position. SPM analysis revealed two significant clusters of activation within the RSC and area PFm of the IPS. For both these cortical regions, there was a period of increased signal and a period of decreased signal relative to baseline, corresponding to the onset and delay periods of the task. The signal in the RSC increased at the commencement of the trial when the presentation of the visual landmark occurred, whereas the signal decreased in PFm during this period. Later, during the delay period, the activity increased in Pfm and decreased in RSC. The BOLD signal within these two cortical regions was negatively correlated ($r(18) = -0.52$, $p<0.05$). The relationship seen in Firure 17 implies RSC and PFm exhibit reciprocal inhibition towards each other and both regions contribute to competing navigation processes.

The orientation selective activation seen during the onset period of the task was in line with previous observations of RSC, which became active upon viewing familiar scenes (Epstein, Higgins, et al., 2007). In addition, the RSC has also been previously implicated in the encoding of directional heading to known landmarks (Baumann & Mattingley, 2010). In contrast, the orientation specific activity of PFm occurred during the delay period of the task (see Figure 17). It is likely that this activation resides within the persistent discharge of parietal neurons. Single cell investigations that utilise a delayed response paradigm typically report persistent activity within PPC neurons that is either related to a planned movement or an expected upcoming visual stimulus (Andersen & Buneo, 2002; Colby, et al., 1996). If the RSC and PFm represent

different navigation mechanisms respectively, then it is logical that an inhibitory relationship exists between these regions, as each system would generate differing output commands and trajectories. As the results indicate that PFm is also sensitive to orientation specificity, the implications arising from the timecourse data indicate that orientation information must first be passed from RSC to PFm once the landmark is visualised and the new orientation is calculated. So while a cursory look at the timecourse data implies an inhibitory relationship between the two regions, the actual relationship might be much more complex.

All animals exhibit two processes of navigation, one based on landmarks and a second process called path integration that is independent of landmarks. When these findings are paired with the results obtained in Study One, it appears the RSC is involved in the processing of visual landmark information in order to determine orientation within the environment. The activity of PFm is likely to reflect the competing process of path integration.

The PPC is known to integrate sensory information from multiple sources such as optic flow, vestibular and motor corollary signals that are required for path integration (Andersen, 1989). In addition, the PPC also receives a vast amount of visual information that it uses to plan, transform and coordinate meaningful motor actions (Andersen & Buneo, 2002; Andersen, et al., 1997; Cohen & Andersen, 2002; Colby & Goldberg, 1999). Therefore, it is likely that PPC maintains a perception of orientation in the absence of visual landmarks.

6.3 **Methods**

6.3.1 Participants

Twelve right-handed male and female participants with a mean age of 21.4 (S.D. = 1.44) participated. These particiapnts also completed the task in Study One and the order in which the tasks were completed was fully counterbalanced. The ethics committees of Barwon Health and Swinburne University of Technology approved this research. The same exclusion criteria from Study One (see section 5.3.1) was also used in this investigation.

6.3.2 Test Protocol

Prior to the fMRI experimental session, all participants attended a practice session that lasted for approximately 20 minutes (see section 6.3.3). In the experimental sessions, participants completed the task whilst undergoing fMRI scanning.

6.3.3 Paradigm

The task contained a single landmark in a visually sparse 3D environment (see Figure 19). The landmark was a red striped pillar that was clearly distinguishable from the black sky and brown patterned ground. The object of this task was to re-orient towards the pillar after a deviation either to the left or right by either 25 or 45 degrees.

At the start of each trial, the participants were rotated either to the left or right of the landmark and continued on a straight trajectory. Eight seconds after the beginning of the trial, the pillar disappeared and the participant was rotated towards the location of the pillar by pressing either the left or right mouse buttons, until they determined they were on a heading directly towards where the landmark had been. At the completion of each trial the pillar reappeared offering a visual confirmation of accuracy.

In the initial segment of the task, the participants were able to determine their orientation by direct visual observation of the landmark (landmark component). After the landmark had disappeared, participants changed their orientation towards the landmark. The only cue they had for estimating their orientation was the rotation of the textured ground of the virtual 3D environment that provided optic flow information. Integration of the optic flow arising from the texture of the ground during the rotation was required to determine the correct orientation towards the invisible landmark and complete the task (path integration component). The BOLD signal from these two components of the task was compared. This task was developed in house at the Faculty of Life and Social Science using Adobe FLASH™.

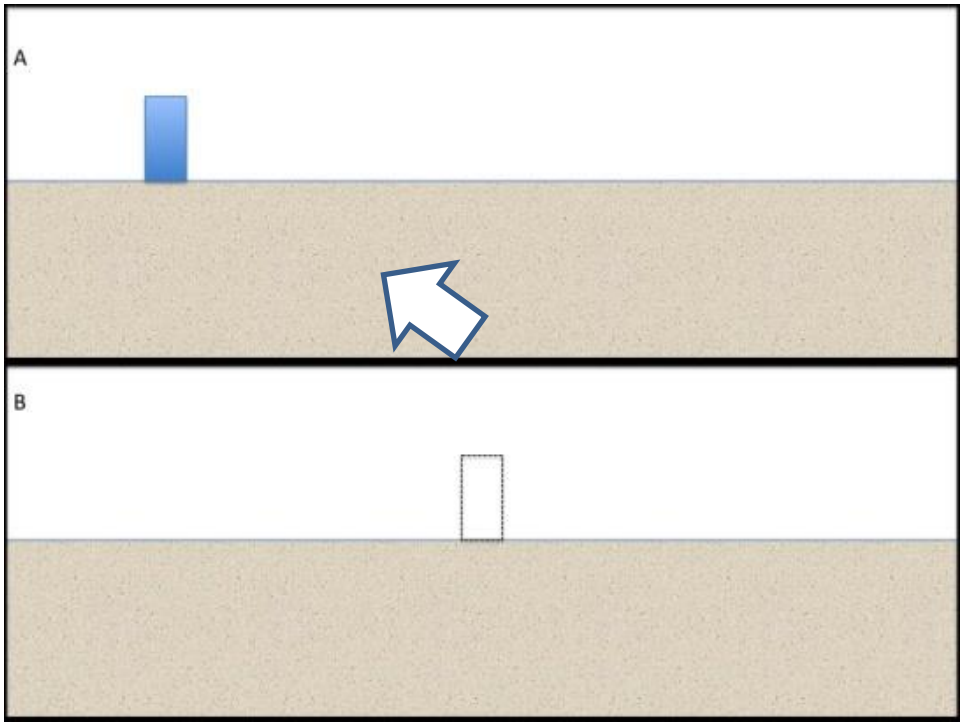

Figure 19: First person view of the "Pillar Task"

A. Subjects travelled in a straight line with the landmark to the left of the centre of the screen. B. When the landmark disappeared, the subjects pushed a button to turn left (or right) and head in the direction of where the landmark had been.

6.3.4 Imaging

FMRI data was acquired in one imaging session that lasted approximately 1 hr in duration. A session contained two functional imaging runs and two structural imaging blocks. The durations of these blocks varied in time. The Pillar task had a duration of 19 mins 30 sec, the T1 structural scan had a duration of 4 mins 36 seconds and the T2 structural scan had a duration of 2 mins 36 secs. Participants lay on their backs in the bore of the magnet and viewed the stimuli via a 45-degree mirror that was attached to the head coil. Whole brain echo-planar imaging (EPI) was conducted using a 3T

Siemens TIM Trio MRI scanner with a 32-channel head coil (Siemens, Munich, Bavaria, Germany). Thirty-Two BOLD sensitive T2* echoplanar images were obtained in the axial plane with a repetition time of 2.5 seconds (Flip angle = 90°, TE = 30ms, 64 x 64 matrix, 192 x 192 FOV, voxel size = 3.0x3.1x3.1) at 3mm thickness for full brain coverage. In addition a 3-D T1 weighted image (208 images; TR = 1900ms; E = 2.25ms; TI = 900ms; flip angle 9°; 23cm FOV; 232x256 matrix) was also acquired.

6.3.5 Data Analysis

This investigation ultised the same analysis approach used in Study One. For more detail, please refer to section 5.3.4.

6.3.6 First Level Modelling

FMRI time series were modelled as an event related paradigm and analysed by fitting two convolved canonical HRFs and their temporal derivatives to two distinct periods in the task. The first HRF was specified as an epoch with a duration of either 3 seconds (for perturbations of 25 degrees) or 4 seconds (for perturbations of 45 degrees). This condition was specified as the Landmark condition. The second HRF was also specified as an epoch with a duration of either 4 seconds (for 25 degree perturbations) or 5 seconds (for 45 degree perturbations). The difference in duration is due to the greater amount of time needed to get back into a desired orientation after a 45 perturbation. This HRF corresponded to the period after the rotation, when the participants were moving forward through the environment without any landmark

present (path integration condition), so that visual stimulation from the optic flow did not corrupt the data.

For each participant, statistical parametric maps of the t-statistic were generated from the linear contrasts comparing the "Landmark" and "Path integration" components of the task (Landmark>Path integration & Path Integration>Landmark). The "Landmark" component consisted of the period at the start of each trial when the subject was able to derive their orientation from the visible landmark. The contrast images from this analysis were subsequently included in a second level analysis using the single sample t-test statistic (please refer to Appendices section 9.3 for the MATLAB script used to create this model). Using standard GLM notation the formula used in this model was expressed as:

$Y = \beta_0 + \beta_1 * X_1 + \beta_2 * X_2 + \xi$

Where;

β_0 = Parameter estimate for implicit baseline

β_1 = Parameter estimate for Landmark condition

β_2 = Parameter estimate for Path Integration

ξ = Error Term

6.3.7 Second Level Modelling

Several random effects models were calculated to investigate the effects of orientation change on cortical areas. This was first accomplished by computing the model on each individual's data, followed by running one sample t-test on the

contrasts. Significant activation for second level t-statistic maps was determined by correcting for family-wise error (FWE) over the whole brain at the cluster level using random field theory as implemented in SPM8 with a standard alpha criterion (α=.05). The co-ordinates of peak voxels reported are in the stereotactic space defined by the Montreal Neurological Institute (MNI space). In addition, SPMs were overlayed with probabilistic cytoarchitectonic maps using the SPM Anatomy tool box in standard Montreal Neurological Institute space (MNI, Eickhoff, et al., 2005).

6.4 **Results**

Second level whole brain analysis revealed a large significant cluster for the contrast of Landmark>Path Integration in the RSC ($T(11) = 6.67$, $p<0.05$ FWE corrected, peak voxel = -5 -54 18, cluster size = 1065). Additionally, significant clusters were also found in the right anterior parietal lobe, in Brodmann area 3 ($T(11) = 8.65$, $p<0.05$ FWE corrected, peak voxel = 42 -30 64, cluster size = 135); right fusiform gyrus ($T(11) = 5.55$, $p<0.05$ FWE corrected, peak voxel = 54 -6 -24, cluster size = 129) and orbitofrontal cortex (OFC) corresponding to Brodmann area 11 ($T(11) = 4.83$, $p<0.05$ FWE corrected, peak voxel = 2 48 -14, cluster size = 198). The SPM displaying significant activity in the RSC during this contrast is displayed in Figure 20.

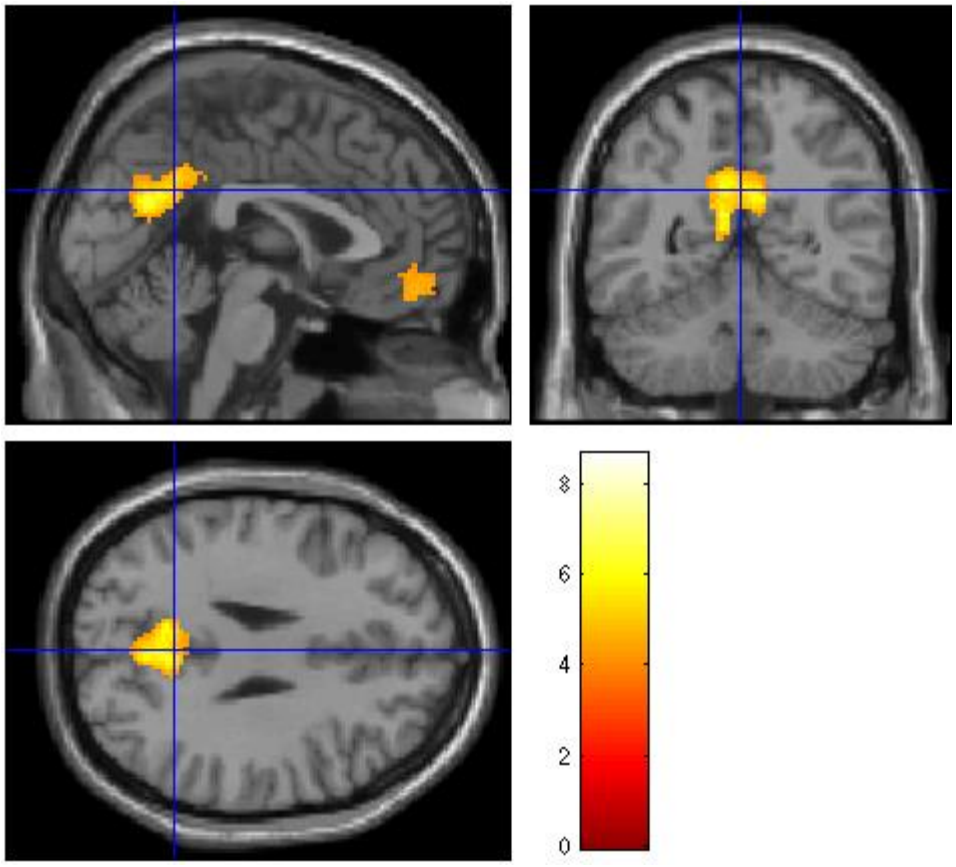

Figure 20: SPM of RSC activation during the visual landmark>path integration contrast.

For the contrast of Path Integration>Landmark a significant cluster was found in area PFm of the PPC (T(11) = 6.22, p<0.05 FWE corrected, peak voxel = 60 -44 44, cluster size = 574). In addition, significant clusters were also found in right anterior cingulate cortex (ACC; T (11) = 7.13, p<0.05 FWE corrected, peak voxel = 12 16 44, cluster size = 341); right inferior frontal gyrus (IFG; T (11) = 6.78, p<0.05 FWE corrected, peak voxel = 54 18 2, cluster size = 842); right superior frontal gyrus (SFG, BA 6; T (11) =

4.91, p<0.05 FWE corrected, peak voxel = 16 10 66, cluster size = 142). The SPM for the above contrast is displayed inFigure 21.

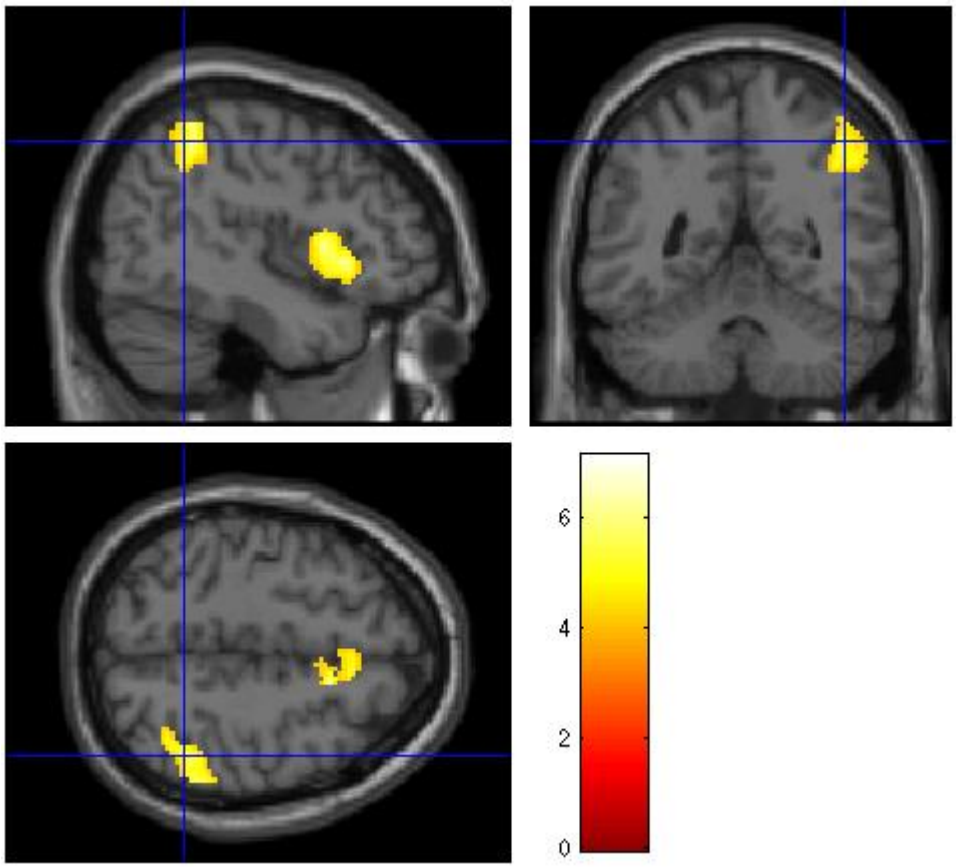

Figure 21: SPM of PFm & IFG activation during the path integration>visual landmark contrast.

6.5 **Discussion**

In the first experiment in this thesis, orientation specific activity was demonstrated in two regions of the brain, PPC and RSC. The cluster of activity within

PPC had peak activation within area 40 of the IPL and is cytoarchitectonically defined as PFm (Eickhoff, et al., 2005).

In the second experiment, the RSC and PFm were shown to be active during navigation based on visual landmarks and path integration respectively. These results imply that PFm is performing path integration by integrating optic flow information with the current estimate of orientation to provide an updated estimate of orientation within the environment.

6.5.1 Landmark Condition

Our results showed that when a participant is navigating through the virtual environment with a visual landmark present, the RSC is active. When this landmark is removed and the participant must rely solely on optic flow for directional information, area PFm is active. In addition to the RSC activation during the visual landmark condition, the primary somatosensory cortex (BA 3), right fusiform gyrus and OFC were also significantly activated. These regions have been previously implicated in decision making processes (OFC, Wallis, 2007), memory for object identity (right fusiform gyrus, Burgess, Maguire, Spiers, & O'Keefe, 2001; Köhler, Moscovitch, Winocur, Houle, & McIntosh, 1998; Moscovitch, Kapur, Köhler, & Houle, 1995; Postle, Stern, Rosen, & Corkin, 2000) and sensory processing (BA 3, Waxman, 2003).

6.5.2 Path Integration condition

Analysis of fMRI data during the path integration condition, a condition where the landmark was absent, revealed PFm to be a focal site of activity within the PPC. As this region demonstrated activity specific for orientation (Study One) it is likely PFm is an important region for navigation and its activity in the absence of a visual landmark is highly suggestive that the region is central to path integration. Path integration is a navigational process that allows people to maintain an accurate representation of direction and location by integrating linear and angular movements (Etienne, et al., 1996; McNaughton, Battaglia, Jensen, Moser, & Moser, 2006; Müller & Wehner, 1988). In rodents, these processes are largely accounted for by MTL areas that have specialised cells that process location in the environment (Hafting, et al., 2005; O'Keefe & Dostrovsky, 1971) such as head direction cells (Ranck, 1973; Taube & Bassett, 2003; Taube, et al., 1990). In humans and primates, the PPC is likely to be a large contributor to this process. Neurons within the PPC process proprioceptive information regarding the position of body limbs and may integrate this information with visual and motor corollary signals (Andersen, et al., 1997), information which is essential for PI. Neurons in area 7a of primate PPC respond to the body's orientation in space (Snyder, et al., 1998) and when lesioned, cause disturbances in the perception of peripersonal space (Matelli, et al., 1984). Path integration is an important navigation process that affords a means of maintaining a stable percept of location and orientation in the environment when no visual landmarks are available to confirm our orientation. The idea that a

region in PPC is central to this process is consistent with current theories of the function of PPC. Single cell recording studies of PPC in primates suggest the region integrates information from multiple sensory modalities as well as from corollary discharges from motor areas to maintain a stable spatial percept (Andersen, et al., 1997). Our results suggest that PFm is the cortical region within PPC that integrates the internal signals within the brain to maintain a stable percept of our orientation within the environment when visual landmarks are not present

In addition to the activation of PFm during the path integration condition, the IFG, ACC and SFG were also activated. The IFG has a role in speech production (via Broca's area) and a role in response inhibition (Aron, Behrens, Smith, Frank, & Poldrack, 2007; Aron, Robbins, & Poldrack, 2004; Hampshire, Chamberlain, Monti, Duncan, & Owen, 2010). In this task, participants were required to actively withhold from making a button press during the trials until they were given a 'go' signal (the landmark disappearing). However, as the IFG was only active during the time period after the button press had been made, it is unlikely the activation of the IFG reflects response inhibition in this task. The activation of the ACC during this condition may reflect involvement in error detection as suggested by previous investigations (Bush et al., 2002; Carter et al., 1998; Taylor et al., 2006). As the perturbation for each trial was different, a new calculation for each button press was required. At the end of each trial, the landmark reappeared to give the participants visual feedback on their performance in that trial. Previous investigations concerning the role of the ACC in

error detection have reported the region active during feedback on performance (Bush, et al., 2002; Taylor, et al., 2006), which implies the region evaluates responses.

The cluster of activity on the anterior surface of BA6 contains the supplementary motor area (SMA). The motor planning and preparatory activity of the SMA is well known and established (Hanakawa, et al., 2008; Picard & Strick, 2003).

6.6 **Conclusion**

Results from this study have identified two regions within the left parietal lobe that are activated during two distinct navigational periods in the task. The RSC was activated during the period of time when the landmark was present. Conversely, PFm was activated during the period of time when the landmark was invisible. As the only source of orientation information could be derived from optic flow, it is likely that PFm contributes to the process of path integration.

7 *General Discussion*

7.1 **Overview**

The aim of this thesis was to advance our understanding of the parietal cortex in spatial navigation. Although this region has already received a tremendous amount of attention in the sciences, its role in navigation is not well understood. By employing the use of simplified navigation paradigms with fMRI, we were able to identify a region within the PPC that appears to be central to path integration, an essential component of navigation. The purpose of this chapter is to discuss these results in light of previous findings and in light of what remains unresolved.

7.2 **Previous literature**

Considering the amount of evidence concerning the involvement of the PPC in the spatial processing, it is somewhat surprising that its involvement in spatial navigation has not been clearly established. Much of our knowledge regarding how the human brain performs navigation tasks is derived from clinical studies detailing impairments that arise from injuries to different cortical regions. To date three main cortical regions have been implicated in topographical disorientation, the parahippocampus, the RS and the PPC. As mentioned in section 5.2, patients with lesions to the parahippocampal cortex display an impaired ability to represent environmental stimuli such as visual landmarks and consequently have difficulty

perceiving and identifying previously familiar buildings or landscapes (Aguirre & D'Esposito, 1999; Barrash, 1998; Barrash, et al., 2000; Takahashi & Kawamura, 2002). Patients with RS lesions develop heading disorientation, a condition where they are unable to extract any directional information from environmental landmarks, while those with lesions to the PPC develop egocentric disorientation, a condition where there is an inability to represent the location of objects with respect to oneself (Aguirre & D'Esposito, 1999; Barrash, 1998). This is commonly seen as misreaching for objects, but patients also cannot describe the relationship between two objects (Holmes & Horrax, 1919; M. Stark, 1996).

There is a considerable amount of functional evidence regarding the RS and parahippocampal cortex in spatial processing. The PPA is a visual landmark responsive region within the parahippocampal cortex, and its processing is believed to reflect a representation of a local scene (Epstein, 2008; Epstein & Kanwisher, 1998). The RSC is also a visual landmark responsive region, but the activity in this region is strongly modulated by familiarity and is more strongly active if the scene contains familiar landmarks (Epstein, Higgins, et al., 2007). More recently, the region has also been implicated in the encoding of heading direction (Baumann & Mattingley, 2010) and in the processing of landmark stability (Auger, et al., 2012). The function of the PPC however, has not been well established using functional imaging.

7.3 **Key Findings**

The orientation specific activation of the RSC in the presence of a landmark confirms the findings of a recent investigation reporting the involvement of the region in the encoding of heading direction (Baumann & Mattingley, 2010). These findings are also in agreement with clinical observations of lesioned patients who can recognise landmarks, but cannot extract directional information with respect to those landmarks (Ino, et al., 2007; Katayama, et al., 1999; Takahashi, et al., 1997). Coupling functional and clinical evidence together suggests the RSC is a critical component of navigation that requires the use of landmarks.

Area PFm, a subregion within PPC, shows activation when landmarks are absent (Study Two) and also displays orientation specific activity (Study One), implying the region is a critical component of path integration.

7.4 **Area PFm and navigation**

In Study one, the activation of PFm followed the activation of RSC. During the onset of the task, PFm was deactivated while RSC was activated relative to baseline. In humans, the RSC is specifically active on viewing visual landmarks and contains information on heading direction. It is highly likely that this region calculates heading direction based on the orientation of the visual landmarks (Baumann & Mattingley, 2010). The RSC is also active during the recognition of familiar visual scenes (Epstein, 2008; Epstein, Higgins, et al., 2007; Epstein, Parker, et al., 2007). As participants in this

both investigations were quite familiar with the tasks (taking into account the pre-scan practise and multiple experimental trials per subject), it is likely the initial activation of the RSC was a combination of the both scene familiarity, and the calculation of orientation. The BOLD signal timecourse from Study One implied an inhibitory relationship between RSC and PFm. One explanation for this relationship is that the activity within the two regions may reflect different processes of navigation, one based on visual landmarks and one based on path integration. As each region would produce different outputs and trajectories, selective inhibition between the two regions would be needed to prevent confusion.

In order to further investigate the role of PFm in navigation, a second fMRI experiment was conducted requiring participants to estimate their orientation within a virtual environment based on the memory of heading direction and path integration derived from optic flow. Similarly as in the first experiment, both the RSC and PFm were active at different time periods in the task. When the participant's orientation was changing with the visible landmark present, the RSC was active. When the participants were navigating without the aid of the landmark and had to rely on path integration and memory, PFm was active. This suggests that area PFm is involved in navigation by path integration and RSC is involved in navigation by visual landmarks. A number of features of PFm support the hypothesis that it is involved in path integration.

(1) The area demonstrates activity specific to heading direction and is therefore part of the navigation system. This was demonstrated using inter-trial suppression of orientation within a virtual environment.

(2) The region does not become active on viewing visual landmarks and is therefore not part of the landmark based navigation system. In fact the BOLD signal reduces in this region on viewing landmarks. The negative correlation of BOLD signal between PFm and RSC suggests that they are inhibitory towards each other during navigation tasks, although the exact nature of this relationship is likely to be much more complex. This would be expected as both regions encode heading directions that could be contradictory.

(3) BOLD signal increased in PFm during a task that required heading direction to be computed by optic flow rather than visual landmarks, which is the basis of path integration.

(4) PFm showed increased activity related only to the spatial aspects of navigation, not to the sensory or motor aspects of the task.

7.5 **Limitations of present work and suggestions for future research**

Although there was a great deal of consistency in the results between the two investigations, it should be noted that there are some issues that warrant caution when interpreting these findings. Firstly, as the results were obtained using fMRI, they

cannot be considered definitive. This is due to the nature of the BOLD response (see Chapter 4), which can only be considered a secondary measure of neural activity

In relation to the imaging parameters, one methodological concern that needs to be addressed is the timing of the regressors. Specifically, in Study One both regressors had the same onset periods and therefore will be highly correlated. In statistics this is referred to as multicollinearity. There are two main issues with multicollinearity. The first is that the overall amount of variance in the model is limited. This is a result of each regressor explaining the same variance as opposed to explaining additional variance. The second concern with multicollinearity is identifying the exact amount of variance that each regressor contributes to the model. As both regressors contribute to the same variance, it is difficult to estimate which regressor contributes to the observed effects. One way of examining the contribution of each regressor would be to run the model with only one predictor, which would give a better indication of its contribution to the total variance. Given the fact that both regressors produced different and non-overlapping activations, I would expect to see a stronger activation as the influence of the other regressor is partialled-out. We used long ITI between trials in each of the two tasks in order to limit the effects of correlated regressors. A suggestion for future research using these paradigms would be to also include long ITIs between regressors in some trials in order to reduce and correlation between the regressors. Given the limitations of fMRI, one suggestion for future research that may address these issues would be to employ the use of MEG. There already exists a

significant body of literature implicating theta and gamma bands in spatial processes (Caplan et al., 2003; Cornwell, Johnson, Holroyd, Carver, & Grillon, 2008; de Araujo, Baffa, & Wakai, 2002; Kahana, Sekuler, Caplan, Kirschen, & Madsen, 1999), and future research using this imaging method may benefit from using adapted versions of the paradigms used in this thesis. Additionally, the increased temporal resolution afforded by MEG results in an overall reduction in the interstimulus interval thereby reducing the data collection time for each participant. By using blind source separation, a process which involves the identification and separation of a source signal from a mixed signal we would be able to investigate the origin of electric and magnetic sources which may supplement the findings obtained in this thesis.

The PPC of the non-human primate has many more functionally defined regions when compared to the human PPC. However, it should be noted that current human cytoarchitectonic post-mortem research does indicate the number of parietal regions is much greater than the more traditionally and commonly used Brodmann labelling convention (Eickhoff, et al., 2005; Scheperjans et al., 2008).

Lastly, the sample size of Study Two was low due to timing contraints. Even though this sample was within the recommended size for maintaining 80% power power at $\alpha = 0.05$ (Desmond & Glover, 2002), a greater sample size would have allowed for a much more generalisable result.

7.6 **Conclusion**

Path integration affords a means of maintaining a stable percept of where we are in the environment when no visual landmarks are available to confirm our orientation. The fact that all mobile animals are capable of path integration highlights its importance. The idea that a region in PPC is central to path integration fits well with current theories of the role of PPC. Single cell recording studies in primates suggest that the region integrates information from multiple sensory modalities as well as from corollary discharges from motor areas to maintain a stable percept of the environment (Andersen, et al., 1997). Our results suggest that PFm is the cortical region that integrates the internal signals within the brain to maintain a stable percept of our location in the environment when visual landmarks are not present.

8 *References*

Abela, E., Missimer, J., Wiest, R., Federspiel, A., Hess, C., Sturzenegger, M., et al. (2012). Lesions to Primary Sensory and Posterior Parietal Cortices Impair Recovery from Hand Paresis after Stroke. *PLoS ONE, 7*(2), e31275.

Aggleton, J. P. (2010). Understanding retrosplenial amnesia: insights from animal studies. *Neuropsychologia, 48*(8), 2328-2338.

Aggleton, J. P., & Vann, S. D. (2004). Testing the importance of the retrosplenial navigation system: lesion size but not strain matters: a reply to Harker and Whishaw. *Neurosci Biobehav Rev, 28*(5), 525-531.

Aguirre, G. K., & D'Esposito, M. (1999). Topographical disorientation: a synthesis and taxonomy. *Brain, 122 (Pt 9)*, 1613-1628.

Aguirre, G. K., Detre, J. A., Alsop, D. C., & D'Esposito, M. (1996). The Parahippocampus Subserves Topographical Learning in Man. *Cereb Cortex, 6*(6), 823-829.

Aguirre, G. K., Zarahn, E., & D'Esposito, M. (1997). Empirical Analyses of BOLD fMRI Statistics. *NeuroImage, 5*(3), 199-212.

Aguirre, G. K., Zarahn, E., & D'Esposito, M. (1998). The Variability of Human, BOLD Hemodynamic Responses. *NeuroImage, 8*(4), 360-369.

Amaral, D. G. (2000). The Functional Organization of Perception of Movement. In E. K. Kandel, J. H. Schwartz & T. M. Jessell (Eds.), *Principles of Neural Science* (4 ed.). New York: McGraw-Hill.

Amaro, E., Jr., & Barker, G. J. (2006). Study design in fMRI: basic principles. *Brain Cogn, 60*(3), 220-232.

Andersen, R. A. (1989). Visual and Eye Movement Functions of the Posterior Parietal Cortex. *Annual Review of Neuroscience, 12*(1), 377-403.

Andersen, R. A. (1998). Multimodal Integration for the Representation of Space in the Posterior Parietal Cortex. In N. Burgess, K. J. Jeffery & J. O'Keefe (Eds.), *The Hippocampal and Parietal Foundations of Spatial Cognition*. Oxford: Oxford University Press.

Andersen, R. A., Asanuma, C., Essick, G., & Siegel, R. M. (1990). Corticocortical connections of anatomically and physiologically defined subdivisions within the inferior parietal lobule. *J Comp Neurol, 296*(1), 65-113.

Andersen, R. A., Bracewell, R. M., Barash, S., Gnadt, J. W., & Fogassi, L. (1990). Eye position effects on visual, memory, and saccade-related activity in areas LIP and 7a of macaque. *J Neurosci, 10*(4), 1176-1196.

Andersen, R. A., Brotchie, P. R., & Mazzoni, P. (1992). Evidence for the lateral intraparietal area as the parietal eye field. *Current Opinion in Neurobiology, 2*(6), 840-846.

Andersen, R. A., & Buneo, C. A. (2002). Intentional Maps in Posterior Parietal Cortex. *Annual Review of Neuroscience, 25*(1), 189-220.

Andersen, R. A., Essick, G. K., & Siegel, R. M. (1985). Encoding of spatial location by posterior parietal neurons. *Science, 230*(4724), 456-458.

Andersen, R. A., Essick, G. K., & Siegel, R. M. (1987). Neurons of area 7 activated by both visual stimuli and oculomotor behavior. *Experimental Brain Research, 67*(2), 316-322.

Andersen, R. A., & Mountcastle, V. (1983). The influence of the angle of gaze upon the excitability of the light- sensitive neurons of the posterior parietal cortex. *The Journal of Neuroscience, 3*(3), 532-548.

Andersen, R. A., Snyder, L. H., Bradley, D. C., & Xing, J. (1997). Multimodal Representation of Space in the Posterior Parietal Cortex and its use in Planning Movements. *Annual Review of Neuroscience, 20*(1), 303-330.

Andersen, R. A., Snyder, L. H., Li, C. S., & Stricanne, B. (1993). Coordinate transformations in the representation of spatial information. *Curr Opin Neurobiol, 3*(2), 171-176.

Andersen, R. A., & Zipser, D. (1988). The role of the posterior parietal cortex in coordinate transformations for visual-motor integration. *Can J Physiol Pharmacol, 66*(4), 488-501.

Andersson, J. L., Hutton, C., Ashburner, J., Turner, R., & Friston, K. (2001). Modeling geometric deformations in EPI time series. *NeuroImage, 13*(5), 903-919.

Ando, S., & Moritake, K. (1990). Pure optic ataxia associated with a right parieto-occipital tumour. *J Neurol Neurosurg Psychiatry, 53*(9), 805-806.

Aron, A. R., Behrens, T. E., Smith, S., Frank, M. J., & Poldrack, R. A. (2007). Triangulating a Cognitive Control Network Using Diffusion-Weighted Magnetic Resonance Imaging (MRI) and Functional MRI. *The Journal of Neuroscience, 27*(14), 3743-3752.

Aron, A. R., Robbins, T. W., & Poldrack, R. A. (2004). Inhibition and the right inferior frontal cortex. *Trends in Cognitive Sciences, 8*(4), 170-177.

Auerbach, S. H., & Alexander, M. P. (1981). Pure agraphia and unilateral optic ataxia associated with a left superior parietal lobule lesion. *J Neurol Neurosurg Psychiatry, 44*(5), 430-432.

Auger, S. D., Mullally, S. L., & Maguire, E. A. (2012). Retrosplenial Cortex Codes for Permanent Landmarks. *PLoS ONE, 7*(8), e43620.

Averbeck, B. B., Battaglia-Mayer, A., Guglielmo, C., & Caminiti, R. (2009). Statistical Analysis of Parieto-Frontal Cognitive-Motor Networks. *Journal of Neurophysiology, 102*(3), 1911-1920.

Baker, R. R. (1968). Sun orientation during migration in some British butterflies. *Proceedings of the Royal Entomological Society of London. Series A, General Entomology, 43*(7-9), 89-95.

Baker, R. R. (1969). The Evolution of the Migratory Habit in Butterflies. *Journal of Animal Ecology, 38*(3), 703-746.

Balint, R. (1909). Seelenlahmung des “Schauens,” optische Ataxie, raumliche Storung der Aufmerksamkeit. *Monatsschr. Psychiatr. Neurol., 25*, 51-81.

Bar, M. (2004). Visual objects in context. [10.1038/nrn1476]. *Nat Rev Neurosci, 5*(8), 617-629.

Barash, S., Bracewell, R. M., Fogassi, L., Gnadt, J. W., & Andersen, R. A. (1991). Saccade-related activity in the lateral intraparietal area. I. Temporal properties; comparison with area 7a. *Journal of Neurophysiology, 66*(3), 1095-1108.

Barrash, J. (1998). A historical review of topographical disorientation and its neuroanatomical correlates. *J Clin Exp Neuropsychol, 20*(6), 807-827.

Barrash, J., Damasio, H., Adolphs, R., & Tranel, D. (2000). The neuroanatomical correlates of route learning impairment. *Neuropsychologia, 38*(6), 820-836.

Barry, C., Hayman, R., Burgess, N., & Jeffery, K. J. (2007). Experience-dependent rescaling of entorhinal grids. [Research Support, Non-U.S. Gov't]. *Nat Neurosci, 10*(6), 682-684.

Batista, A. P., & Andersen, R. A. (2001). The parietal reach region codes the next planned movement in a sequential reach task. *J Neurophysiol, 85*(2), 539-544.

Battaglia-Mayer, A., & Caminiti, R. (2002). Optic ataxia as a result of the breakdown of the global tuning fields of parietal neurones. *Brain, 125*(2), 225-237.

Baumann, O., & Mattingley, J. B. (2010). Medial Parietal Cortex Encodes Perceived Heading Direction in Humans. *J. Neurosci., 30*(39), 12897-12901.

Bennett, A. T. (1996). Do animals have cognitive maps? *J Exp Biol, 199*(1), 219-224.

Berman, R. A., Colby, C. L., Genovese, C. R., Voyvodic, J. T., Luna, B., Thulborn, K. R., et al. (1999). Cortical networks subserving pursuit and saccadic eye movements in humans: an FMRI study. *Hum Brain Mapp, 8*(4), 209-225.

Biegler, R., & Morris, R. G. (1993). Landmark stability is a prerequisite for spatial but not discrimination learning. [10.1038/361631a0]. *Nature, 361*(6413), 631-633.

Biegler, R., & Morris, R. G. (1996). Landmark stability: studies exploring whether the perceived stability of the environment influences spatial representation. *Journal of Experimental Biology, 199*(1), 187-193.

Binkofski, F., Buccino, G., Posse, S., Seitz, R. J., Rizzolatti, G., & Freund, H. J. (1999). A fronto-parietal circuit for object manipulation in man: evidence from an fMRI-study. *European Journal of Neuroscience, 11*(9), 3276-3286.

Bisiach, E., & Luzzatti, C. (1978). Unilateral neglect of representational space. *Cortex, 14*(1), 129-133.

Bisley, J. W., & Goldberg, M. E. (2003). Neuronal activity in the lateral intraparietal area and spatial attention. *Science, 299*(5603), 81-86.

Bisley, J. W., & Goldberg, M. E. (2010). Attention, Intention, and Priority in the Parietal Lobe. *Annual Review of Neuroscience, 33*(1).

Blatt, G. J., Andersen, R. A., & Stoner, G. R. (1990). Visual receptive field organization and cortico-cortical connections of the lateral intraparietal area (area LIP) in the macaque. *The Journal of Comparative Neurology, 299*(4), 421-445.

Bodegard, A., Geyer, S., Grefkes, C., Zilles, K., & Roland, P. E. (2001). Hierarchical processing of tactile shape in the human brain. [Research Support, Non-U.S. Gov't]. *Neuron, 31*(2), 317-328.

Borra, E., Belmalih, A., Calzavara, R., Gerbella, M., Murata, A., Rozzi, S., et al. (2008). Cortical Connections of the Macaque Anterior Intraparietal (AIP) Area. *Cerebral Cortex, 18*(5), 1094-1111.

Bremmer, F., Klam, F., Duhamel, J. R., Ben Hamed, S., & Graf, W. (2002). Visual-vestibular interactive responses in the macaque ventral intraparietal area (VIP). *Eur J Neurosci, 16*(8), 1569-1586.

Bremmer, F., Schlack, A., Duhamel, J.-R., Graf, W., & Fink, G. R. (2001). Space Coding in Primate Posterior Parietal Cortex. *NeuroImage, 14*(1), S46-S51.

Bremmer, F., Schlack, A., Shah, N. J., Zafiris, O., Kubischik, M., Hoffmann, K.-P., et al. (2001). Polymodal Motion Processing in Posterior Parietal and Premotor Cortex: A Human fMRI Study Strongly Implies Equivalencies between Humans and Monkeys. *Neuron, 29*(1), 287-296.

Brett, M., Anton, J.-L., Valabregue, R., & Poline, J.-B. (2002). *Region of interest analysis using an SPM toolbox.* Paper presented at the 8th International Conference on Functional Mapping of the Human Brain, Sendai, Japan.

Brodmann, K. (1909). *Vergleichende Lokalisationslehre der Großhirnrinde in ihren Prinzipien dargestellt auf Grund des Zellenbaues*. Leipzig: Johann Ambrosius Barth Verlag.

Brotchie, P. R., Andersen, R. A., Snyder, L. H., & Goodman, S. J. (1995). Head position signals used by parietal neurons to encode locations of visual stimuli. *Nature, 375*(6528), 232-235.

Brotchie, P. R., Lee, M. B., Chen, D.-Y., Lourensz, M., Jackson, G., & Bradley, W. G. (2003). Head Position Modulates Activity in the Human Parietal Eye Fields. *NeuroImage, 18*(1), 178-184.

Buckner, R. L. (1998). Event-related fMRI and the hemodynamic response. *Hum Brain Mapp, 6*(5-6), 373-377.

Burgess, N., Jeffery, K. J., & O'Keefe, J. (1999). Integrating hippocampal and parietal functions: a spatial point of view. In N. Burgess, K. J. Jeffery & J. O'Keefe (Eds.), *The hippocampal and parietal foundations of spatial cognition* (pp. 3-29). Oxford: Oxford University Press.

Burgess, N., Maguire, E. A., Spiers, H. J., & O'Keefe, J. (2001). A Temporoparietal and Prefrontal Network for Retrieving the Spatial Context of Lifelike Events. *NeuroImage, 14*(2), 439-453.

Burgess, N., Spiers, H. J., & Paleologou, E. (2004). Orientational manoeuvres in the dark: dissociating allocentric and egocentric influences on spatial memory. [Research Support, Non-U.S. Gov't]. *Cognition, 94*(2), 149-166.

Busch, N. A., Groh-Bordin, C., Zimmer, H. D., & Herrmann, C. S. (2008). Modes of memory: early electrophysiological markers of repetition suppression and recognition enhancement predict behavioral performance. *Psychophysiology, 45*(1), 25-35.

Bush, G., Vogt, B. A., Holmes, J., Dale, A. M., Greve, D., Jenike, M. A., et al. (2002). Dorsal anterior cingulate cortex: a role in reward-based decision making. *Proc Natl Acad Sci U S A, 99*(1), 523-528.

Buxbaum, L. J., Ferraro, M. K., Veramonti, T., Farne, A., Whyte, J., Ladavas, E., et al. (2004). Hemispatial neglect: Subtypes, neuroanatomy, and disability. *Neurology, 62*(5), 749-756.

Buxton, R. B. Dynamic models of BOLD contrast. *NeuroImage*(0).

Byrne, P., Becker, S., & Burgess, N. (2007). Remembering the past and imagining the future: a neural model of spatial memory and imagery. *Psychol Rev, 114*(2), 340-375.

Caminiti, R., Chafee, M. V., Battaglia-Mayer, A., Averbeck, B. B., Crowe, D. A., & Georgopoulos, A. P. (2010). Understanding the parietal lobe syndrome from a neurophysiological and evolutionary perspective. *European Journal of Neuroscience, 31*(12), 2320-2340.

Caminiti, R., Ferraina, S., & Johnson, P. B. (1996). The sources of visual information to the primate frontal lobe: a novel role for the superior parietal lobule. *Cereb Cortex, 6*(3), 319-328.

Caplan, J. B., Madsen, J. R., Schulze-Bonhage, A., Aschenbrenner-Scheibe, R., Newman, E. L., & Kahana, M. J. (2003). Human theta oscillations related to sensorimotor integration and spatial learning. *J Neurosci, 23*(11), 4726-4736.

Carter, C. S., Braver, T. S., Barch, D. M., Botvinick, M. M., Noll, D., & Cohen, J. D. (1998). Anterior Cingulate Cortex, Error Detection, and the Online Monitoring of Performance. *Science, 280*(5364), 747-749.

Cavada, C., & Goldman-Rakic, P. S. (1989a). Posterior parietal cortex in rhesus monkey: I. Parcellation of areas based on distinctive limbic and sensory corticocortical connections. *The Journal of Comparative Neurology, 287*(4), 393-421.

Cavada, C., & Goldman-Rakic, P. S. (1989b). Posterior parietal cortex in rhesus monkey: II. Evidence for segregated corticocortical networks linking sensory and limbic areas with the frontal lobe. *J Comp Neurol, 287*(4), 422-445.

Chafee, M. V., & Goldman-Rakic, P. S. (1998). Matching Patterns of Activity in Primate Prefrontal Area 8a and Parietal Area 7ip Neurons During a Spatial Working MemoryTask. *Journal of Neurophysiology, 79*(6), 2919-2940.

Chaminade, T., & Decety, J. (2002). Leader or follower? Involvement of the inferior parietal lobule in agency. [Research Support, Non-U.S. Gov't]. *Neuroreport, 13*(15), 1975-1978.

Chan, E., Baumann, O., Bellgrove, M. A., & Mattingley, J. B. (2012). From objects to landmarks: the function of visual location information in spatial navigation. *Front Psychol, 3*, 304.

Choi, H. J., Zilles, K., Mohlberg, H., Schleicher, A., Fink, G. R., Armstrong, E., et al. (2006). Cytoarchitectonic identification and probabilistic mapping of two distinct areas within the anterior ventral bank of the human intraparietal sulcus. *J Comp Neurol, 495*(1), 53-69.

Cohen, Y. E., & Andersen, R. A. (2000). Reaches to sounds encoded in an eye-centered reference frame. *Neuron, 27*(3), 647-652.
Cohen, Y. E., & Andersen, R. A. (2002). A common reference frame for movement plans in the posterior parietal cortex. *Nat Rev Neurosci, 3*(7), 553-562.
Colby, C. L., & Duhamel, J. R. (1991). Heterogeneity of extrastriate visual areas and multiple parietal areas in the Macaque monkey. *Neuropsychologia, 29*(6), 517-537.
Colby, C. L., Duhamel, J. R., & Goldberg, M. E. (1993). Ventral intraparietal area of the macaque: anatomic location and visual response properties. *J Neurophysiol, 69*(3), 902-914.
Colby, C. L., Duhamel, J. R., & Goldberg, M. E. (1996). Visual, presaccadic, and cognitive activation of single neurons in monkey lateral intraparietal area. *J Neurophysiol, 76*(5), 2841-2852.
Colby, C. L., & Goldberg, M. E. (1999). Space and attention in parietal cortex. *Annual Review of Neuroscience, 22*(1), 319-349.
Compte, A., Brunel, N., Goldman-Rakic, P. S., & Wang, X.-J. (2000). Synaptic Mechanisms and Network Dynamics Underlying Spatial Working Memory in a Cortical Network Model. *Cerebral Cortex, 10*(9), 910-923.
Cooke, D. F., Taylor, C. S., Moore, T., & Graziano, M. S. (2003). Complex movements evoked by microstimulation of the ventral intraparietal area. [Research Support, Non-U.S. Gov't
Research Support, U.S. Gov't, P.H.S.]. *Proc Natl Acad Sci U S A, 100*(10), 6163-6168.
Cooper, B. G., Manka, T. F., & Mizumori, S. J. Y. (2001). Finding your way in the dark: The retrosplenial cortex contributes to spatial memory and navigation without visual cues. *Behavioral Neuroscience, 115*(5), 1012-1028.
Cooper, B. G., & Mizumori, S. J. Y. (2001). Temporary Inactivation of the Retrosplenial Cortex Causes a Transient Reorganization of Spatial Coding in the Hippocampus. *J. Neurosci., 21*(11), 3986-4001.
Corbetta, M., Patel, G., & Shulman, G. L. (2008). The Reorienting System of the Human Brain: From Environment to Theory of Mind. *Neuron, 58*(3), 306-324.
Corbetta, M., & Shulman, G. L. (2002). Control of goal-directed and stimulus-driven attention in the brain. [10.1038/nrn755]. *Nat Rev Neurosci, 3*(3), 201-215.
Cornwell, B. R., Johnson, L. L., Holroyd, T., Carver, F. W., & Grillon, C. (2008). Human hippocampal and parahippocampal theta during goal-directed spatial navigation predicts performance on a virtual Morris water maze. *J Neurosci, 28*(23), 5983-5990.
Cressant, A., Muller, R. U., & Poucet, B. (1997). Failure of Centrally Placed Objects to Control the Firing Fields of Hippocampal Place Cells. *J. Neurosci., 17*(7), 2531-2542.
Critchley, M. (1953). *The Parietal Lobes*. London: Edward Arnold.
Darwin, C. (1873). Origin of certain instincts. *Nature, 7*, 417-418.

de Araujo, D. B., Baffa, O., & Wakai, R. T. (2002). Theta oscillations and human navigation: a magnetoencephalography study. *J Cogn Neurosci, 14*(1), 70-78.
deIpolyi, A. R., Rankin, K. P., Mucke, L., Miller, B. L., & Gorno-Tempini, M. L. (2007). Spatial cognition and the human navigation network in AD and MCI. *Neurology, 69*(10), 986-997.
Desgranges, B., Baron, J. C., Lalevée, C., Giffard, B., Viader, F., de la Sayette, V., et al. (2002). The neural substrates of episodic memory impairment in Alzheimer's disease as revealed by FDG–PET: relationship to degree of deterioration. *Brain, 125*(5), 1116-1124.
Desimone, R. (1996). Neural mechanisms for visual memory and their role in attention. *Proceedings of the National Academy of Sciences, 93*(24), 13494-13499.
Desmond, J. E., & Glover, G. H. (2002). Estimating sample size in functional MRI (fMRI) neuroimaging studies: statistical power analyses. *J Neurosci Methods, 118*(2), 115-128.
DiMattia, B. V., & Kesner, R. P. (1988). Spatial cognitive maps: Differential role of parietal cortex and hippocampal formation. *Behavioral Neuroscience, 102*(4), 471-480.
Donaldson, D. I. (2004). Parsing brain activity with fMRI and mixed designs: what kind of a state is neuroimaging in? *Trends Neurosci, 27*(8), 442-444.
Downing, P. E., Chan, A. W., Peelen, M. V., Dodds, C. M., & Kanwisher, N. (2006). Domain specificity in visual cortex. *Cereb Cortex, 16*(10), 1453-1461.
Duhamel, J.-R., Bremmer, F., BenHamed, S., & Graf, W. (1997). Spatial invariance of visual receptive fields in parietal cortex neurons. [10.1038/39865]. *Nature, 389*(6653), 845-848.
Duhamel, J.-R., Colby, C. L., & Goldberg, M. E. (1998). Ventral Intraparietal Area of the Macaque: Congruent Visual and Somatic Response Properties. *J Neurophysiol, 79*(1), 126-136.
Economo, C. v. (1929). *The Cytoarchitectonics of the Human Cerebral Cortex*. London: Oxford University Press.
Eichenbaum, H. (1997). Declarative memory: Insights from cognitive neurobiology. [Article]. *Annual Review of Psychology, 48*(1), 547.
Eichenbaum, H., Dudchenko, P., Wood, E., Shapiro, M., & Tanila, H. (1999). The Hippocampus, Memory, and Place Cells: Is It Spatial Memory or a Memory Space? *Neuron, 23*(2), 209-226.
Eickhoff, S. B., Stephan, K. E., Mohlberg, H., Grefkes, C., Fink, G. R., Amunts, K., et al. (2005). A new SPM toolbox for combining probabilistic cytoarchitectonic maps and functional imaging data. *NeuroImage, 25*(4), 1325-1335.
Ekstrom, A. D., Kahana, M. J., Caplan, J. B., Fields, T. A., Isham, E. A., Newman, E. L., et al. (2003). Cellular networks underlying human spatial navigation. *Nature, 425*(6954), 184-188.
Enright, J. T. (1972). When the beachhopper looks at the moon: The moon compass

hypothesis. In S. R. Galler, K. Schmidt-Koenig, G. J. Jacobs & R. E. Bellevile (Eds.), *Animal orientation and navigation.* (pp. 523-555). Washington, DC,: NASA US Government Printing Office.

Epstein, R. A. (2008). Parahippocampal and retrosplenial contributions to human spatial navigation. *Trends Cogn Sci, 12*(10), 388-396.

Epstein, R. A., Higgins, J. S., Jablonski, K., & Feiler, A. M. (2007). Visual scene processing in familiar and unfamiliar environments. *J Neurophysiol, 97*(5), 3670-3683.

Epstein, R. A., & Kanwisher, N. (1998). A cortical representation of the local visual environment. *Nature, 392*(6676), 598-601.

Epstein, R. A., Parker, W. E., & Feiler, A. M. (2007). Where Am I Now? Distinct Roles for Parahippocampal and Retrosplenial Cortices in Place Recognition. *The Journal of Neuroscience, 27*(23), 6141-6149.

Epstein, R. A., Parker, W. E., & Feiler, A. M. (2008). Two Kinds of fMRI Repetition Suppression? Evidence for Dissociable Neural Mechanisms. *Journal of Neurophysiology, 99*(6), 2877-2886.

Etienne, A. S., & Jeffery, K. J. (2004). Path integration in mammals. *Hippocampus, 14*(2), 180-192.

Etienne, A. S., Maurer, R., & Seguinot, V. (1996). Path integration in mammals and its interaction with visual landmarks. *J Exp Biol, 199*(Pt 1), 201-209.

Fang, F., Murray, S. O., Kersten, D., & He, S. (2005). Orientation-Tuned fMRI Adaptation in Human Visual Cortex. *Journal of Neurophysiology, 94*(6), 4188-4195.

Faraji, J., Lehmann, H., Metz, G. A., & Sutherland, R. J. (2008). Rats with hippocampal lesion show impaired learning and memory in the ziggurat task: A new task to evaluate spatial behavior. *Behavioural Brain Research, 189*(1), 17-31.

Fox, S. E., & Ranck Jr, J. B. (1975). Localization and anatomical identification of theta and complex spike cells in dorsal hippocampal formation of rats. *Experimental Neurology, 49*(1), 299-313.

Frackowiak, R. S., Friston, K., & Frith, C. D. (2003). *Human Brain Function*. London: Academic Press.

Franzius, M., Vollgraf, R., & Wiskott, L. (2007). From grids to places. *J Comput Neurosci, 22*(3), 297-299.

Frey, S. H., Vinton, D., Norlund, R., & Grafton, S. T. (2005). Cortical topography of human anterior intraparietal cortex active during visually guided grasping. *Brain Res Cogn Brain Res, 23*(2-3), 397-405.

Friston, K. J. (2003). Introduction: experimental design and statistical parametric mapping. In K. J. Friston, J. Ashburner & W. Penny (Eds.), *Human Brain Fuction* (2nd ed.). London.

Friston, K. J., Ashburner, J., Buchel, C., Kiebel, S., & Nichols, T. (Eds.). (2007). *Statistical Parametric Mapping: The Analysis of Functional Brain Images.*
(1st Edition ed.).

Friston, K. J., Jezzard, P., & Turner, R. (1994). Analysis of functional MRI time-series. *Hum Brain Mapp, 1*(2), 153-171.

Friston, K. J., Williams, S., Howard, R., Frackowiak, R. S., & Turner, R. (1996). Movement-related effects in fMRI time-series. *Magn Reson Med, 35*(3), 346-355.

Friston, K. J., Zarahn, E., Josephs, O., Henson, R. N., & Dale, A. M. (1999). Stochastic designs in event-related fMRI. *NeuroImage, 10*(5), 607-619.

Gallistel, C. R. (1993). *The Organization of Learning*. Cambridge, MA: MIT Press.

Gallistel, C. R., & Cramer, A. E. (1996). Computations on metric maps in mammals: getting oriented and choosing a multi-destination route. *J Exp Biol, 199*(Pt 1), 211-217.

Gnadt, J. W., & Andersen, R. A. (1988). Memory related motor planning activity in posterior parietal cortex of macaque. *Exp Brain Res, 70*(1), 216-220.

Goldberg, M. E., Colby, C. L., & Duhamel, J. R. (1990). Representation of visuomotor space in the parietal lobe of the monkey. *Cold Spring Harb Symp Quant Biol, 55*, 729-739.

Goodale, M. A., & Milner, A. D. (1992). Separate visual pathways for perception and action. *Trends in Neurosciences, 15*(1), 20-25.

Goodrich-Hunsaker, N. J., Hunsaker, M. R., & Kesner, R. P. (2005). Dissociating the role of the parietal cortex and dorsal hippocampus for spatial information processing. [Comparative Study

Research Support, N.I.H., Extramural

Research Support, U.S. Gov't, Non-P.H.S.]. *Behav Neurosci, 119*(5), 1307-1315.

Gothard, K. M., Skaggs, W. E., Moore, K. M., & McNaughton, B. L. (1996). Binding of hippocampal CA1 neural activity to multiple reference frames in a landmark-based navigation task. [Research Support, U.S. Gov't, Non-P.H.S.]. *J Neurosci, 16*(2), 823-835.

Gray, H. (1918). *Anatomy of the human body, by Henry Gray. 20th ed., thoroughly rev. and re-edited by Warren H. Lewis.* (20th ed.). Philadelphia

Lea & Febiger.

Greene, K. K., Donders, J., & Thoits, T. (2006). Topographical heading disorientation: a case study. *Appl Neuropsychol, 13*(4), 269-274.

Grefkes, C., & Fink, G. R. (2005). The functional organization of the intraparietal sulcus in humans and monkeys. [Review]. *J Anat, 207*(1), 3-17.

Grefkes, C., Geyer, S., Schormann, T., Roland, P., & Zilles, K. (2001). Human somatosensory area 2: observer-independent cytoarchitectonic mapping, interindividual variability, and population map. [Research Support, Non-U.S. Gov't

Research Support, U.S. Gov't, P.H.S.]. *NeuroImage, 14*(3), 617-631.

Grefkes, C., Ritzl, A., Zilles, K., & Fink, G. R. (2004). Human medial intraparietal cortex subserves visuomotor coordinate transformation. [Research Support, Non-U.S. Gov't]. *NeuroImage, 23*(4), 1494-1506.

Grefkes, C., Weiss, P. H., Zilles, K., & Fink, G. R. (2002). Crossmodal Processing of Object Features in Human Anterior Intraparietal Cortex: An fMRI Study Implies Equivalencies between Humans and Monkeys. *Neuron, 35*(1), 173-184.

Grill-Spector, K., Henson, R., & Martin, A. (2006). Repetition and the brain: neural models of stimulus-specific effects. *Trends in Cognitive Sciences, 10*(1), 14-23.

Grill-Spector, K., Kushnir, T., Edelman, S., Avidan, G., Itzchak, Y., & Malach, R. (1999). Differential Processing of Objects under Various Viewing Conditions in the Human Lateral Occipital Complex. *Neuron, 24*(1), 187-203.

Gron, G., Wunderlich, A. P., Spitzer, M., Tomczak, R., & Riepe, M. W. (2000). Brain activation during human navigation: gender-different neural networks as substrate of performance. *Nat Neurosci, 3*(4), 404-408.

Grootoonk, S., Hutton, C., Ashburner, J., Howseman, A. M., Josephs, O., Rees, G., et al. (2000). Characterization and correction of interpolation effects in the realignment of fMRI time series. *NeuroImage, 11*(1), 49-57.

Grossi, D., Fasanaro, A. M., Cecere, R., Salzano, S., & Trojano, L. (2007). Progressive topographical disorientation: a case of focal Alzheimer's disease. *Neurol Sci, 28*(2), 107-110.

Guthrie, E. R. (1930). Conditioning as a principle of learning. *Psychological Review, 37*(5), 412-428.

Guzowski, J. F., Knierim, J. J., & Moser, E. I. (2004). Ensemble Dynamics of Hippocampal Regions CA3 and CA1. *Neuron, 44*(4), 581-584.

Hafting, T., Fyhn, M., Molden, S., Moser, M. B., & Moser, E. I. (2005). Microstructure of a spatial map in the entorhinal cortex. *Nature, 436*(7052), 801-806.

Hampshire, A., Chamberlain, S. R., Monti, M. M., Duncan, J., & Owen, A. M. (2010). The role of the right inferior frontal gyrus: inhibition and attentional control. *NeuroImage, 50*(3), 1313-1319.

Hanakawa, T., Dimyan, M. A., & Hallett, M. (2008). Motor planning, imagery, and execution in the distributed motor network: a time-course study with functional MRI. *Cereb Cortex, 18*(12), 2775-2788.

Harker, K. T., & Whishaw, I. Q. (2004a). Impaired place navigation in place and matching-to-place swimming pool tasks follows both retrosplenial cortex lesions and cingulum bundle lesions in rats. *Hippocampus, 14*(2), 224-231.

Harker, K. T., & Whishaw, I. Q. (2004b). A reaffirmation of the retrosplenial contribution to rodent navigation: reviewing the influences of lesion, strain, and task. *Neurosci Biobehav Rev, 28*(5), 485-496.

Hartley, T., Trinkler, I., & Burgess, N. (2004). Geometric determinants of human spatial memory. *Cognition, 94*(1), 39-75.

Heide, W., Binkofski, F., Seitz, R. J., Posse, S., Nitschke, M. F., Freund, H. J., et al. (2001). Activation of frontoparietal cortices during memorized triple-step sequences of saccadic eye movements: an fMRI study. *Eur J Neurosci, 13*(6), 1177-1189.

Heiser, L. M., & Colby, C. L. (2006). Spatial Updating in Area LIP Is Independent of Saccade Direction. *J Neurophysiol, 95*(5), 2751-2767.

Henson, R. (Ed.). (2003). *Analysis of fMRI Timeseries: Linear Time-Invariant Models, Event-related fMRI and Optimal Experimental Design*. London: Academic Press.
Hikosaka, O., & Wurtz, R. H. (1983). Visual and oculomotor functions of monkey substantia nigra pars reticulata. III. Memory-contingent visual and saccade responses. *J Neurophysiol, 49*(5), 1268-1284.
Holmes, G. (1918). Disuturbances of Visual Orientation. *The British Journal of Ophthalmology, 2*(9), 449-468.
Holmes, G., & Horrax, G. (1919). DIsturbances of spatial orientation and visual attention, with loss of stereoscopic vision. *Archives of Neurology And Psychiatry, 1*(4), 385-407.
Hömke, L., Amunts, K., Bönig, L., Fretz, C., Binkofski, F., Zilles, K., et al. (2009). Analysis of lesions in patients with unilateral tactile agnosia using cytoarchitectonic probabilistic maps. *Hum Brain Mapp, 30*(5), 1444-1456.
Hu, X., & Yacoub, E. The story of the initial dip in fMRI. *NeuroImage*(0).
Hull, C. L. (1940). *Mathematico deductive theory of rote learning: a study in scientific methodology*. New Haven: Yale University Press.
Ino, T., Doi, T., Hirose, S., Kimura, T., Ito, J., & Fukuyama, H. (2007). Directional Disorientation Following Left Retrosplenial Hemorrhage: a Case Report with FMRI Studies. *Cortex, 43*(2), 248-254.
Ito, M. (1989). Long-term depression. *Annu Rev Neurosci, 12*, 85-102.
Jacobs, S., Danielmeier, C., & Frey, S. H. (2010). Human anterior intraparietal and ventral premotor cortices support representations of grasping with the hand or a novel tool. [Research Support, N.I.H., Extramural
Research Support, Non-U.S. Gov't]. *J Cogn Neurosci, 22*(11), 2594-2608.
James, T. W., & Gauthier, I. (2006). Repetition-induced changes in BOLD response reflect accumulation of neural activity. *Hum Brain Mapp, 27*(1), 37-46.
Jones, E. G., Coulter, J. D., & Hendry, S. H. C. (1978). Intracortical connectivity of architectonic fields in the somatic sensory, motor and parietal cortex of monkeys. *The Journal of Comparative Neurology, 181*(2), 291-347.
Kaas, J. H., Nelson, R. J., Sur, M., Lin, C.-S., & Merzenich, M. M. (1979). Multiple Representations of the Body Within the Primary Somatosensory Cortex of Primates. *Science, 204*(4392), 521-523.
Kahana, M. J., Sekuler, R., Caplan, J. B., Kirschen, M., & Madsen, J. R. (1999). Human theta oscillations exhibit task dependence during virtual maze navigation. *Nature, 399*(6738), 781-784.
Kalaska, J. F., Caminiti, R., & Georgopoulos, A. P. (1983). Cortical mechanisms related to the direction of two-dimensional arm movements: relations in parietal area 5 and comparison with motor cortex. *Exp Brain Res, 51*(2), 247-260.
Karnath, H.-O. (1998). Spatial orientation and the representation of space with parietal lobe lesions. In N. Burgess, K. J. Jeffery & J. O'Keefe (Eds.), *The Hippocampal and Parietal Foundations of Spatial Cognition*. Oxford: Oxford University Press.

Kase, C. S., Troncoso, J. F., Court, J. E., Tapia, J. F., & Mohr, J. P. (1977). Global spatial disorientation. Clinico-pathologic correlations. *J Neurol Sci, 34*(2), 267-278.

Katayama, K., Takahashi, N., Ogawara, K., & Hattori, T. (1999). Pure Topographical Disorientation Due to Right Posterior Cingulate Lesion. *Cortex, 35*(2), 279-282.

Kesner, R. P., Farnsworth, G., & DiMattia, B. V. (1989). Double dissociation of egocentric and allocentric space following medial prefrontal and parietal cortex lesions in the rat. [Research Support, U.S. Gov't, P.H.S.]. *Behav Neurosci, 103*(5), 956-961.

Kesner, R. P., Farnsworth, G., & Kametani, H. (1991). Role of Parietal Cortex and Hippocampus in Representing Spatial Information. *Cerebral Cortex, 1*(5), 367-373.

Klam, F., & Graf, W. (2003). Vestibular signals of posterior parietal cortex neurons during active and passive head movements in macaque monkeys. [Research Support, Non-U.S. Gov't]. *Ann N Y Acad Sci, 1004*, 271-282.

Knierim, J. J., Kudrimoti, H. S., & McNaughton, B. L. (1995). Place cells, head direction cells, and the learning of landmark stability. *J Neurosci, 15*(3 Pt 1), 1648-1659.

Kobayashi, Y., & Amaral, D. G. (2003). Macaque monkey retrosplenial cortex: II. Cortical afferents. *The Journal of Comparative Neurology, 466*(1), 48-79.

Köhler, S., Moscovitch, M., Winocur, G., Houle, S., & McIntosh, A. R. (1998). Networks of domain-specific and general regions involved in episodic memory for spatial location and object identity. *Neuropsychologia, 36*(2), 129-142.

Koyama, M., Hasegawa, I., Osada, T., Adachi, Y., Nakahara, K., & Miyashita, Y. (2004). Functional magnetic resonance imaging of macaque monkeys performing visually guided saccade tasks: comparison of cortical eye fields with humans. [Comparative Study

Research Support, Non-U.S. Gov't]. *Neuron, 41*(5), 795-807.

Kramer, G. (1951). *Eine neve methode zur erforsching der zugorientierung und die bisher damit erzielten Ergebnisse.* Paper presented at the Proceedeings of the 10th Ornithological Congress, Upsala.

Krekelberg, B., Boynton, G. M., & van Wezel, R. J. (2006). Adaptation: from single cells to BOLD signals. *Trends Neurosci, 29*(5), 250-256.

Lewis, J. W., & Van Essen, D. C. (2000a). Corticocortical connections of visual, sensorimotor, and multimodal processing areas in the parietal lobe of the macaque monkey. *J Comp Neurol, 428*(1), 112-137.

Lewis, J. W., & Van Essen, D. C. (2000b). Mapping of architectonic subdivisions in the macaque monkey, with emphasis on parieto-occipital cortex. *J Comp Neurol, 428*(1), 79-111.

Lueschow, A., Miller, E. K., & Desimone, R. (1994). Inferior temporal mechanisms for invariant object recognition. *Cereb Cortex, 4*(5), 523-531.

Maguire, E. A., Burgess, N., Donnett, J. G., Frackowiak, R. S., Frith, C. D., & O'Keefe, J. (1998). Knowing Where and Getting There: A Human Navigation Network. *Science, 280*(5365), 921-924.

Maguire, E. A., Frackowiak, R. S. J., & Frith, C. D. (1997). Recalling Routes around London: Activation of the Right Hippocampus in Taxi Drivers. *J. Neurosci., 17*(18), 7103-7110.

Maguire, E. A., Frith, C. D., Burgess, N., Donnett, J. G., & O'Keefe, J. (1998). Knowing where things are: parahippocampal involvement in encoding object locations in virtual large-scale space. *Journal of Cognitive Neuroscience, v10*(n1), p61(16).

Markram, H., & Tsodyks, M. (1996). Redistribution of synaptic efficacy between neocortical pyramidal neurons. [10.1038/382807a0]. *Nature, 382*(6594), 807-810.

Markus, E. J., Qin, Y. L., Leonard, B., Skaggs, W. E., McNaughton, B. L., & Barnes, C. A. (1995). Interactions between location and task affect the spatial and directional firing of hippocampal neurons. *J. Neurosci., 15*(11), 7079-7094.

Marr, D. (1982). *Vision*. San Francisco: W. H. Freeman.

Martini, F. H. (2001). *Fundamentals of Anatomy and Physiology*. Upper Sadle River, New Jersey: Prentice Hall.

Matelli, M., Gallese, V., & Rizzolatti, G. (1984). Neurological deficit following a lesion in the parietal area 7b in the monkey. *Deficit neurologici conseguenti a lesione dell'area parietale 7b nella scimmia., 60*(4), 839-844.

Matsumura, N., Nishijo, H., Tamura, R., Eifuku, S., Endo, S., & Ono, T. (1999). Spatial- and task-dependent neuronal responses during real and virtual translocation in the monkey hippocampal formation. *J Neurosci, 19*(6), 2381-2393.

Maunsell, J. H., & van Essen, D. C. (1983). The connections of the middle temporal visual area (MT) and their relationship to a cortical hierarchy in the macaque monkey. *J Neurosci, 3*(12), 2563-2586.

May, J. G., & Andersen, R. A. (1986). Different patterns of corticopontine projections from separate cortical fields within the inferior parietal lobule and dorsal prelunate gyrus of the macaque. *Exp Brain Res, 63*(2), 265-278.

Mazzoni, P., Bracewell, R. M., Barash, S., & Andersen, R. A. (1996). Spatially tuned auditory responses in area LIP of macaques performing delayed memory saccades to acoustic targets. [Research Support, Non-U.S. Gov't

Research Support, U.S. Gov't, Non-P.H.S.

Research Support, U.S. Gov't, P.H.S.]. *J Neurophysiol, 75*(3), 1233-1241.

McAdams, C. J., & Maunsell, J. H. R. (2000). Attention to Both Space and Feature Modulates Neuronal Responses in Macaque Area V4. *Journal of Neurophysiology, 83*(3), 1751-1755.

McDonald, R. J., & White, N. M. (1994). Parallel information processing in the water maze: evidence for independent memory systems involving dorsal striatum and hippocampus. *Behav Neural Biol, 61*(3), 260-270.

McNamara, T. P., Sluzenski, J., & Rump, B. (2008). Human spatial memory and navigation. In J. H. Byrne (Ed.), *Learning and Memory: A Comprehensive Reference* (pp. Elsevier).

McNaughton, B. L., Barnes, C. A., & O'Keefe, J. (1983). The contributions of position, direction, and velocity to single unit activity in the hippocampus of freely-moving rats. *Exp Brain Res, 52*(1), 41-49.

McNaughton, B. L., Battaglia, F. P., Jensen, O., Moser, E. I., & Moser, M. B. (2006). Path integration and the neural basis of the 'cognitive map'. *Nat Rev Neurosci, 7*(8), 663-678.

McNaughton, B. L., Chen, L. L., & Markus, E. J. (1991). "Dead reckoning", landmark learning, and the sense of direction: A neurophysiological and computational hypothesis. *J Cogn Neurosci, 3*(2), 190-202.

Medalla, M., & Barbas, H. (2006). Diversity of laminar connections linking periarcuate and lateral intraparietal areas depends on cortical structure. *Eur J Neurosci, 23*(1), 161-179.

Miranda, R., Blanco, E., Begega, A., Rubio, S., & Arias, J. L. (2006). Hippocampal and caudate metabolic activity associated with different navigational strategies. *Behav Neurosci, 120*(3), 641-650.

Moran, J., & Desimone, R. (1985). Selective attention gates visual processing in the extrastriate cortex. *Science, 229*(4715), 782-784.

Morris, R. G. M., Garrud, P., Rawlins, J. N. P., & O'Keefe, J. (1982). Place navigation impaired in rats with hippocampal lesions. [10.1038/297681a0]. *Nature, 297*(5868), 681-683.

Moscovitch, C., Kapur, S., Köhler, S., & Houle, S. (1995). Distinct neural correlates of visual long-term memory for spatial location and object identity: a positron emission tomography study in humans. *Proceedings of the National Academy of Sciences, 92*(9), 3721-3725.

Moser, E. I., Kropff, E., & Moser, M.-B. (2008). Place Cells, Grid Cells, and the Brain's Spatial Representation System. *Annual Review of Neuroscience, 31*(1).

Moser, E. I., & Moser, M.-B. (2008). A metric for space. *Hippocampus, 18*(12), 1142-1156.

Motter, B. C. (1994). Neural correlates of attentive selection for color or luminance in extrastriate area V4. *The Journal of Neuroscience, 14*(4), 2178-2189.

Motter, B. C., & Mountcastle, V. B. (1981). The functional properties of the light-sensitive neurons of the posterior parietal cortex studied in waking monkeys: foveal sparing and opponent vector organization. *J Neurosci, 1*(1), 3-26.

Mou, W., & McNamara, T. P. (2002). Intrinsic frames of reference in spatial memory. *J Exp Psychol Learn Mem Cogn, 28*(1), 162-170.

Mountcastle, V. B., Lynch, J. C., Georgopoulos, A., Sakata, H., & Acuna, C. (1975). Posterior parietal association cortex of the monkey: command functions for operations within extrapersonal space. *Journal of Neurophysiology, 38*(4), 871-908.

Müller, M., & Wehner, R. (1988). Path integration in desert ants, Cataglyphis fortis. *Proceedings of the National Academy of Sciences, 85*(14), 5287-5290.

Muller, R., & Kubie, J. (1987). The effects of changes in the environment on the spatial firing of hippocampal complex-spike cells. *J. Neurosci., 7*(7), 1951-1968.
Murphy, J. J. (1873). Instinct: A Mechanical Analogy. *Nature, 7*, 483.
Nair, D. G. (2005). About being BOLD. *Brain Research Reviews, 50*(2), 229-243.
Neal, J. W., Pearson, R. C. A., & Powell, T. P. S. (1987). The cortico-cortical connections of area 7b, PF, in the parietal lobe of the monkey. *Brain Research, 419*(1-2), 341-346.
Neal, J. W., Pearson, R. C. A., & Powell, T. P. S. (1988). The cortico-cortical connections within the parieto-temporal lobe of area PG, 7a, in the monkey. *Brain Research, 438*(1-2), 343-350.
Neal, J. W., Pearson, R. C. A., & Powell, T. P. S. (1990). The connections of area PG, 7a, with cortex in the parietal, occipital and temporal lobes of the monkey. *Brain Research, 532*(1-2), 249-264.
Nunez, P. L., & Silberstein, R. B. (2000). On the Relationship of Synaptic Activity to Macroscopic Measurements: Does Co-Registration of EEG with fMRI Make Sense? *Brain Topography, 13*(2), 79-96.
O'Craven, K. M., & Kanwisher, N. (2000). Mental Imagery of Faces and Places Activates Corresponding Stimulus-Specific Brain Regions. *Journal of Cognitive Neuroscience, 12*(6), 1013-1023.
O'Keefe, J., & Burgess, N. (1996). Geometric determinants of the place fields of hippocampal neurons. *Nature, 381*(6581), 425-428.
O'Keefe, J., & Conway, D. H. (1978). Hippocampal place units in the freely moving rat: why they fire where they fire. *Exp Brain Res, 31*(4), 573-590.
O'Keefe, J., & Dostrovsky, J. (1971). The hippocampus as a spatial map. Preliminary evidence from unit activity in the freely-moving rat. *Brain Res, 34*(1), 171-175.
O'Keefe, J., & Nadel, L. (1978). *The Hippocampus as a Cognitive Map*. Oxford: Oxford University Press.
Packard, M. G., & McGaugh, J. L. (1992). Double dissociation of fornix and caudate nucleus lesions on acquisition of two water maze tasks: further evidence for multiple memory systems. *Behav Neurosci, 106*(3), 439-446.
Pandya, D. N., & Kuypers, H. G. J. M. (1969). Cortico-cortical connections in the rhesus monkey. *Brain Research, 13*(1), 13-36.
Pandya, D. N., & Seltzer, B. (1982). Intrinsic connections and architectonics of posterior parietal cortex in the rhesus monkey. *J Comp Neurol, 204*(2), 196-210.
Papi, F., & Pardi, L. (1963). On the Lunar Orientation of Sandhoppers (Amphipoda Talitridae). *Biological Bulletin, 124*(1), 97-105.
Paul, R. L., Merzenich, M., & Goodman, H. (1972). Representation of slowly and rapidly adapting cutaneous mechanoreceptors of the hand in brodmann's areas 3 and 1 of Macaca Mulatta. *Brain Research, 36*(2), 229-249.
Penfield, W. (1968). Engrams in the human brain. Mechanisms of memory. *Proc R Soc Med, 61*(8), 831-840.

Penfield, W., & Rasmussen, T. (1950). *The Cerebral Cortex of Man: A Clinical Study of the localization of Function*. New York: Macmillan.

Perenin, M.-T., & Vighetto, A. (1988). Optic Ataxia: A Specfic Disruption in Visuomotor Mechanims. *Brain, 111*(3), 643-674.

Petit, L., & Haxby, J. V. (1999). Functional anatomy of pursuit eye movements in humans as revealed by fMRI. *J Neurophysiol, 82*(1), 463-471.

Picard, N., & Strick, P. L. (2003). Activation of the supplementary motor area (SMA) during performance of visually guided movements. *Cereb Cortex, 13*(9), 977-986.

Pierrot-Deseilligny, C., Milea, D., & Muri, R. M. (2004). Eye movement control by the cerebral cortex. *Curr Opin Neurol, 17*(1), 17-25.

Postle, B. R., Stern, C. E., Rosen, B. R., & Corkin, S. (2000). An fMRI Investigation of Cortical Contributions to Spatial and Nonspatial Visual Working Memory. *NeuroImage, 11*(5), 409-423.

Pothuizen, H. H. J., Aggleton, J. P., & Vann, S. D. (2008). Do rats with retrosplenial cortex lesions lack direction? *European Journal of Neuroscience, 28*(12), 2486-2498.

Pothuizen, H. H. J., Davies, M., Aggleton, J. P., & Vann, S. D. (2010). Effects of selective granular retrosplenial cortex lesions on spatial working memory in rats. *Behavioural Brain Research, 208*(2), 566-575.

Powell, T. P., & Mountcastle, V. B. (1959). Some aspects of the functional organization of the cortex of the postcentral gyrus of the monkey: a correlation of findings obtained in a single unit analysis with cytoarchitecture. *Bull Johns Hopkins Hosp, 105*, 133-162.

Ranck, J. B., Jr. (1973). Studies on single neurons in dorsal hippocampal formation and septum in unrestrained rats. I. Behavioral correlates and firing repertoires. *Exp Neurol, 41*(2), 461-531.

Rauchs, G., Orban, P., Balteau, E., Schmidt, C., Degueldre, C., Luxen, A., et al. (2008). Partially segregated neural networks for spatial and contextual memory in virtual navigation. *Hippocampus, 18*(5), 503-518.

Rivard, B., Li, Y., Lenck-Santini, P. P., Poucet, B., & Muller, R. U. (2004). Representation of objects in space by two classes of hippocampal pyramidal cells. [Research Support, Non-U.S. Gov't

Research Support, U.S. Gov't, P.H.S.]. *J Gen Physiol, 124*(1), 9-25.

Rizzolatti, G., & Matelli, M. (2003). Two different streams form the dorsal visual system: anatomy and functions. *Experimental Brain Research, 153*(2), 146-157.

Rock, I. (1973). *Orientation and Form*. New york: Academic Press.

Rodriguez, P. F. (2010). Human navigation that requires calculating heading vectors recruits parietal cortex in a virtual and visually sparse water maze task in fMRI. *Behavioral Neuroscience, 124*(4), 532-540.

Rogers, J. L., & Kesner, R. P. (2006). Lesions of the Dorsal Hippocampus or Parietal Cortex Differentially Affect Spatial Information Processing. *Behavioral Neuroscience, 120*(4), 852-860.

Rolls, E. T., & O'Mara, S. M. (1995). View-responsive neurons in the primate hippocampal complex. *Hippocampus, 5*(5), 409-424.

Rolls, E. T., Robertson, R. G., & Georges-Francois, P. (1997). Spatial view cells in the primate hippocampus. *Eur J Neurosci, 9*(8), 1789-1794.

Rozzi, S., Calzavara, R., Belmalih, A., Borra, E., Gregoriou, G. G., Matelli, M., et al. (2006). Cortical Connections of the Inferior Parietal Cortical Convexity of the Macaque Monkey. *Cerebral Cortex, 16*(10), 1389-1417.

Rugg, M. D., Fletcher, P. C., Frith, C. D., Frackowiak, R. S., & Dolan, R. J. (1997). Brain regions supporting intentional and incidental memory: a PET study. *Neuroreport, 8*(5), 1283-1287.

Rushworth, M. F. S., Behrens, T. E. J., & Johansen-Berg, H. (2006). Connection Patterns Distinguish 3 Regions of Human Parietal Cortex. *Cerebral Cortex, 16*(10), 1418-1430.

Rushworth, M. F. S., Nixon, P. D., & Passingham, R. E. (1997a). Parietal cortex and movement I. Movement selection and reaching. *Experimental Brain Research, 117*(2), 292-310.

Rushworth, M. F. S., Nixon, P. D., & Passingham, R. E. (1997b). Parietal cortex and movement II. Spatial representation. *Experimental Brain Research, 117*(2), 311-323.

Sakata, H., Taira, M., Kusunoki, M., Murata, A., & Tanaka, Y. (1997). The TINS Lecture The parietal association cortex in depth perception and visual control of hand action. *Trends in Neurosciences, 20*(8), 350-357.

Sakata, H., Taira, M., Murata, A., & Mine, S. (1995). Neural Mechanisms of Visual Guidance of Hand Action in the Parietal Cortex of the Monkey. *Cerebral Cortex, 5*(5), 429-438.

Sakata, H., Takaoka, Y., Kawarasaki, A., & Shibutani, H. (1973). Somatosensory properties of neurons in the superior parietal cortex (area 5) of the rhesus monkey. *Brain Research, 64*, 85-102.

Sandstrom, N. J., Kaufman, J., & Huettel, S. A. (1998). Males and females use different distal cues in a virtual environment navigation task. *Cognitive Brain Research, 6*(4), 351-360.

Santschi, F. (1911). Observations et remarques critiques sur le mécanisme de l'orientation chez les fourmis. *Rev. Suisse Zool, 19*, 305-338.

Sargolini, F., Fyhn, M., Hafting, T., McNaughton, B. L., Witter, M. P., Moser, M. B., et al. (2006). Conjunctive representation of position, direction, and velocity in entorhinal cortex. *Science, 312*(5774), 758-762.

Sauer, E. G. F., & Sauer, E. M. (1960). Star navigation of nocturnal migrating birds. *Cold Spring Habor Symposia on Quantitative Biology, 25*, 463-473.

Save, E., Guazzelli, A., & Poucet, B. (2001). Dissociation of the effects of bilateral lesions of the dorsal hippocampus and parietal cortex on path integration in the rat. [Research Support, Non-U.S. Gov't]. *Behav Neurosci, 115*(6), 1212-1223.

Save, E., Paz-Villagran, V., Alexinsky, T., & Poucet, B. (2005). Functional interaction between the associative parietal cortex and hippocampal place cell firing in the rat. *European Journal of Neuroscience, 21*(2), 522-530.

Save, E., & Poucet, B. (2000). Involvement of the hippocampus and associative parietal cortex in the use of proximal and distal landmarks for navigation. *Behavioural Brain Research, 109*(2), 195-206.

Save, E., Poucet, B., Foreman, N., & Buhot, M. C. (1992). Object exploration and reactions to spatial and nonspatial changes in hooded rats following damage to parietal cortex or hippocampal formation. [Research Support, Non-U.S. Gov't]. *Behav Neurosci, 106*(3), 447-456.

Sayres, R., & Grill-Spector, K. (2006). Object-selective cortex exhibits performance-independent repetition suppression. *J Neurophysiol, 95*(2), 995-1007.

Scheperjans, F., Eickhoff, S. B., Homke, L., Mohlberg, H., Hermann, K., Amunts, K., et al. (2008). Probabilistic maps, morphometry, and variability of cytoarchitectonic areas in the human superior parietal cortex. *Cereb Cortex, 18*(9), 2141-2157.

Scoville, W. B. (1954). The limbic lobe in man. *J Neurosurg, 11*(1), 64-66.

Scoville, W. B., & Milner, B. (1957). Loss of recent memory after bilateral hippocampal lesions. *J Neurol Neurosurg Psychiatry, 20*(1), 11-21.

Seltzer, B., & Pandya, D. N. (1980). Converging visual and somatic sensory cortical input to the intraparietal sulcus of the rhesus monkey. *Brain Research, 192*(2), 339-351.

Seltzer, B., & Pandya, D. N. (1984). Further observations on parieto-temporal connections in the rhesus monkey. *Experimental Brain Research, 55*(2), 301-312.

Seltzer, B., & Van Hoesen, G. W. (1979). A direct inferior parietal lobule projection to the presubiculum in the rhesus monkey. *Brain Research, 179*(1), 157-161.

Shibutani, H., Sakata, H., & Hyvarinen, J. (1984). Saccade and blinking evoked by microstimulation of the posterior parietal association cortex of the monkey. *Exp Brain Res, 55*(1), 1-8.

Shulman, G. L., McAvoy, M. P., Cowan, M. C., Astafiev, S. V., Tansy, A. P., d'Avossa, G., et al. (2003). Quantitative analysis of attention and detection signals during visual search. [Research Support, U.S. Gov't, P.H.S.]. *J Neurophysiol, 90*(5), 3384-3397.

Siegel, A. W., & White, S. H. (Eds.). (1975). *The development of spatial representations of large-scale environments.* (Vol. 10). New York: Academic Press.

Simon, O., Mangin, J. F., Cohen, L., Le Bihan, D., & Dehaene, S. (2002). Topographical layout of hand, eye, calculation, and language-related areas in the human parietal lobe. [Research Support, Non-U.S. Gov't]. *Neuron, 33*(3), 475-487.

Snyder, L. H., Batista, A. P., & Andersen, R. A. (1997). Coding of intention in the posterior parietal cortex. [10.1038/386167a0]. *Nature, 386*(6621), 167-170.
Snyder, L. H., Batista, A. P., & Andersen, R. A. (2000). Intention-related activity in the posterior parietal cortex: a review. *Vision Res, 40*(10-12), 1433-1441.
Snyder, L. H., Grieve, K. L., Brotchie, P. R., & Andersen, R. A. (1998). Separate body- and world-referenced representations of visual space in parietal cortex. *Nature, 394*(6696), 887-891.
Soechting, J. F., & Flanders, M. (1992). Moving in Three-Dimensional Space: Frames of Reference, Vectors, and Coordinate Systems. *Annu Rev Neurosci, 15*(1), 167-191.
Spiers, H. J., & Maguire, E. A. (2006). Thoughts, behaviour, and brain dynamics during navigation in the real world. *NeuroImage, 31*(4), 1826-1840.
Spiers, H. J., & Maguire, E. A. (2007a). A navigational guidance system in the human brain. *Hippocampus, 17*(8), 618-626.
Spiers, H. J., & Maguire, E. A. (2007b). The neuroscience of remote spatial memory: A tale of two cities. *Neuroscience, 149*(1), 7-27.
Squire, L. R. (1987). *Memory and Brain*. New York: Oxford University Press.
Stankiewicz, B. J., & Kalia, A. A. (2007). Acquisition of structural versus object landmark knowledge. *J Exp Psychol Hum Percept Perform, 33*(2), 378-390.
Stark, C. E. L., & Squire, L. R. (2001). When zero is not zero: The problem of ambiguous baseline conditions in fMRI. *Proceedings of the National Academy of Sciences, 98*(22), 12760-12766.
Stark, M. (1996). Impairment of an Egocentric Map of Locations: Implications for Perception and Action. *Cognitive Neuropsychology, 13*(4), 481 - 524.
Stern, C. E., Corkin, S., Gonzalez, R. G., Guimaraes, A. R., Baker, J. R., Jennings, P. J., et al. (1996). The hippocampal formation participates in novel picture encoding: evidence from functional magnetic resonance imaging. *Proc Natl Acad Sci U S A, 93*(16), 8660-8665.
Stricanne, B., Andersen, R. A., & Mazzoni, P. (1996). Eye-centered, head-centered, and intermediate coding of remembered sound locations in area LIP. [Research Support, Non-U.S. Gov't
Research Support, U.S. Gov't, Non-P.H.S.
Research Support, U.S. Gov't, P.H.S.]. *J Neurophysiol, 76*(3), 2071-2076.
Sugiura, M., Shah, N. J., Zilles, K., & Fink, G. R. (2005). Cortical representations of personally familiar objects and places: functional organization of the human posterior cingulate cortex. *J Cogn Neurosci, 17*(2), 183-198.
Taira, M., Mine, S., Georgopoulos, A. P., Murata, A., & Sakata, H. (1990). Parietal cortex neurons of the monkey related to the visual guidance of hand movement. *Exp Brain Res, 83*(1), 29-36.
Takahashi, N., & Kawamura, M. (2002). Pure Topographical Disorientation —The Anatomical Basis of Landmark Agnosia. *Cortex, 38*(5), 717-725.

Takahashi, N., Kawamura, M., Shiota, J., Kasahata, N., & Hirayama, K. (1997). Pure topographic disorientation due to right retrosplenial lesion. *Neurology, 49*(2), 464-469.

Taube, J. S. (1998). Head direction cells and the neurophysiological basis for a sense of direction. *Progress in Neurobiology, 55*(3), 225-256.

Taube, J. S., & Bassett, J. P. (2003). Persistent neural activity in head direction cells. *Cereb Cortex, 13*(11), 1162-1172.

Taube, J. S., Muller, R. U., & Ranck, J. B., Jr. (1990). Head-direction cells recorded from the postsubiculum in freely moving rats. II. Effects of environmental manipulations. *J. Neurosci., 10*(2), 436-447.

Taylor, S. F., Martis, B., Fitzgerald, K. D., Welsh, R. C., Abelson, J. L., Liberzon, I., et al. (2006). Medial frontal cortex activity and loss-related responses to errors. *J Neurosci, 26*(15), 4063-4070.

Thorndike, E. (1932). *The Fundamentals of Learning.* New York: Teachers College Press.

Tian, J., Schlag, J., & Schlag-Rey, M. (2000). Testing quasi-visual neurons in the monkey's frontal eye field with the triple-step paradigm. *Exp Brain Res, 130*(4), 433-440.

Tolman, E. C. (1948). Cognitive maps in rats and men. *Psychological Review, 55*(4), 189-208.

Touretzky, D. S., & Redish, A. D. (1996). Theory of rodent navigation based on interacting representations of space. *Hippocampus, 6*(3), 247-270.

Tunik, E., Frey, S. H., & Grafton, S. T. (2005). Virtual lesions of the anterior intraparietal area disrupt goal-dependent on-line adjustments of grasp. [Comparative Study
Research Support, N.I.H., Extramural
Research Support, U.S. Gov't, P.H.S.]. *Nat Neurosci, 8*(4), 505-511.

Ungerleider, L. G., & Desimone, R. (1986). Cortical connections of visual area MT in the macaque. *J Comp Neurol, 248*(2), 190-222.

Ungerleider, L. G., & Mishkin, M. (1982). Two cortical visual systems. In D. J. Ingle & M. A. Goodale (Eds.), *Analysis of Visual Behavior.* (pp. 549-586). MA: MIT.

van Turennout, M., Bielamowicz, L., & Martin, A. (2003). Modulation of neural activity during object naming: effects of time and practice. *Cereb Cortex, 13*(4), 381-391.

Vann, S. D., & Aggleton, J. P. (2004). Testing the importance of the retrosplenial guidance system: effects of different sized retrosplenial cortex lesions on heading direction and spatial working memory. *Behavioural Brain Research, 155*(1), 97-108.

Vann, S. D., Aggleton, J. P., & Maguire, E. A. (2009). What does the retrosplenial cortex do? [10.1038/nrn2733]. *Nat Rev Neurosci, 10*(11), 792-802.

Vann, S. D., Kristina Wilton, L. A., Muir, J. L., & Aggleton, J. P. (2003). Testing the importance of the caudal retrosplenial cortex for spatial memory in rats. *Behavioural Brain Research, 140*(1–2), 107-118.

Vogt, C., & Vogt, O. (1919). Allgemeinere Ergebnisse unserer Hirnforschung. *J. Psychol. Neurol, 25*, 279-461.
Von Bonin, G., & Bailey, P. (1947). *The neocortex of Macaca Mulatta.* Urbana: University of Illinois Press.
Wallis, J. D. (2007). Orbitofrontal cortex and its contribution to decision-making. [Research Support, N.I.H., Extramural
Research Support, Non-U.S. Gov't
Review]. *Annu Rev Neurosci, 30*, 31-56.
Waxman, S. G. (2003). *Clinical Neuroanatomy*. New York: Mc Graw-Hill.
Weniger, G., Ruhleder, M., Wolf, S., Lange, C., & Irle, E. (2009). Egocentric memory impaired and allocentric memory intact as assessed by virtual reality in subjects with unilateral parietal cortex lesions. *Neuropsychologia, 47*(1), 59-69.
Whishaw, I. Q., Maaswinkel, H., Gonzalez, C. L. R., & Kolb, B. (2001). Deficits in allothetic and idiothetic spatial behavior in rats with posterior cingulate cortex lesions. *Behavioural Brain Research, 118*(1), 67-76.
Wilson, B. A., Berry, E., Gracey, F., Harrison, C., Stow, I., Macniven, J., et al. (2005). Egocentric Disorientation following Bilateral Parietal Lobe Damage. *Cortex, 41*(4), 547-554.
Wilson, M., & McNaughton, B. (1993). Dynamics of the hippocampal ensemble code for space. *Science, 261*(5124), 1055-1058.
Wolbers, T., & Buchel, C. (2005). Dissociable Retrosplenial and Hippocampal Contributions to Successful Formation of Survey Representations. *The Journal of Neuroscience, 25*(13), 3333-3340.
Yacoub, E., Shmuel, A., Pfeuffer, J., Van De Moortele, P.-F., Adriany, G., Ugurbil, K., et al. (2001). Investigation of the initial dip in fMRI at 7 Tesla. *NMR in Biomedicine, 14*(7-8), 408-412.
Zhang, K., Ginzburg, I., McNaughton, B. L., & Sejnowski, T. J. (1998). Interpreting neuronal population activity by reconstruction: unified framework with application to hippocampal place cells. *J Neurophysiol, 79*(2), 1017-1044.

9 *Appendices*

9.1 **MATLAB script for pre-processing of individual participant data**

```
run (preprocess);
matlabbatch{1}.spm.temporal.st.scans = {
{ 'C:\Subjectdata\'      %Insert directory of subject data and each
volume%

matlabbatch{1}.spm.temporal.st.nslices = 32;
```

```
matlabbatch{1}.spm.temporal.st.tr = 2.5;
matlabbatch{1}.spm.temporal.st.ta = 2.421875;
matlabbatch{1}.spm.temporal.st.so = [1 2 3 4 5 6 7 8 9 10 11 12 13 14
15 16 17 18 19 20 21 22 23 24 25 26 27 28 29 30 31 32];
matlabbatch{1}.spm.temporal.st.refslice = 16;
matlabbatch{1}.spm.temporal.st.prefix = 'a';
matlabbatch{2}.spm.spatial.realign.estwrite.data{1}(1) = cfg_dep;
matlabbatch{2}.spm.spatial.realign.estwrite.data{1}(1).tname =
'Session';
matlabbatch{2}.spm.spatial.realign.estwrite.data{1}(1).tgt_spec{1}(1).n
ame = 'filter';
matlabbatch{2}.spm.spatial.realign.estwrite.data{1}(1).tgt_spec{1}(1).v
alue = 'image';
matlabbatch{2}.spm.spatial.realign.estwrite.data{1}(1).tgt_spec{1}(2).n
ame = 'strtype';
matlabbatch{2}.spm.spatial.realign.estwrite.data{1}(1).tgt_spec{1}(2).v
alue = 'e';
matlabbatch{2}.spm.spatial.realign.estwrite.data{1}(1).sname = 'Slice
Timing: Slice Timing Corr. Images (Sess 1)';
matlabbatch{2}.spm.spatial.realign.estwrite.data{1}(1).src_exbranch =
substruct('.','val', '{}',{1}, '.','val', '{}',{1}, '.','val',
'{}',{1});
matlabbatch{2}.spm.spatial.realign.estwrite.data{1}(1).src_output =
substruct('()',{1}, '.','files');
matlabbatch{2}.spm.spatial.realign.estwrite.data{2}(1) = cfg_dep;
matlabbatch{2}.spm.spatial.realign.estwrite.data{2}(1).tname =
'Session';
matlabbatch{2}.spm.spatial.realign.estwrite.data{2}(1).tgt_spec{1}(1).n
ame = 'filter';
matlabbatch{2}.spm.spatial.realign.estwrite.data{2}(1).tgt_spec{1}(1).v
alue = 'image';
matlabbatch{2}.spm.spatial.realign.estwrite.data{2}(1).tgt_spec{1}(2).n
ame = 'strtype';
matlabbatch{2}.spm.spatial.realign.estwrite.data{2}(1).tgt_spec{1}(2).v
alue = 'e';
matlabbatch{2}.spm.spatial.realign.estwrite.data{2}(1).sname = 'Slice
Timing: Slice Timing Corr. Images (Sess 2)';
matlabbatch{2}.spm.spatial.realign.estwrite.data{2}(1).src_exbranch =
substruct('.','val', '{}',{1}, '.','val', '{}',{1}, '.','val',
'{}',{1});
matlabbatch{2}.spm.spatial.realign.estwrite.data{2}(1).src_output =
substruct('()',{2}, '.','files');
matlabbatch{2}.spm.spatial.realign.estwrite.data{3}(1) = cfg_dep;
matlabbatch{2}.spm.spatial.realign.estwrite.data{3}(1).tname =
'Session';
matlabbatch{2}.spm.spatial.realign.estwrite.data{3}(1).tgt_spec{1}(1).n
ame = 'filter';
matlabbatch{2}.spm.spatial.realign.estwrite.data{3}(1).tgt_spec{1}(1).v
alue = 'image';
matlabbatch{2}.spm.spatial.realign.estwrite.data{3}(1).tgt_spec{1}(2).n
ame = 'strtype';
matlabbatch{2}.spm.spatial.realign.estwrite.data{3}(1).tgt_spec{1}(2).v
alue = 'e';
matlabbatch{2}.spm.spatial.realign.estwrite.data{3}(1).sname = 'Slice
Timing: Slice Timing Corr. Images (Sess 3)';
```

```
matlabbatch{2}.spm.spatial.realign.estwrite.data{3}(1).src_exbranch =
substruct('.','val', '{}',{1}, '.','val', '{}',{1}, '.','val',
'{}',{1});
matlabbatch{2}.spm.spatial.realign.estwrite.data{3}(1).src_output =
substruct('()',{3}, '.','files');
matlabbatch{2}.spm.spatial.realign.estwrite.eoptions.quality = 1;
matlabbatch{2}.spm.spatial.realign.estwrite.eoptions.sep = 4;
matlabbatch{2}.spm.spatial.realign.estwrite.eoptions.fwhm = 5;
matlabbatch{2}.spm.spatial.realign.estwrite.eoptions.rtm = 0;
matlabbatch{2}.spm.spatial.realign.estwrite.eoptions.interp = 2;
matlabbatch{2}.spm.spatial.realign.estwrite.eoptions.wrap = [0 0 0];
matlabbatch{2}.spm.spatial.realign.estwrite.eoptions.weight = {''};
matlabbatch{2}.spm.spatial.realign.estwrite.roptions.which = [0 1];
matlabbatch{2}.spm.spatial.realign.estwrite.roptions.interp = 4;
matlabbatch{2}.spm.spatial.realign.estwrite.roptions.wrap = [0 0 0];
matlabbatch{2}.spm.spatial.realign.estwrite.roptions.mask = 1;
matlabbatch{2}.spm.spatial.realign.estwrite.roptions.prefix = 'r';
matlabbatch{3}.spm.spatial.coreg.estimate.ref(1) = cfg_dep;
matlabbatch{3}.spm.spatial.coreg.estimate.ref(1).tname = 'Reference
Image';
matlabbatch{3}.spm.spatial.coreg.estimate.ref(1).tgt_spec{1}(1).name =
'filter';
matlabbatch{3}.spm.spatial.coreg.estimate.ref(1).tgt_spec{1}(1).value =
'image';
matlabbatch{3}.spm.spatial.coreg.estimate.ref(1).tgt_spec{1}(2).name =
'strtype';
matlabbatch{3}.spm.spatial.coreg.estimate.ref(1).tgt_spec{1}(2).value =
'e';
matlabbatch{3}.spm.spatial.coreg.estimate.ref(1).sname = 'Realign:
Estimate & Reslice: Mean Image';
matlabbatch{3}.spm.spatial.coreg.estimate.ref(1).src_exbranch =
substruct('.','val', '{}',{2}, '.','val', '{}',{1}, '.','val',
'{}',{1}, '.','val', '{}',{1});
matlabbatch{3}.spm.spatial.coreg.estimate.ref(1).src_output =
substruct('.','rmean');
matlabbatch{3}.spm.spatial.coreg.estimate.source = {'E:\2010
MRI\Converted filename.img }; %Subject T1%
matlabbatch{3}.spm.spatial.coreg.estimate.other = {''};
matlabbatch{3}.spm.spatial.coreg.estimate.eoptions.cost_fun = 'nmi';
matlabbatch{3}.spm.spatial.coreg.estimate.eoptions.sep = [4 2];
matlabbatch{3}.spm.spatial.coreg.estimate.eoptions.tol = [0.02 0.02
0.02 0.001 0.001 0.001 0.01 0.01 0.01 0.001 0.001 0.001];
matlabbatch{3}.spm.spatial.coreg.estimate.eoptions.fwhm = [7 7];
matlabbatch{4}.spm.spatial.normalise.estwrite.subj.source = {'E:\2010
MRI\ filename.img,1     '};
matlabbatch{4}.spm.spatial.normalise.estwrite.subj.wtsrc = '';
matlabbatch{4}.spm.spatial.normalise.estwrite.subj.resample = {'E:\2010
MRI\filename.img,1'};
matlabbatch{4}.spm.spatial.normalise.estwrite.eoptions.template =
{'C:\XXXXX\spm8\templates\T1.nii,1'}; %Location of SPM templates
directory%
matlabbatch{4}.spm.spatial.normalise.estwrite.eoptions.weight = '';
matlabbatch{4}.spm.spatial.normalise.estwrite.eoptions.smosrc = 8;
matlabbatch{4}.spm.spatial.normalise.estwrite.eoptions.smoref = 0;
matlabbatch{4}.spm.spatial.normalise.estwrite.eoptions.regtype = 'mni';
```

```
matlabbatch{4}.spm.spatial.normalise.estwrite.eoptions.cutoff = 25;
matlabbatch{4}.spm.spatial.normalise.estwrite.eoptions.nits = 16;
matlabbatch{4}.spm.spatial.normalise.estwrite.eoptions.reg = 1;
matlabbatch{4}.spm.spatial.normalise.estwrite.roptions.preserve = 0;
matlabbatch{4}.spm.spatial.normalise.estwrite.roptions.bb = [-78 -112 -
50
                                                            78 76 85];
matlabbatch{4}.spm.spatial.normalise.estwrite.roptions.vox = [2 2 2];
matlabbatch{4}.spm.spatial.normalise.estwrite.roptions.interp = 1;
matlabbatch{4}.spm.spatial.normalise.estwrite.roptions.wrap = [0 0 0];
matlabbatch{4}.spm.spatial.normalise.estwrite.roptions.prefix = 'w';
matlabbatch{5}.spm.spatial.normalise.write.subj(1).matname(1) =
cfg_dep;
matlabbatch{5}.spm.spatial.normalise.write.subj(1).matname(1).tname =
'Parameter File';
matlabbatch{5}.spm.spatial.normalise.write.subj(1).matname(1).tgt_spec{
1}(1).name = 'filter';
matlabbatch{5}.spm.spatial.normalise.write.subj(1).matname(1).tgt_spec{
1}(1).value = 'mat';
matlabbatch{5}.spm.spatial.normalise.write.subj(1).matname(1).tgt_spec{
1}(2).name = 'strtype';
matlabbatch{5}.spm.spatial.normalise.write.subj(1).matname(1).tgt_spec{
1}(2).value = 'e';
matlabbatch{5}.spm.spatial.normalise.write.subj(1).matname(1).sname =
'Normalise: Estimate & Write: Norm Params File (Subj 1)';
matlabbatch{5}.spm.spatial.normalise.write.subj(1).matname(1).src_exbra
nch = substruct('.','val', '{}',{4}, '.','val', '{}',{1}, '.','val',
'{}',{1}, '.','val', '{}',{1});
matlabbatch{5}.spm.spatial.normalise.write.subj(1).matname(1).src_outpu
t = substruct('()',{1}, '.','params');
matlabbatch{5}.spm.spatial.normalise.write.subj(1).resample(1) =
cfg_dep;
matlabbatch{5}.spm.spatial.normalise.write.subj(1).resample(1).tname =
'Images to Write';
matlabbatch{5}.spm.spatial.normalise.write.subj(1).resample(1).tgt_spec
{1}(1).name = 'filter';
matlabbatch{5}.spm.spatial.normalise.write.subj(1).resample(1).tgt_spec
{1}(1).value = 'image';
matlabbatch{5}.spm.spatial.normalise.write.subj(1).resample(1).tgt_spec
{1}(2).name = 'strtype';
matlabbatch{5}.spm.spatial.normalise.write.subj(1).resample(1).tgt_spec
{1}(2).value = 'e';
matlabbatch{5}.spm.spatial.normalise.write.subj(1).resample(1).sname =
'Realign: Estimate & Reslice: Realigned Images (Sess 1)';
matlabbatch{5}.spm.spatial.normalise.write.subj(1).resample(1).src_exbr
anch = substruct('.','val', '{}',{2}, '.','val', '{}',{1}, '.','val',
'{}',{1}, '.','val', '{}',{1});
matlabbatch{5}.spm.spatial.normalise.write.subj(1).resample(1).src_outp
ut = substruct('.','sess', '()',{1}, '.','cfiles');
matlabbatch{5}.spm.spatial.normalise.write.subj(2).matname(1) =
cfg_dep;
matlabbatch{5}.spm.spatial.normalise.write.subj(2).matname(1).tname =
'Parameter File';
matlabbatch{5}.spm.spatial.normalise.write.subj(2).matname(1).tgt_spec{
1}(1).name = 'filter';
```

```
matlabbatch{5}.spm.spatial.normalise.write.subj(2).matname(1).tgt_spec{
1}(1).value = 'mat';
matlabbatch{5}.spm.spatial.normalise.write.subj(2).matname(1).tgt_spec{
1}(2).name = 'strtype';
matlabbatch{5}.spm.spatial.normalise.write.subj(2).matname(1).tgt_spec{
1}(2).value = 'e';
matlabbatch{5}.spm.spatial.normalise.write.subj(2).matname(1).sname =
'Normalise: Estimate & Write: Norm Params File (Subj 1)';
matlabbatch{5}.spm.spatial.normalise.write.subj(2).matname(1).src_exbra
nch = substruct('.','val', '{}',{4}, '.','val', '{}',{1}, '.','val',
'{}',{1}, '.','val', '{}',{1});
matlabbatch{5}.spm.spatial.normalise.write.subj(2).matname(1).src_outpu
t = substruct('()',{1}, '.','params');
matlabbatch{5}.spm.spatial.normalise.write.subj(2).resample(1) =
cfg_dep;
matlabbatch{5}.spm.spatial.normalise.write.subj(2).resample(1).tname =
'Images to Write';
matlabbatch{5}.spm.spatial.normalise.write.subj(2).resample(1).tgt_spec
{1}(1).name = 'filter';
matlabbatch{5}.spm.spatial.normalise.write.subj(2).resample(1).tgt_spec
{1}(1).value = 'image';
matlabbatch{5}.spm.spatial.normalise.write.subj(2).resample(1).tgt_spec
{1}(2).name = 'strtype';
matlabbatch{5}.spm.spatial.normalise.write.subj(2).resample(1).tgt_spec
{1}(2).value = 'e';
matlabbatch{5}.spm.spatial.normalise.write.subj(2).resample(1).sname =
'Realign: Estimate & Reslice: Realigned Images (Sess 2)';
matlabbatch{5}.spm.spatial.normalise.write.subj(2).resample(1).src_exbr
anch = substruct('.','val', '{}',{2}, '.','val', '{}',{1}, '.','val',
'{}',{1}, '.','val', '{}',{1});
matlabbatch{5}.spm.spatial.normalise.write.subj(2).resample(1).src_outp
ut = substruct('.','sess', '()',{2}, '.','cfiles');
matlabbatch{5}.spm.spatial.normalise.write.subj(3).matname(1) =
cfg_dep;
matlabbatch{5}.spm.spatial.normalise.write.subj(3).matname(1).tname =
'Parameter File';
matlabbatch{5}.spm.spatial.normalise.write.subj(3).matname(1).tgt_spec{
1}(1).name = 'filter';
matlabbatch{5}.spm.spatial.normalise.write.subj(3).matname(1).tgt_spec{
1}(1).value = 'mat';
matlabbatch{5}.spm.spatial.normalise.write.subj(3).matname(1).tgt_spec{
1}(2).name = 'strtype';
matlabbatch{5}.spm.spatial.normalise.write.subj(3).matname(1).tgt_spec{
1}(2).value = 'e';
matlabbatch{5}.spm.spatial.normalise.write.subj(3).matname(1).sname =
'Normalise: Estimate & Write: Norm Params File (Subj 1)';
matlabbatch{5}.spm.spatial.normalise.write.subj(3).matname(1).src_exbra
nch = substruct('.','val', '{}',{4}, '.','val', '{}',{1}, '.','val',
'{}',{1}, '.','val', '{}',{1});
matlabbatch{5}.spm.spatial.normalise.write.subj(3).matname(1).src_outpu
t = substruct('()',{1}, '.','params');
matlabbatch{5}.spm.spatial.normalise.write.subj(3).resample(1) =
cfg_dep;
matlabbatch{5}.spm.spatial.normalise.write.subj(3).resample(1).tname =
'Images to Write';
```

```
matlabbatch{5}.spm.spatial.normalise.write.subj(3).resample(1).tgt_spec
{1}(1).name = 'filter';
matlabbatch{5}.spm.spatial.normalise.write.subj(3).resample(1).tgt_spec
{1}(1).value = 'image';
matlabbatch{5}.spm.spatial.normalise.write.subj(3).resample(1).tgt_spec
{1}(2).name = 'strtype';
matlabbatch{5}.spm.spatial.normalise.write.subj(3).resample(1).tgt_spec
{1}(2).value = 'e';
matlabbatch{5}.spm.spatial.normalise.write.subj(3).resample(1).sname =
'Realign: Estimate & Reslice: Realigned Images (Sess 3)';
matlabbatch{5}.spm.spatial.normalise.write.subj(3).resample(1).src_exbr
anch = substruct('.','val', '{}',{2}, '.','val', '{}',{1}, '.','val',
'{}',{1}, '.','val', '{}',{1});
matlabbatch{5}.spm.spatial.normalise.write.subj(3).resample(1).src_outp
ut = substruct('.','sess', '()',{3}, '.','cfiles');
matlabbatch{5}.spm.spatial.normalise.write.roptions.preserve = 0;
matlabbatch{5}.spm.spatial.normalise.write.roptions.bb = [-78 -112 -50
                                                          78 76 85];
matlabbatch{5}.spm.spatial.normalise.write.roptions.vox = [2 2 2];
matlabbatch{5}.spm.spatial.normalise.write.roptions.interp = 1;
matlabbatch{5}.spm.spatial.normalise.write.roptions.wrap = [0 0 0];
matlabbatch{5}.spm.spatial.normalise.write.roptions.prefix = 'w';
matlabbatch{6}.spm.spatial.smooth.data(1) = cfg_dep;
matlabbatch{6}.spm.spatial.smooth.data(1).tname = 'Images to Smooth';
matlabbatch{6}.spm.spatial.smooth.data(1).tgt_spec{1}(1).name =
'filter';
matlabbatch{6}.spm.spatial.smooth.data(1).tgt_spec{1}(1).value =
'image';
matlabbatch{6}.spm.spatial.smooth.data(1).tgt_spec{1}(2).name =
'strtype';
matlabbatch{6}.spm.spatial.smooth.data(1).tgt_spec{1}(2).value = 'e';
matlabbatch{6}.spm.spatial.smooth.data(1).sname = 'Normalise: Write:
Normalised Images (Subj 1)';
matlabbatch{6}.spm.spatial.smooth.data(1).src_exbranch =
substruct('.','val', '{}',{5}, '.','val', '{}',{1}, '.','val',
'{}',{1}, '.','val', '{}',{1});
matlabbatch{6}.spm.spatial.smooth.data(1).src_output =
substruct('()',{1}, '.','files');
matlabbatch{6}.spm.spatial.smooth.data(2) = cfg_dep;
matlabbatch{6}.spm.spatial.smooth.data(2).tname = 'Images to Smooth';
matlabbatch{6}.spm.spatial.smooth.data(2).tgt_spec{1}(1).name =
'filter';
matlabbatch{6}.spm.spatial.smooth.data(2).tgt_spec{1}(1).value =
'image';
matlabbatch{6}.spm.spatial.smooth.data(2).tgt_spec{1}(2).name =
'strtype';
matlabbatch{6}.spm.spatial.smooth.data(2).tgt_spec{1}(2).value = 'e';
matlabbatch{6}.spm.spatial.smooth.data(2).sname = 'Normalise: Write:
Normalised Images (Subj 2)';
matlabbatch{6}.spm.spatial.smooth.data(2).src_exbranch =
substruct('.','val', '{}',{5}, '.','val', '{}',{1}, '.','val',
'{}',{1}, '.','val', '{}',{1});
matlabbatch{6}.spm.spatial.smooth.data(2).src_output =
substruct('()',{2}, '.','files');
matlabbatch{6}.spm.spatial.smooth.data(3) = cfg_dep;
```

```
matlabbatch{6}.spm.spatial.smooth.data(3).tname = 'Images to Smooth';
matlabbatch{6}.spm.spatial.smooth.data(3).tgt_spec{1}(1).name =
'filter';
matlabbatch{6}.spm.spatial.smooth.data(3).tgt_spec{1}(1).value =
'image';
matlabbatch{6}.spm.spatial.smooth.data(3).tgt_spec{1}(2).name =
'strtype';
matlabbatch{6}.spm.spatial.smooth.data(3).tgt_spec{1}(2).value = 'e';
matlabbatch{6}.spm.spatial.smooth.data(3).sname = 'Normalise: Write:
Normalised Images (Subj 3)';
matlabbatch{6}.spm.spatial.smooth.data(3).src_exbranch =
substruct('.','val', '{}',{5}, '.','val', '{}',{1}, '.','val',
'{}',{1}, '.','val', '{}',{1});
matlabbatch{6}.spm.spatial.smooth.data(3).src_output =
substruct('()',{3}, '.','files');
matlabbatch{6}.spm.spatial.smooth.fwhm = [8 8 8];
matlabbatch{6}.spm.spatial.smooth.dtype = 0;
matlabbatch{6}.spm.spatial.smooth.im = 0;
matlabbatch{6}.spm.spatial.smooth.prefix = 's';
end
```

9.2 MATLAB script for creating statistical model used in Study One

```
run (ssnt task);
matlabbatch{1}.spm.stats.fmri_spec.dir = {'E:\2010
MRI\Converted\subject\Level1\SSNT\'};
matlabbatch{1}.spm.stats.fmri_spec.timing.units = 'secs';
matlabbatch{1}.spm.stats.fmri_spec.timing.RT = 2.5;
matlabbatch{1}.spm.stats.fmri_spec.timing.fmri_t = 16;
matlabbatch{1}.spm.stats.fmri_spec.timing.fmri_t0 = 1;
%%
matlabbatch{1}.spm.stats.fmri_spec.sess.scans
{ 'C:\Subjectdata\'      %Insert directory of subject data and each
volume%
matlabbatch{1}.spm.stats.fmri_spec.sess.cond(1).name = 'Left Movement';
%%
matlabbatch{1}.spm.stats.fmri_spec.sess.cond(1).onset = [0
                                                         78
                                                         128
                                                         178
                                                         224
                                                         240
                                                         304
                                                         336
                                                         414
                                                         464
                                                         514
                                                         560
                                                         576
                                                         640
                                                         672
                                                         750
```

```
                                                                800
                                                                850
                                                                896
                                                                912
                                                                976];
%%
%%
matlabbatch{1}.spm.stats.fmri_spec.sess.cond(1).duration = [0
                                                             0
                                                             0
                                                             0
                                                             0
                                                             0
                                                             0
                                                             0
                                                             0
                                                             0
                                                             0
                                                             0
                                                             0
                                                             0
                                                             0
                                                             0
                                                             0];
%%
matlabbatch{1}.spm.stats.fmri_spec.sess.cond(1).tmod = 0;
matlabbatch{1}.spm.stats.fmri_spec.sess.cond(1).pmod = struct('name',
{}, 'param', {}, 'poly', {});
matlabbatch{1}.spm.stats.fmri_spec.sess.cond(2).name = 'Right
Movement';
%%
matlabbatch{1}.spm.stats.fmri_spec.sess.cond(2).onset = [14
                                                         64
                                                         96
                                                         160
                                                         192
                                                         258
                                                         274
                                                         350
                                                         400
                                                         432
                                                         496
                                                         528
                                                         594
                                                         610
                                                         686
                                                         736
                                                         768
                                                         832
                                                         864
                                                         930
```

```
                                                                946];
%%
%%
matlabbatch{1}.spm.stats.fmri_spec.sess.cond(2).duration = [0
                                                            0
                                                            0
                                                            0
                                                            0
                                                            0
                                                            0
                                                            0
                                                            0
                                                            0
                                                            0
                                                            0
                                                            0
                                                            0
                                                            0
                                                            0
                                                            0
                                                            0];
%%
matlabbatch{1}.spm.stats.fmri_spec.sess.cond(2).tmod = 0;
matlabbatch{1}.spm.stats.fmri_spec.sess.cond(2).pmod = struct('name',
{}, 'param', {}, 'poly', {});
matlabbatch{1}.spm.stats.fmri_spec.sess.cond(3).name = 'No Movement';
%%
matlabbatch{1}.spm.stats.fmri_spec.sess.cond(3).onset = [30
                                                         48
                                                         114
                                                         144
                                                         206
                                                         288
                                                         322
                                                         366
                                                         384
                                                         450
                                                         480
                                                         542
                                                         624
                                                         658
                                                         702
                                                         720
                                                         786
                                                         816
                                                         878
                                                         960
                                                         994];
%%
%%
matlabbatch{1}.spm.stats.fmri_spec.sess.cond(3).duration = [0
                                                            0
```

```
                                                                    0
                                                                    0
                                                                    0
                                                                    0
                                                                    0
                                                                    0
                                                                    0
                                                                    0
                                                                    0
                                                                    0
                                                                    0
                                                                    0
                                                                    0
                                                                    0
                                                                    0
                                                                    0
                                                                    0];
%%
matlabbatch{1}.spm.stats.fmri_spec.sess.cond(3).tmod = 0;
matlabbatch{1}.spm.stats.fmri_spec.sess.cond(3).pmod = struct('name',
{}, 'param', {}, 'poly', {});
matlabbatch{1}.spm.stats.fmri_spec.sess.multi = {''};
matlabbatch{1}.spm.stats.fmri_spec.sess.regress = struct('name', {},
'val', {});
matlabbatch{1}.spm.stats.fmri_spec.sess.multi_reg = {'E:\2010
MRI\Converted\subject\SSNT1\rp_1.txt'};
matlabbatch{1}.spm.stats.fmri_spec.sess.hpf = 128;
matlabbatch{1}.spm.stats.fmri_spec.fact = struct('name', {}, 'levels',
{});
matlabbatch{1}.spm.stats.fmri_spec.bases.hrf.derivs = [0 0];
matlabbatch{1}.spm.stats.fmri_spec.volt = 1;
matlabbatch{1}.spm.stats.fmri_spec.global = 'None';
matlabbatch{1}.spm.stats.fmri_spec.mask = {''};
matlabbatch{1}.spm.stats.fmri_spec.cvi = 'AR(1)';
matlabbatch{2}.spm.stats.fmri_est.spmmat(1) = cfg_dep;
matlabbatch{2}.spm.stats.fmri_est.spmmat(1).tname = 'Select SPM.mat';
matlabbatch{2}.spm.stats.fmri_est.spmmat(1).tgt_spec = {};
matlabbatch{2}.spm.stats.fmri_est.spmmat(1).sname = 'fMRI model
specification: SPM.mat File';
matlabbatch{2}.spm.stats.fmri_est.spmmat(1).src_exbranch =
substruct('.','val', '{}',{1}, '.','val', '{}',{1}, '.','val',
'{}',{1});
matlabbatch{2}.spm.stats.fmri_est.spmmat(1).src_output =
substruct('.','spmmat');
matlabbatch{2}.spm.stats.fmri_est.method.Classical = 1;
matlabbatch{3}.spm.stats.con.spmmat(1) = cfg_dep;
matlabbatch{3}.spm.stats.con.spmmat(1).tname = 'Select SPM.mat';
matlabbatch{3}.spm.stats.con.spmmat(1).tgt_spec = {};
matlabbatch{3}.spm.stats.con.spmmat(1).sname = 'Model estimation:
SPM.mat File';
matlabbatch{3}.spm.stats.con.spmmat(1).src_exbranch =
substruct('.','val', '{}',{2}, '.','val', '{}',{1}, '.','val',
'{}',{1});
```

```
matlabbatch{3}.spm.stats.con.spmmat(1).src_output =
substruct('.','spmmat');
matlabbatch{3}.spm.stats.con.consess{1}.tcon.name = 'move > no move';
matlabbatch{3}.spm.stats.con.consess{1}.tcon.convec = [0.5 0.5 -1 0 0 0
0 0 0];
matlabbatch{3}.spm.stats.con.consess{1}.tcon.sessrep = 'none';
matlabbatch{3}.spm.stats.con.consess{2}.tcon.name = 'left move > right
move';
matlabbatch{3}.spm.stats.con.consess{2}.tcon.convec = [1 -1 0 0 0 0 0 0
0];
matlabbatch{3}.spm.stats.con.consess{2}.tcon.sessrep = 'none';
matlabbatch{3}.spm.stats.con.consess{3}.tcon.name = 'right move > left
move';
matlabbatch{3}.spm.stats.con.consess{3}.tcon.convec = [-1 1 0 0 0 0 0 0
0];
matlabbatch{3}.spm.stats.con.consess{3}.tcon.sessrep = 'none';
matlabbatch{3}.spm.stats.con.consess{4}.tcon.name = 'left move >
baseline';
matlabbatch{3}.spm.stats.con.consess{4}.tcon.convec = [1 0 0 0 0 0 0 0
0];
matlabbatch{3}.spm.stats.con.consess{4}.tcon.sessrep = 'none';
matlabbatch{3}.spm.stats.con.consess{5}.tcon.name = 'right move >
baseline';
matlabbatch{3}.spm.stats.con.consess{5}.tcon.convec = [0 1 0 0 0 0 0 0
0];
matlabbatch{3}.spm.stats.con.consess{5}.tcon.sessrep = 'none';
matlabbatch{3}.spm.stats.con.consess{6}.tcon.name = 'no move >
baseline';
matlabbatch{3}.spm.stats.con.consess{6}.tcon.convec = [0 0 1 0 0 0 0 0
0];
matlabbatch{3}.spm.stats.con.consess{6}.tcon.sessrep = 'none';
matlabbatch{3}.spm.stats.con.delete = 0;
end
```

9.3 MATLAB script for creating statistical model used in Study Two

```
matlabbatch{1}.cfg_basicio.cfg_mkdir.parent = {'E:\2010
MRI\Converted\PillarModel\'};
matlabbatch{1}.cfg_basicio.cfg_mkdir.name = 'Peter';
matlabbatch{2}.spm.stats.fmri_spec.dir(1) = cfg_dep;
matlabbatch{2}.spm.stats.fmri_spec.dir(1).tname = 'Directory';
matlabbatch{2}.spm.stats.fmri_spec.dir(1).tgt_spec{1}(1).name =
'filter';
matlabbatch{2}.spm.stats.fmri_spec.dir(1).tgt_spec{1}(1).value = 'dir';
matlabbatch{2}.spm.stats.fmri_spec.dir(1).tgt_spec{1}(2).name =
'strtype';
matlabbatch{2}.spm.stats.fmri_spec.dir(1).tgt_spec{1}(2).value = 'e';
matlabbatch{2}.spm.stats.fmri_spec.dir(1).sname = 'Make Directory: Make
Directory ''Peter''';
matlabbatch{2}.spm.stats.fmri_spec.dir(1).src_exbranch =
substruct('.','val', '{}',{1}, '.','val', '{}',{1});
```

```
matlabbatch{2}.spm.stats.fmri_spec.dir(1).src_output =
substruct('.','dir');
matlabbatch{2}.spm.stats.fmri_spec.timing.units = 'secs';
matlabbatch{2}.spm.stats.fmri_spec.timing.RT = 2.5;
matlabbatch{2}.spm.stats.fmri_spec.timing.fmri_t = 16;
matlabbatch{2}.spm.stats.fmri_spec.timing.fmri_t0 = 1;

matlabbatch{2}.spm.stats.fmri_spec.sess(1).scans = {

'E:\DIRECTORY\swaghdf000000-0006-00001-000001-01.img,1'
'E:\DIRECTORY\swaghdf000000-0006-00481-000481-01.img
%Include directory of each volume%

matlabbatch{2}.spm.stats.fmri_spec.sess(1).cond(1).name = 'Start
+25deg';
matlabbatch{2}.spm.stats.fmri_spec.sess(1).cond(1).onset = [0
                                                            210
                                                            300
                                                            390
                                                            480
                                                            690
                                                            780
                                                            870
                                                            960
                                                            1170];
matlabbatch{2}.spm.stats.fmri_spec.sess(1).cond(1).duration = 0;
matlabbatch{2}.spm.stats.fmri_spec.sess(1).cond(1).tmod = 0;
matlabbatch{2}.spm.stats.fmri_spec.sess(1).cond(1).pmod =
struct('name', {}, 'param', {}, 'poly', {});
matlabbatch{2}.spm.stats.fmri_spec.sess(1).cond(2).name = 'Disappear
+25deg';
matlabbatch{2}.spm.stats.fmri_spec.sess(1).cond(2).onset = [10
                                                            220
                                                            310
                                                            400
                                                            490
                                                            700
                                                            790
                                                            880
                                                            970
                                                            1180];
matlabbatch{2}.spm.stats.fmri_spec.sess(1).cond(2).duration = 0;
matlabbatch{2}.spm.stats.fmri_spec.sess(1).cond(2).tmod = 0;
matlabbatch{2}.spm.stats.fmri_spec.sess(1).cond(2).pmod =
struct('name', {}, 'param', {}, 'poly', {});
matlabbatch{2}.spm.stats.fmri_spec.sess(1).cond(3).name = 'Reappear
+25deg';
matlabbatch{2}.spm.stats.fmri_spec.sess(1).cond(3).onset = [18
                                                            228
                                                            318
                                                            408
                                                            498
                                                            708
                                                            798
                                                            888
```

```
                                                                978
                                                                1188];
matlabbatch{2}.spm.stats.fmri_spec.sess(1).cond(3).duration = 0;
matlabbatch{2}.spm.stats.fmri_spec.sess(1).cond(3).tmod = 0;
matlabbatch{2}.spm.stats.fmri_spec.sess(1).cond(3).pmod =
struct('name', {}, 'param', {}, 'poly', {});
matlabbatch{2}.spm.stats.fmri_spec.sess(1).cond(4).name = 'Start
+45deg';
matlabbatch{2}.spm.stats.fmri_spec.sess(1).cond(4).onset = [30
                                                                120
                                                                330
                                                                420
                                                                510
                                                                600
                                                                810
                                                                900
                                                                1020
                                                                1080];
matlabbatch{2}.spm.stats.fmri_spec.sess(1).cond(4).duration = 0;
matlabbatch{2}.spm.stats.fmri_spec.sess(1).cond(4).tmod = 0;
matlabbatch{2}.spm.stats.fmri_spec.sess(1).cond(4).pmod =
struct('name', {}, 'param', {}, 'poly', {});
matlabbatch{2}.spm.stats.fmri_spec.sess(1).cond(5).name = 'Disappear
+45deg';
matlabbatch{2}.spm.stats.fmri_spec.sess(1).cond(5).onset = [40
                                                                130
                                                                340
                                                                430
                                                                520
                                                                610
                                                                820
                                                                910
                                                                1030
                                                                1090];
matlabbatch{2}.spm.stats.fmri_spec.sess(1).cond(5).duration = 0;
matlabbatch{2}.spm.stats.fmri_spec.sess(1).cond(5).tmod = 0;
matlabbatch{2}.spm.stats.fmri_spec.sess(1).cond(5).pmod =
struct('name', {}, 'param', {}, 'poly', {});
matlabbatch{2}.spm.stats.fmri_spec.sess(1).cond(6).name = 'Appear
+45deg';
matlabbatch{2}.spm.stats.fmri_spec.sess(1).cond(6).onset = [48
                                                                138
                                                                348
                                                                438
                                                                528
                                                                618
                                                                828
                                                                918
                                                                1038
                                                                1098];
matlabbatch{2}.spm.stats.fmri_spec.sess(1).cond(6).duration = 0;
matlabbatch{2}.spm.stats.fmri_spec.sess(1).cond(6).tmod = 0;
matlabbatch{2}.spm.stats.fmri_spec.sess(1).cond(6).pmod =
struct('name', {}, 'param', {}, 'poly', {});
```

```
matlabbatch{2}.spm.stats.fmri_spec.sess(1).cond(7).name = 'Start -
25deg';
matlabbatch{2}.spm.stats.fmri_spec.sess(1).cond(7).onset = [60
                                                            150
                                                            240
                                                            450
                                                            540
                                                            630
                                                            720
                                                            930
                                                            990
                                                            1110];
matlabbatch{2}.spm.stats.fmri_spec.sess(1).cond(7).duration = 0;
matlabbatch{2}.spm.stats.fmri_spec.sess(1).cond(7).tmod = 0;
matlabbatch{2}.spm.stats.fmri_spec.sess(1).cond(7).pmod =
struct('name', {}, 'param', {}, 'poly', {});
matlabbatch{2}.spm.stats.fmri_spec.sess(1).cond(8).name = 'Disappear -
25deg';
matlabbatch{2}.spm.stats.fmri_spec.sess(1).cond(8).onset = [70
                                                            160
                                                            250
                                                            460
                                                            550
                                                            640
                                                            730
                                                            940
                                                            1000
                                                            1120];
matlabbatch{2}.spm.stats.fmri_spec.sess(1).cond(8).duration = 0;
matlabbatch{2}.spm.stats.fmri_spec.sess(1).cond(8).tmod = 0;
matlabbatch{2}.spm.stats.fmri_spec.sess(1).cond(8).pmod =
struct('name', {}, 'param', {}, 'poly', {});
matlabbatch{2}.spm.stats.fmri_spec.sess(1).cond(9).name = 'Appear -
25deg';
matlabbatch{2}.spm.stats.fmri_spec.sess(1).cond(9).onset = [78
                                                            168
                                                            258
                                                            468
                                                            558
                                                            648
                                                            738
                                                            948
                                                            1008
                                                            1128];
matlabbatch{2}.spm.stats.fmri_spec.sess(1).cond(9).duration = 0;
matlabbatch{2}.spm.stats.fmri_spec.sess(1).cond(9).tmod = 0;
matlabbatch{2}.spm.stats.fmri_spec.sess(1).cond(9).pmod =
struct('name', {}, 'param', {}, 'poly', {});
matlabbatch{2}.spm.stats.fmri_spec.sess(1).cond(10).name = 'Start -
45deg';
matlabbatch{2}.spm.stats.fmri_spec.sess(1).cond(10).onset = [90
                                                             180
                                                             270
                                                             360
                                                             570
```

```
                                                                660
                                                                750
                                                                840
                                                                1050
                                                                1140];
matlabbatch{2}.spm.stats.fmri_spec.sess(1).cond(10).duration = 0;
matlabbatch{2}.spm.stats.fmri_spec.sess(1).cond(10).tmod = 0;
matlabbatch{2}.spm.stats.fmri_spec.sess(1).cond(10).pmod =
struct('name', {}, 'param', {}, 'poly', {});
matlabbatch{2}.spm.stats.fmri_spec.sess(1).cond(11).name = 'Disappear -
45deg';
matlabbatch{2}.spm.stats.fmri_spec.sess(1).cond(11).onset = [100
                                                                190
                                                                280
                                                                370
                                                                580
                                                                670
                                                                760
                                                                850
                                                                1060
                                                                1150];
matlabbatch{2}.spm.stats.fmri_spec.sess(1).cond(11).duration = 0;
matlabbatch{2}.spm.stats.fmri_spec.sess(1).cond(11).tmod = 0;
matlabbatch{2}.spm.stats.fmri_spec.sess(1).cond(11).pmod =
struct('name', {}, 'param', {}, 'poly', {});
matlabbatch{2}.spm.stats.fmri_spec.sess(1).cond(12).name = 'Reappear -
45deg';
matlabbatch{2}.spm.stats.fmri_spec.sess(1).cond(12).onset = [108
                                                                198
                                                                288
                                                                378
                                                                588
                                                                678
                                                                768
                                                                858
                                                                1068
                                                                1158];
matlabbatch{2}.spm.stats.fmri_spec.sess(1).cond(12).duration = 0;
matlabbatch{2}.spm.stats.fmri_spec.sess(1).cond(12).tmod = 0;
matlabbatch{2}.spm.stats.fmri_spec.sess(1).cond(12).pmod =
struct('name', {}, 'param', {}, 'poly', {});
matlabbatch{2}.spm.stats.fmri_spec.sess(1).multi = {''};
matlabbatch{2}.spm.stats.fmri_spec.sess(1).regress = struct('name', {},
'val', {});
matlabbatch{2}.spm.stats.fmri_spec.sess(1).multi_reg = {'E:\2010
MRI\Converted\Peter\Pillar1\rp_aghdf000000-0006-00001-000001-01.txt'};
matlabbatch{2}.spm.stats.fmri_spec.sess(1).hpf = 200;

%session 2%
matlabbatch{2}.spm.stats.fmri_spec.sess(2).scans = {
'E:\DIRECTORY\swaghdf000000-0006-00001-000001-01.img,1'
'E:\DIRECTORY\swaghdf000000-0006-00481-000481-01.img
%Include directory of each volume%
```

```
matlabbatch{2}.spm.stats.fmri_spec.sess.cond(1).name = 'Face+Turn
+25degrees';
matlabbatch{2}.spm.stats.fmri_spec.sess.cond(1).onset = [0
                                                         210
                                                         300
                                                         390
                                                         480
                                                         690
                                                         780
                                                         870
                                                         960
                                                         1170];
matlabbatch{2}.spm.stats.fmri_spec.sess.cond(1).duration = 3;
matlabbatch{2}.spm.stats.fmri_spec.sess.cond(1).tmod = 0;
matlabbatch{2}.spm.stats.fmri_spec.sess.cond(1).pmod = struct('name',
{}, 'param', {}, 'poly', {});
matlabbatch{2}.spm.stats.fmri_spec.sess.cond(2).name = 'Face+Turn -
25degrees';
matlabbatch{2}.spm.stats.fmri_spec.sess.cond(2).onset = [60
                                                         150
                                                         240
                                                         450
                                                         540
                                                         630
                                                         720
                                                         930
                                                         990
                                                         1110];
matlabbatch{2}.spm.stats.fmri_spec.sess.cond(2).duration = 3;
matlabbatch{2}.spm.stats.fmri_spec.sess.cond(2).tmod = 0;
matlabbatch{2}.spm.stats.fmri_spec.sess.cond(2).pmod = struct('name',
{}, 'param', {}, 'poly', {});
matlabbatch{2}.spm.stats.fmri_spec.sess.cond(3).name = 'Target Visible
+25degrees';
matlabbatch{2}.spm.stats.fmri_spec.sess.cond(3).onset = [3
                                                         213
                                                         303
                                                         393
                                                         483
                                                         693
                                                         783
                                                         873
                                                         963
                                                         1173];
matlabbatch{2}.spm.stats.fmri_spec.sess.cond(3).duration = 7;
matlabbatch{2}.spm.stats.fmri_spec.sess.cond(3).tmod = 0;
matlabbatch{2}.spm.stats.fmri_spec.sess.cond(3).pmod = struct('name',
{}, 'param', {}, 'poly', {});
matlabbatch{2}.spm.stats.fmri_spec.sess.cond(4).name = 'Target Visible
-25degrees';
matlabbatch{2}.spm.stats.fmri_spec.sess.cond(4).onset = [63
                                                         153
                                                         243
                                                         453
                                                         543
```

```
                                                                633
                                                                723
                                                                933
                                                                993
                                                                1113];
matlabbatch{2}.spm.stats.fmri_spec.sess.cond(4).duration = 7;
matlabbatch{2}.spm.stats.fmri_spec.sess.cond(4).tmod = 0;
matlabbatch{2}.spm.stats.fmri_spec.sess.cond(4).pmod = struct('name',
{}, 'param', {}, 'poly', {});
matlabbatch{2}.spm.stats.fmri_spec.sess.cond(5).name = 'Disappear
+25degrees';
matlabbatch{2}.spm.stats.fmri_spec.sess.cond(5).onset = [10
                                                                220
                                                                310
                                                                400
                                                                490
                                                                700
                                                                790
                                                                880
                                                                970
                                                                1180];
matlabbatch{2}.spm.stats.fmri_spec.sess.cond(5).duration = 0;
matlabbatch{2}.spm.stats.fmri_spec.sess.cond(5).tmod = 0;
matlabbatch{2}.spm.stats.fmri_spec.sess.cond(5).pmod = struct('name',
{}, 'param', {}, 'poly', {});
matlabbatch{2}.spm.stats.fmri_spec.sess.cond(5).name = 'Disappear -
25degrees';
matlabbatch{2}.spm.stats.fmri_spec.sess.cond(5).onset = [70
                                                                160
                                                                250
                                                                460
                                                                550
                                                                640
                                                                730
                                                                940
                                                                1000
                                                                1120];
matlabbatch{2}.spm.stats.fmri_spec.sess.cond(5).duration = 0;
matlabbatch{2}.spm.stats.fmri_spec.sess.cond(5).tmod = 0;
matlabbatch{2}.spm.stats.fmri_spec.sess.cond(5).pmod = struct('name',
{}, 'param', {}, 'poly', {});
matlabbatch{2}.spm.stats.fmri_spec.sess.cond(6).name = 'Subj Move +25
degrees';
matlabbatch{2}.spm.stats.fmri_spec.sess.cond(6).onset = [10
                                                                220
                                                                310
                                                                400
                                                                490
                                                                700
                                                                790
                                                                880
                                                                970
                                                                1180];
matlabbatch{2}.spm.stats.fmri_spec.sess.cond(6).duration = 3;
matlabbatch{2}.spm.stats.fmri_spec.sess.cond(6).tmod = 0;
```

```
matlabbatch{2}.spm.stats.fmri_spec.sess.cond(6).pmod = struct('name',
{}, 'param', {}, 'poly', {});
matlabbatch{2}.spm.stats.fmri_spec.sess.cond(7).name = 'Subj Move -25
degrees';
matlabbatch{2}.spm.stats.fmri_spec.sess.cond(7).onset = [70
                                                         160
                                                         250
                                                         460
                                                         550
                                                         640
                                                         730
                                                         940
                                                         1000
                                                         1120];
matlabbatch{2}.spm.stats.fmri_spec.sess.cond(7).duration = 3;
matlabbatch{2}.spm.stats.fmri_spec.sess.cond(7).tmod = 0;
matlabbatch{2}.spm.stats.fmri_spec.sess.cond(7).pmod = struct('name',
{}, 'param', {}, 'poly', {});
matlabbatch{2}.spm.stats.fmri_spec.sess.cond(8).name = 'Invisible
heading +25';
matlabbatch{2}.spm.stats.fmri_spec.sess.cond(8).onset = [13
                                                         223
                                                         313
                                                         403
                                                         493
                                                         703
                                                         793
                                                         883
                                                         973
                                                         1183];
matlabbatch{2}.spm.stats.fmri_spec.sess.cond(8).duration = 5;
matlabbatch{2}.spm.stats.fmri_spec.sess.cond(8).tmod = 0;
matlabbatch{2}.spm.stats.fmri_spec.sess.cond(8).pmod = struct('name',
{}, 'param', {}, 'poly', {});
matlabbatch{2}.spm.stats.fmri_spec.sess.cond(9).name = 'Invisible
heading -25';
matlabbatch{2}.spm.stats.fmri_spec.sess.cond(9).onset = [73
                                                         163
                                                         253
                                                         463
                                                         553
                                                         643
                                                         733
                                                         943
                                                         1003
                                                         1123];
matlabbatch{2}.spm.stats.fmri_spec.sess.cond(9).duration = 5;
matlabbatch{2}.spm.stats.fmri_spec.sess.cond(9).tmod = 0;
matlabbatch{2}.spm.stats.fmri_spec.sess.cond(9).pmod = struct('name',
{}, 'param', {}, 'poly', {});
matlabbatch{2}.spm.stats.fmri_spec.sess.cond(10).name = 'reappear +25';
matlabbatch{2}.spm.stats.fmri_spec.sess.cond(10).onset = [18
                                                          228
                                                          318
                                                          408
```

```
                                                                498
                                                                708
                                                                798
                                                                888
                                                                978
                                                                1188];
matlabbatch{2}.spm.stats.fmri_spec.sess.cond(10).duration = 0;
matlabbatch{2}.spm.stats.fmri_spec.sess.cond(10).tmod = 0;
matlabbatch{2}.spm.stats.fmri_spec.sess.cond(10).pmod = struct('name',
{}, 'param', {}, 'poly', {});
matlabbatch{2}.spm.stats.fmri_spec.sess.cond(11).name = 'reappear -25';
matlabbatch{2}.spm.stats.fmri_spec.sess.cond(11).onset = [18
                                                                228
                                                                318
                                                                408
                                                                498
                                                                708
                                                                798
                                                                888
                                                                978
                                                                1188];
matlabbatch{2}.spm.stats.fmri_spec.sess.cond(11).duration = 0;
matlabbatch{2}.spm.stats.fmri_spec.sess.cond(11).tmod = 0;
matlabbatch{2}.spm.stats.fmri_spec.sess.cond(11).pmod = struct('name',
{}, 'param', {}, 'poly', {});
matlabbatch{2}.spm.stats.fmri_spec.sess.cond(12).name = 'Face+Turn
+45degrees';
matlabbatch{2}.spm.stats.fmri_spec.sess.cond(12).onset = [30
                                                                120
                                                                330
                                                                420
                                                                510
                                                                600
                                                                810
                                                                900
                                                                1020
                                                                1080];
matlabbatch{2}.spm.stats.fmri_spec.sess.cond(12).duration = 4;
matlabbatch{2}.spm.stats.fmri_spec.sess.cond(12).tmod = 0;
matlabbatch{2}.spm.stats.fmri_spec.sess.cond(12).pmod = struct('name',
{}, 'param', {}, 'poly', {});
matlabbatch{2}.spm.stats.fmri_spec.sess.cond(13).name = 'Face+Turn -
45degrees';
matlabbatch{2}.spm.stats.fmri_spec.sess.cond(13).onset = [90
                                                                180
                                                                270
                                                                360
                                                                570
                                                                660
                                                                750
                                                                840
                                                                1050
                                                                1140];
matlabbatch{2}.spm.stats.fmri_spec.sess.cond(13).duration = 4;
matlabbatch{2}.spm.stats.fmri_spec.sess.cond(13).tmod = 0;
```

```
matlabbatch{2}.spm.stats.fmri_spec.sess.cond(13).pmod = struct('name',
{}, 'param', {}, 'poly', {});
matlabbatch{2}.spm.stats.fmri_spec.sess.cond(14).name = 'Target Visible
+45degrees';
matlabbatch{2}.spm.stats.fmri_spec.sess.cond(14).onset = [34
                                                          124
                                                          334
                                                          424
                                                          514
                                                          604
                                                          814
                                                          904
                                                          1024
                                                          1084];
matlabbatch{2}.spm.stats.fmri_spec.sess.cond(14).duration = 6;
matlabbatch{2}.spm.stats.fmri_spec.sess.cond(14).tmod = 0;
matlabbatch{2}.spm.stats.fmri_spec.sess.cond(14).pmod = struct('name',
{}, 'param', {}, 'poly', {});
matlabbatch{2}.spm.stats.fmri_spec.sess.cond(15).name = 'Target Visible
-45degrees';
matlabbatch{2}.spm.stats.fmri_spec.sess.cond(15).onset = [94
                                                          184
                                                          274
                                                          364
                                                          574
                                                          664
                                                          754
                                                          844
                                                          1054
                                                          1144];
matlabbatch{2}.spm.stats.fmri_spec.sess.cond(15).duration = 6;
matlabbatch{2}.spm.stats.fmri_spec.sess.cond(15).tmod = 0;
matlabbatch{2}.spm.stats.fmri_spec.sess.cond(15).pmod = struct('name',
{}, 'param', {}, 'poly', {});
matlabbatch{2}.spm.stats.fmri_spec.sess.cond(5).name = 'Disappear
+45degrees';
matlabbatch{2}.spm.stats.fmri_spec.sess.cond(5).onset = [40
                                                         130
                                                         340
                                                         430
                                                         520
                                                         610
                                                         820
                                                         910
                                                         1030
                                                         1090];
matlabbatch{2}.spm.stats.fmri_spec.sess.cond(5).duration = 0;
matlabbatch{2}.spm.stats.fmri_spec.sess.cond(5).tmod = 0;
matlabbatch{2}.spm.stats.fmri_spec.sess.cond(5).pmod = struct('name',
{}, 'param', {}, 'poly', {});
matlabbatch{2}.spm.stats.fmri_spec.sess.cond(5).name = 'Disappear -
45degrees';
matlabbatch{2}.spm.stats.fmri_spec.sess.cond(5).onset = [100
                                                         190
                                                         280
```

```
                                                                370
                                                                580
                                                                670
                                                                760
                                                                850
                                                                1060
                                                                1150];
matlabbatch{2}.spm.stats.fmri_spec.sess.cond(5).duration = 0;
matlabbatch{2}.spm.stats.fmri_spec.sess.cond(5).tmod = 0;
matlabbatch{2}.spm.stats.fmri_spec.sess.cond(5).pmod = struct('name',
{}, 'param', {}, 'poly', {});
matlabbatch{2}.spm.stats.fmri_spec.sess.cond(7).name = 'Subj Move +45
degrees';
matlabbatch{2}.spm.stats.fmri_spec.sess.cond(7).onset = [40
                                                                130
                                                                340
                                                                430
                                                                520
                                                                610
                                                                820
                                                                910
                                                                1030
                                                                1090];
matlabbatch{2}.spm.stats.fmri_spec.sess.cond(7).duration = 4;
matlabbatch{2}.spm.stats.fmri_spec.sess.cond(7).tmod = 0;
matlabbatch{2}.spm.stats.fmri_spec.sess.cond(7).pmod = struct('name',
{}, 'param', {}, 'poly', {});
tlabbatch{2}.spm.stats.fmri_spec.sess.cond(7).name = 'Subj Move -45
degrees';
matlabbatch{2}.spm.stats.fmri_spec.sess.cond(7).onset = [100
                                                                190
                                                                280
                                                                370
                                                                580
                                                                670
                                                                760
                                                                850
                                                                1060
                                                                1150];
matlabbatch{2}.spm.stats.fmri_spec.sess.cond(7).duration = 4;
matlabbatch{2}.spm.stats.fmri_spec.sess.cond(7).tmod = 0;
matlabbatch{2}.spm.stats.fmri_spec.sess.cond(7).pmod = struct('name',
{}, 'param', {}, 'poly', {});
matlabbatch{2}.spm.stats.fmri_spec.sess.cond(8).name = 'Invisible
heading +45';
matlabbatch{2}.spm.stats.fmri_spec.sess.cond(8).onset = [44
                                                                134
                                                                344
                                                                434
                                                                524
                                                                614
                                                                824
                                                                914
                                                                1034
                                                                1094];
```

```
matlabbatch{2}.spm.stats.fmri_spec.sess.cond(8).duration = 4;
matlabbatch{2}.spm.stats.fmri_spec.sess.cond(8).tmod = 0;
matlabbatch{2}.spm.stats.fmri_spec.sess.cond(8).pmod = struct('name',
{}, 'param', {}, 'poly', {});
matlabbatch{2}.spm.stats.fmri_spec.sess.cond(9).name = 'Invisible
heading -45';
matlabbatch{2}.spm.stats.fmri_spec.sess.cond(9).onset = [104
                                                         194
                                                         284
                                                         374
                                                         584
                                                         674
                                                         764
                                                         854
                                                         1064
                                                         1154];
matlabbatch{2}.spm.stats.fmri_spec.sess.cond(9).duration = 4;
matlabbatch{2}.spm.stats.fmri_spec.sess.cond(9).tmod = 0;
matlabbatch{2}.spm.stats.fmri_spec.sess.cond(9).pmod = struct('name',
{}, 'param', {}, 'poly', {});
matlabbatch{2}.spm.stats.fmri_spec.sess.cond(10).name = 'reappear +45';
matlabbatch{2}.spm.stats.fmri_spec.sess.cond(10).onset = [48
                                                          138
                                                          348
                                                          438
                                                          528
                                                          618
                                                          828
                                                          918
                                                          1038
                                                          1098];
matlabbatch{2}.spm.stats.fmri_spec.sess.cond(10).duration = 0;
matlabbatch{2}.spm.stats.fmri_spec.sess.cond(10).tmod = 0;
matlabbatch{2}.spm.stats.fmri_spec.sess.cond(10).pmod = struct('name',
{}, 'param', {}, 'poly', {});
matlabbatch{2}.spm.stats.fmri_spec.sess.cond(10).name = 'reappear -45';
matlabbatch{2}.spm.stats.fmri_spec.sess.cond(10).onset = [108
                                                          198
                                                          288
                                                          378
                                                          588
                                                          678
                                                          768
                                                          858
                                                          1068
                                                          1158];
matlabbatch{2}.spm.stats.fmri_spec.sess.cond(10).duration = 0;
matlabbatch{2}.spm.stats.fmri_spec.sess.cond(10).tmod = 0;
matlabbatch{2}.spm.stats.fmri_spec.sess.cond(10).pmod = struct('name',
{}, 'param', {}, 'poly', {});
matlabbatch{2}.spm.stats.fmri_spec.sess.multi = {''};
matlabbatch{2}.spm.stats.fmri_spec.sess.regress = struct('name', {},
'val', {});
matlabbatch{2}.spm.stats.fmri_spec.sess.multi_reg = {'E:\FMRI\2010
MRI\Converted\subject\Pillar2\rp_aghdf999-0024-00001-000001-01.txt'};
```

```
matlabbatch{2}.spm.stats.fmri_spec.sess.hpf = 200;
matlabbatch{2}.spm.stats.fmri_spec.fact = struct('name', {}, 'levels',
{});
matlabbatch{2}.spm.stats.fmri_spec.bases.hrf.derivs = [0 0];
matlabbatch{2}.spm.stats.fmri_spec.volt = 1;
matlabbatch{2}.spm.stats.fmri_spec.global = 'None';
matlabbatch{2}.spm.stats.fmri_spec.mask = {''};
matlabbatch{2}.spm.stats.fmri_spec.cvi = 'AR(1)';

end.
```

9.4 **Ethical approvals**

OFFICE FOR RESEARCH
P.O. Box 281
Geelong Victoria 3220
Telephone: 03 5226 7920
Facsimile: 03 5226 7306
e-mail: hrec@BarwonHealth.org.au

Correspondence: A/Prof Peter Brotchie
BMI
Barwon Health
Geelong Hospital

ETHICS COMMITTEE ADDITIONAL APPROVAL STATEMENT

HREC Project Number	09/98
Site	Barwon Health
Date Approved	24/05/2010
Principal Investigator	Dr Peter Brotchie
Title:	Investigating Navigation performance in Humans using Functional Magnetic Resonance Imaging (fMRI)
Co investigators	Professor David Crewther - Swinburne University Dr Shoan Ip- Swinburne University
Student names	Mr Shaun Seixas - PhD Student , Swinburne University

In addition to the study approval dated 24/05/2010 , the following was reviewed and approved

Item:	Approval Date
Noted that BH HREC had requested that people taking illicit drugs should be excluded form the study. This was further refined by the student's home HREC, Swinburne in relation to NS section 4.6. BH HREC approved these changes on 07/03/11 Application for amendment as a result of Swinburne HREC advice: - Updated participant information and consent dated 03.02.11 - Recruiting poster version 2	7/03/2011

Name:.....

Signature.....

BERNICE DAVIES
RGO and HREC MANAGER
BARWON HEALTH
TELEPHONE:(03) 5226 7978
FAX: (03) 6260 3023
EMAIL: hrec@barwonhealth.org.au

Human Research Ethics Committee
Chair: Mr Simon French

Reseearch Review Committee
Chair: Dr Mary Lou Chatterton

17/03/2011

Project Number: 09/98

The Barwon Health Human Research Ethics Committee (HREC)) operates in accordance to guidelines established by the Nationa Health and Medical Research Council, National Statement on Ethical Conduct in Human Research (2007).

HUMAN RESEARCH ETHICS COMMITTEE

Telephone: 03 5226 7978
Facsimile: 03 5226 7306
e-mail: hrec@barwonhealth.org.au

The Geelong Hospital,
Ryrie Street P.O. Box 281
Geelong Victoria 3220

Correspondence: A/Prof Peter Brotchie
BMI
Barwon Health
Geelong Hospital

ETHICS COMMITTEE APPROVAL STATEMENT

Project Number	**09/98**
Site	**Barwon Health**
Principal Investigator:	**Dr Peter Brotchie**
Title:	**Investigating Navigation performance in Humans using Functional Magnetic Resonance Imaging (fMRI)**
Co investigators	Professor David Crewther - Swinburne University Dr Shoan Ip- Swinburne University
Student names	Mr Shaun Seixas - PhD Student , Swinburne University

Thankyou for submitting your application with the Human Research Ethics Committee.

Full approval was granted on 24/05/2010 for three years or until the anticipated completion date, 15/01/2011 ,whichever is the closer.

In addition any items approved in support of this project are listed below:

	Date Approved	*Item*		*Document Date*
1	24/05/2010	Participant Information and Consent Form	ver 4	02/11/2009
2	24/05/2010	Screening tool	Ver 1	
3	24/05/2010	Advertisement	ver 2	

I have attached a current list of the HREC membership. Committee members are required to disclose any actual or potential conflict of interest in the research under consideration. Members who do disclose a conflict, such as involvement in the research team, are not permitted to participate in the deliberations or decisions relating to the approval of this project.

Please note your annual report is in the month of: **May**

Dear David and Shaun,

SUHREC Project 2010/202 Investigating navigation performance in humans using functional magnetic resonance imaging (MRI)
Prof David Crewther; Mr Shaun Seixas; Dr Peter Brotchie; Dr Shoane Ip; Dr Matthew Hughes
Approved duration: 23/02/2011 to 31/08/2011 [Extended to 31/12/2012; Modified November 2011]

I refer to your request to modify the approved protocol for the above project as per your email of 7 and 15 November 2011 with attachments. The request was put to the Chair of SUHREC for consideration.

I am pleased to advise that, as submitted to date, the modified protocol has approval to proceed in line with the on-going ethics clearance conditions previously communicated.

Approval is given on the condition that Barwon Health approval of the modifications is submitted to this office.

Please contact me if you have any queries or concerns about on-going ethics clearance citing the SUHREC project number.

Best wishes for the continuing project.

Yours sincerely

Ann Gaeth
For Keith Wilkins
Secretary, SUHREC